1987

Synthesis and characterization of reduced ternary alkali metal molybdenum oxides

Lorraine Esther Aleandri
Iowa State University

Order Number 8805036

Synthesis and characterization of reduced ternary alkali metal molybdenum oxides

Aleandri, Lorraine Esther, Ph.D.

Iowa State University, 1987

U·M·I
300 N. Zeeb Rd.
Ann Arbor, MI 48106

Synthesis and characterization of reduced ternary alkali metal molybdenum oxides

by

Lorraine Esther Aleandri

A Dissertation Submitted to the
Graduate Faculty in Partial Fulfillment of the
Requirements for the Degree of
DOCTOR OF PHILOSOPHY

Department: Chemistry
Major: Inorganic Chemistry

Approved:

Signature was redacted for privacy.

In Charge of Major Work

Signature was redacted for privacy.

For the Major Department

Signature was redacted for privacy.

For the Graduate College

Iowa State University

Ames, Iowa

1987

TABLE OF CONTENTS

LIST OF TABLES

LIST OF FIGURES

GENERAL INTRODUCTION

Traditionally, the study of alkali metal Mo oxides has centered upon bronzes structurally consisting of MoO_6 and AO_n polyhedra with isolated Mo atoms. In 1979, the discovery of the ternary alkali metal Mo-oxide, $NaMo_4O_6$[1], opened a new area of synthetic effort toward highly reduced Mo oxides. Further work in this field has revealed a variety of compounds yielding novel structures with extended Mo clustering.

Infinite chains of trans edge-shared molybdenum octahedra are the characteristic feature of several structure types, typified by $NaMo_4O_6$[1], $Sc_{0.75}Zn_{1.25}Mo_4O_7$[2], $Mn_{1.5}Mo_8O_{11}$[3], and $Ca_{5.45}Mo_{18}O_{32}$[4]. In each of these structure types the infinite chains are extended along one crystallographic axis to produce a material having pseudo one-dimensional character.

A three dimensional network with orthogonal nonintersecting molybdenum octahedral cluster chains is observed in the compounds, $LiMo_8O_{10}$ and $ZnMo_8O_{10}$[5].

The hollandite structures of $Ba_{1.14}Mo_8O_{16}$[6], $Na_{0.35}BaMo_8O_{16}$[7], $Li_{0.34}BaMo_8O_{16}$[7], and $K_2Mo_8O_{16}$[8] reveal another type of pseudo one-dimensional framework with a different type of molybdenum clustering. These compounds show segmented chains comprised of discrete molybdenum rhomboidal cluster units.

Recently, new structural forms with discrete clusters derived from Mo octahedral units have been prepared with main group and rare earth metals serving as the counter cations, i.e., $In_{11}Mo_{40}O_{62}$[9] and $NdMo_8O_{14}$[10].

Synthetic exploration of reduced molybdenum oxides related to

$Na_2Mo_3O_6$, reported by Hubert[11] in 1966, has led to the isolation of a series of monoclinic layered Na-Mo-oxides, Na_xMoO_2 (Section 1). The two dimensional framework, consisting of oxide layers with alternate sheets of Na and Mo atoms, is quite unique among the previously observed structure types.

Layered oxide systems may be potential hosts suitable for use as cathodes in batteries. Li_xMoO_2 owing to the the smaller size and potentially greater mobility of the Li ions may be promising than Na_xMoO_2 with respect to application of these compounds as battery cathodes. Thus, the high temperature preparation of Li-Mo-oxides was studied, yielding the monoclinic phase, $Li_{0.74}MoO_2$ (Section 3); and the hexagonal material, $LiMoO_2$ (Section 2).

As detailed in the final section, work in the heavier alkali metal ternary system, K-Mo-O, led to a compound reminiscent of $In_{11}Mo_{40}O_{62}$[9] and $NdMo_8O_{14}$[10].

Explanation of Dissertation Format

This dissertation consists of four sections, the first three are written in a form suitable for publication in a technical journal, while the final section summarizes some incomplete work. Although references cited in the general introduction are found at the end of the dissertation, each section contains an independent listing of references and notes which are cited in that section.

SECTION 1. SYNTHESIS AND STRUCTURES OF NOVEL LAYERED PHASES CONTAINING RIBBONS OF FUSED MOLYBDENUM RHOMBOIDAL CLUSTERS: $Na_{0.41}MoO_2$, $Na_{0.51}MoO_2$, AND $Na_{0.66}MoO_2$

INTRODUCTION

Traditionally, the study of ternary Mo oxides has centered upon bronzes structurally consisting of MoO_6 and AO_n polyhedra with isolated Mo atoms. In 1979, the discovery of $NaMo_4O_6$[1] opened a new branch of study in the field concerned with highly reduced Mo oxides. Exploration of this area has revealed a variety of compounds yielding novel structures with extended Mo clustering.

Infinite chains of trans edge-shared molybdenum octahedra are the characteristic feature of several structure types, typified by $NaMo_4O_6$[1], $Sc_{0.75}Zn_{1.25}Mo_4O_7$[2], $Mn_{1.5}Mo_8O_{11}$[3], and $Ca_{5.45}Mo_{18}O_{32}$[4]. In each of these structure types the infinite chains are extended along one crystallographic axis to produce a material having pseudo one-dimensional character.

A three dimensional network with orthogonal nonintersecting molybdenum octahedral cluster chains is observed in the compounds, $LiMo_8O_{10}$ and $ZnMo_8O_{10}$[5].

The hollandite structures of $Ba_{1.14}Mo_8O_{16}$[6], $Na_{0.35}BaMo_8O_{16}$[7], $Li_{0.34}BaMo_8O_{16}$[7], and $K_2Mo_8O_{16}$[8] reveal another type of pseudo one-dimensional framework with a different type of molybdenum clustering. These compounds show segmented chains comprised of discrete molybdenum rhomboidal cluster units.

The structures of these low oxidation state molybdenum oxides are sensitive to the interplay among several factors such as the size and number of the ternary metal cations, and more importantly the extent the molybdenum is reduced. Whenever molybdenum is found in an oxidation state below +4, extensive metal-metal bonding is observed.

Synthetic exploration of reduced molybdenum oxides related to $Na_2Mo_3O_6$, reported by Hubert[9] in 1966, has led to the isolation of a series of layered sodium molybdenum oxides. The two dimensional framework is quite unique among the previously observed structure types. This section will detail the synthesis and structures of such phases, $Na_{0.41}MoO_2$, $Na_{0.51}Moo_2$, and $Na_{0.66}MoO_2$.

EXPERIMENTAL AND RESULTS

Materials

Sodium molybdate dihydrate (Fisher Certified A.C.S.) was dehydrated by drying at 125°C under dynamic vacuum overnight. Since the material is hygroscopic it was stored either over $CaSO_4$ or within a dry box. Molybdenum dioxide was obtained from Alfa Products (99%), molybdenum powder from Aldrich Chemical Co. (99.99%), molybdenum wire from laboratory stock, and elemental sodium from Fisher Scientific Co. Nickel and copper tubing employed for reaction vessels was supplied from Tubes Sales Company and laboratory stock, respectively.

Syntheses

$Na_{0.41}MoO_2$ was first discovered in the product of a reaction intended to prepare $Na_2Mo_3O_6$[4]. A mixture of Na_2MoO_4 and MoO_2 in the mol ratio of 3:2 was ground together and placed along with three pieces of Mo wire in an evacuated Ni tube. The welded reaction vessel was then sealed in an evacuated, protective fused-silica jacket. The reaction was warmed to 900°C in 300° per day increments. At some time between 48-72 hours at 900°C something went wrong with the temperature control and the reaction was found at room temperature within the furnace on the third day. The fused silica tube was destroyed and the Ni vessel was swollen but intact. The new compound grew from the surface of the Mo wires as thin black platelets. The composition, $Na_{0.41}MoO_2$, was determined from the single crystal X-ray diffraction data (see below). Subsequent work showed that pure samples of the material could be

isolated from the reaction between $NaMo_4O_6$ and a large excess of Na_2MoO_4. The mixture was cold welded in an evacuated copper vessel and fired at 900° for six days. The product was washed several times with deionized water to remove the excess sodium molybdate, and vacuum dried at 120°C. A Guinier X-ray powder diffraction pattern of the washed product revealed lines of only $Na_{0.41}MoO_2$. In order to verify the composition established by the single crystal X-ray refinement, quantitative analyses of Na and Mo were carried out. A precipitation method was employed for the determination of molybdenum. Samples were decomposed in a basic solution and neutralized to methyl red using an acetic acid/sodium acetate buffer. Quantitative precipitation of $MoO_2(ONC_9H_6)_2$ was effected by addition of a solution of 8-hydroxyquinoline. The precipitate was filtered into previously tared fritted crucibles and dried at 140°C overnight. The Na content was determined via atomic absorption techniques. The analyses yielded the apparent formula $Na_{0.52}MoO_2$. Calc. for $Na_{0.52}MoO_2$: Mo, 68.6%; Na, 8.55%. Found: Mo, 68.26%; Na, 8.52%.

Single crystals of a different structural variant, $Na_{0.51}MoO_2$, were isolated in the product of a different, longer firing of the same reaction, the oxidation of $NaMo_4O_6$ by Na_2MoO_4, A reactant mixture consisting of $NaMo_4O_6$ and Na_2MoO_4 in a mol ratio of 5:6 with a 200% excess of sodium molybdate was sealed within an evacuated Cu vessel and fired for 3.5 days at 900°C. The reaction vessel was then opened in a dry box, the contents were reground, then cold welded into a new Cu reaction container, and fired at 900°C for an additional seven days. The Guinier powder pattern of the washed and vacuum dried product,

showed lines that could be assigned to either the new form, $Na_{0.51}MoO_2$, γ for clarity, or a sodium layered phase, Na_xMoO_2 (β), discovered by Professor Simon's group in Stuttgart[10]. (The first compound discussed, $Na_{0.41}MoO_2$, is appropriately called α.) The longer reaction time in this case does not dictate the formation of the β or γ phases over the α form. Reactions utilizing $NaMo_4O_6$ and excess Na_2MoO_4 with a shorter firing time of about 5.5 days also result in mixtures of the β and γ forms. Product mixtures containing all three forms can be obtained by reducing MoO_2 with elemental sodium (mol ratio of 1:0.6 or 0.65 respectively) at 900°C for 4 to 4.5 days.

Via comparison of the X-ray powder patterns of these layered phases with that reported by Hubert[9] for $Na_2Mo_3O_6$, it was determined that the latter material represents yet another form of the layered framework. As described by Reau et al.[11], $Na_2Mo_3O_6$, or reformulated here as $Na_{0.66}MoO_2$, can be synthesized by reacting stoichiometric amounts of Na_2MoO_4, MoO_2, and Mo for several days at 700°C. This material reacts with water to form the α phase which can be easily understood in terms of the electrochemical data collected by Tarascon and Hull[12]. In their study, they observe the electrochemical oxidation of $Na_{0.66}MoO_2$ to the α phase at 2.2 Volts. Recalling that the reaction of sodium with water occurs at 2.7 Volts, one can conclude that the deintercalation involves sodium atoms moving out of the layers to react with water to form sodium hydroxide and hydrogen gas.

$$Na + H_2O \text{ ----------> } NaOH + 1/2H_2(g) \qquad +2.7V$$

$$Na_{0.66}MoO_2 \text{ ----------> } Na_{0.41}MoO_2 + 0.25Na \qquad \sim -2.2V$$

$$Na_{0.66}MoO_2 + 0.25H_2O \text{ ----> } Na_{0.41}MoO_2 + 0.25NaOH + 0.125H_2(g)$$

X-ray Single Crystal Analysis for $Na_{0.41}MoO_2$

A single crystal of $Na_{0.41}MoO_2$ in the form of a black thin plate was mounted on the tip of a glass fiber with epoxy adhesive and used for X-ray data collection. The crystal was placed on an automated four circle diffractometer, designed and built in Ames Laboratory[13]. Utilizing an automatic indexing program[14] that uses reflections taken from several ω-oscillation photographs as input, the crystal was indexed based on a triclinic cell. Crystal data and details of parameters associated with data collection are tabulated in Table 1.1. Final unit cell parameters and their estimated standard deviation were obtained by a least squares refinement of 2θ values of 18 independent reflections randomly distributed in reciprocal space having $30^o < 2\theta < 42^o$. The results were $a = 4.934(1)$, $b = 6.387(1)$, $c = 2.886(1)\text{Å}$, $\alpha = 102.79(2)^o$, $\beta = 90.19(2)^o$, $\gamma = 76.33(2)^o$.

The Patterson technique was employed to locate the molybdenum atom position in the cell employing the symmetry $P\bar{1}$ (no. 2). Sodium and oxygen positions were found from electron density and difference maps. Molybdenum and oxygen atoms were refined in general positions while the sodium atoms were refined in special positions. Ultimately all unconstrained positional and anisotropic temperature parameters were allowed to vary along with the multiplier for the sodium atoms. A final unweighted residual R of 5.4% was achieved after absorption and secondary ex n corrections were applied. However a final difference map showed peaks of electron density near the Mo atoms as high as $11e^-/\text{Å}^3$.

Because of these peaks and the seemingly higher symmetry of the unit

cell, the data were reinterpreted on the basis of a monoclinic unit cell: a = 12.448(7), b = 2.893(3), c = 4.934(3)Å, β = 104.02(6)°. 292 observed independent reflections were used to refine the structure in the space group C2/m (no. 12) indicated by the data satisfying the extinction h + k = 2n + 1. Atom positions were inferred as above and all atoms were found to be located on special positions. All unconstrained positional and anisotropic temperature parameters plus the sodium multipliers were allowed to vary. Following absorption and secondary extinction corrections, the refinement proceeded to a final R factor of 4.5% and a weighted R_w of 5.5%. The final difference map again showed high peaks of $2e^-/Å^3$ near the molybdenum sites.

The atomic scattering factors were taken from Hansen et al.[15] for neutral atoms and molybdenum was corrected for the real and imaginary parts of anomalous dispersion[16]. The positional and, thermal parameters, and selected interatomic distances are tabulated in Tables 1.2, 1.3, and 1.4, respectively.

X-ray Single Crystal Analysis for $Na_{0.51}MoO_2$

An hexagonal shaped black crystal with the dimensions 0.08mm x 0.08mm x 0.02mm was selected for film work. Oscillation and Weissenberg photographs indicated that the Laue group was 2/m with the unit cell parameters: a = 5.25, b = 4.94, c = 2.34Å, and β = 101°. Since the crystal was so small and the diffraction pattern weak, the accuracy of the cell parameters was poor. However, the cell constants were significantly different from that of $Na_{0.41}MoO_2$ (α) suggesting that the

crystal had provided a new variant of the layered framework.

The crystal was transferred and centered on a Datex four circle diffractometer[17]. The preliminary unit cell constants and orientation matrix were determined through an automatic indexing program[14] using seven reflections obtained from ω-oscillation pictures. The data set was collected on the basis of a primitive monoclinic cell. The crystallographic data and parameters associated with data collection are given in Table 1.5. Final unit cell parameters, obtained from a least-squares refinement of peak positions of 22 accurately centered high angle (2θ = 23 - 33°) reflections, were a = 2.897(4), b = 4.931(6), c = 12.433(15)Å, and β = 103.73(15)°.

Lorentz and polarization corrections were applied. Scattering factors[15] for neutral atoms were used throughout the calculations. Both the real and imaginary components of anomalous dispersion[16] were included for molybdenum atoms. Examination of the the intensity data set revealed that there were no extinctions in hkl reflections. However, h0l reflections obeyed the l = 2n condition and 0k0 reflections revealed a k = 2n + 1 extinction. Thus the space group no. 14, $P2_1/c$, was selected.

The molybdenum atom position was located using a Patterson function map. A few cycles of least-squares refinement of the positional parameters of the molybdenum atom led to R = 17.9% and R_w = 25.1%. A Fourier synthesis then led to the locations of the sodium and the two oxygen atoms. Refinement of positional parameters, sodium multipliers, and anisotropic temperature factors converged at R = 5.5% and R_w = 7.7%. At this point, since the β_{22} thermal parameter of O1 was negative, the thermal parameter was allowed to refine isotropically and no change in the agreement factors was noted. The maximum residual electron density

on the difference map was $2e^-/Å^3$. Tables 1.6, 1.7, and 1.8 list the atomic positions, thermal parameters, and interatomic distances, respectively.

X-ray Powder Diffraction Data

An Enraf Nonius Delft triple focusing Guinier camera was used with Cu $K\alpha_1$ radiation (λ = 1.54056Å) to obtain the powder diffraction pattern and unit cell data. National Bureau of Standards silicon powder was mixed with all samples as an internal standard. The observed vs. calculated d-spacings for $Na_{0.41}MoO_2$ and $Na_{0.51}MoO_2$ are listed in Tables 1.9 and 1.10. The cell unit dimensions for $Na_{0.41}MoO_2$ and $Na_{0.51}MoO_2$ were determined by a least squares method and the results are tabulated in Table 1.12 in comparison to single crystal results. The lattice parameters for $Na_{0.41}MoO_2$ were calculated using the strongest 15 powder lines, and the lattice parameters for $Na_{0.51}MoO_2$ were computed using the strongest 11 lines. Table 1.11 contains the d-spacings Hubert observed for $Na_2Mo_3O_6$ which can be indexed on the basis of a monoclinic cell as recorded in Table 1.12. For comparison the calculated d-spacings and intensities of the structural model proposed for $Na_{0.66}MoO_2$ (see below) are included.

Structural Model for $Na_{0.66}MoO_2$

As noted above, the powder pattern of Hubert's $Na_2Mo_3O_6$, appropriately reformulated as $Na_{0.66}MoO_2$, can be indexed to yield a monoclinic cell with lattice parameters similar to the other sodium

layered compounds. Upon examination of the indices for the indexed reflections, the condition h = 2n was noted for h00 and h0l reflections. Since the 010 reflection (d-spacing = 2.880) was absent from the pattern, it was assumed that the condition k = 2n for 0k0 reflections is fulfilled. On the basis of these extinctions, the space group with the highest possible symmetry would be $P2_1/a$. Other symmetry choices, ignoring one or both types of extinction, would include P2/a, $P2_1/m$, P2/m, Pa, Pm, $P2_1$, and P2.

An x-ray powder pattern was calculated for the structural model using the space group $P2_1/a$ with the atomic positions and isotropic thermal parameters listed in Table 1.13 and lattice parameters noted in Table 1.12. This model produced a pattern quite similar to that observed. However, the structure was discarded because the calculations that indicated there should be a moderately strong line at 2.486Å corresponding to the $\bar{1}11$ reflection, and an even stronger reflection at 2.255Å for $\bar{3}11$.

Thus, a different space group had to used. The condition h = 2n for h0l reflections was ignored for a trial with the space group $P2_1/m$ (no. 11). A layered structure employing this space group generated a calculated powder pattern with all observed reflections with approximately the correct intensities. Hence, the correct space group is $P2_1/m$. The calculated intensities along with the d-spacings for this model are listed in Table 1.11. The atomic positions and isotropic thermal parameters employed in the model are given in Table 1.14, while the interatomic distances are listed in Table 1.15.

To assure that this was the best model, structures based on the space groups, P2/a and Pa, were determined and diffraction patterns

computed. The centric possibility was eliminated because the calculated powder pattern called for moderate lines at 2.486Å, 2.346Å, 2.255Å, and 1.975Å. The structure corresponding to Pa was rejected on the basis of intensity data. For example, in the observed pattern, the reflection at 2.18Å is weak while the line at 2.075Å is moderately strong. The computed intensities, based on the structural model with Pa symmetry, for these lines are 15% and 14%, respectively.

DESCRIPTION OF STRUCTURES

$Na_{0.41}MoO_2$

Figure 1.1 illustrates the framework of $Na_{0.41}MoO_2$ (α) as viewed down the monoclinic b axis. Overall, the structure consists of molybdenum dioxide sheets sandwiched between layers of sodium ions. Each molybdenum dioxide slab can be viewed as a close-packed arrangement of two oxygen layers with the metal atoms occupying interstitial octahedral sites. However, the molybdenum atoms are shifted from ideal octahedral sites toward neighboring metal atoms to form infinite metal-metal bonded chains which run parallel to the unique axis. Due to this distortion, each molybdenum atom is found in a nonideal octahedral site consisting of three intra-chain (inner) oxygens (d(Mo-O1) 2.058 to 2.083Å) and three inter-chain (ausser) oxygens (d(Mo-O2) 2.070 to 2.108Å). The metal-metal bonding can be seen better in the drawing of the b-c plane given in Figure 1.2. The structure has one crystallographically unique molybdenum atom. Each metal atom is bonded to two metal atoms parallel to the chain direction at a distance corresponding to the monoclinic b lattice constant, 2.890Å, and to two other molybdenum atoms via zig-zag bonds at 2.535Å. The Mo-Mo bonding can be viewed as a condensation of distorted rhomboidal clusters leading to infinite ribbons. The interchain Mo-Mo distance, 3.200Å, indicates there is only very weak interaction between Mo atoms of neighboring ribbons.

The results of the crystal structure determination showed two unique sodium atoms each occupying distinct octahedral sites within the cation

layer. Na1 occupies a more "regular" octahedral site, above and below the molybdenum chains, consisting of four inner oxygens (d(Na1-O1) 2.485Å) and two ausser oxygens (d(Na1-O2) 2.357Å). The second type of sodium, Na2, is also coordinated to four inner oxygens at a distance of 2.514Å and to two ausser oxygens at 2.302Å. This more distorted NaO_6 octahedron is located above and below the interchain links. The multipliers of the two sodiums refined to essentially the same value, 0.098(6) and 0.105(6), for Na1 and Na2, respectively. Overall, the refinement for Na yielded a total sodium-site occupation of 41%, leading to the stoichiometry, $Na_{0.41}MoO_2$. The sodium ions are arranged in a rectangular net (Figure 1.3) rather than an hexagonal array.

$Na_{0.51}MoO_2$

This compound reveals a different structural variation of the layered framework seen in $Na_{0.41}MoO_2$. The contrast will be outlined in detail in the discussion section. The structure of $Na_{0.51}MoO_2$ (γ) is shown in Figure 1.4 viewed down the monoclinic a axis. Similar to the α form, the framework is comprised of molybdenum dioxide layers with sodium intercalating the inter-layer spaces. Within the molybdenum oxide slabs, the metal atoms are shifted from ideal octahedral sites toward neighboring metal atoms to form chains of condensed rhomboidal clusters. This material shows slightly longer Mo-Mo distances, 2.897Å along the chain direction and 2.537Å diagonally, while the interchain spacing remains 3.200Å. From Figure 1.4, it can be seen that in the γ-form the metal chains are staggered from layer to layer while in the α

compound the chains are aligned. Because of this shifted arrangement of the ribbons, there is only one type of octahedral site occupied by Na between the molybdenum dioxide slabs. This distorted site is made up of four inner oxygens (O1) with Na-O distances ranging from 2.486 to 2.522Å and two ausser oxygens (O2) with distances of 2.318 and 2.366Å. Like the first compound, the sodium ions are found on a rectangular sublattice.

$Na_{0.66}MoO_2$

Figure 1.5 illustrates the structural model proposed for $Na_{0.66}MoO_2$ looking down the monoclinic b axis. From this diagram, it can be assessed that the framework is quite similar to the two forms discussed above: molybdenum dioxide slabs with sodium in the interlayer space; and Mo-Mo bonding in the form of chains of condensed rhomboids. Similar to the α form, the metal ribbons are eclipsed along the layering axis. The model reveals unrefined Mo-Mo distances of 2.552 and 2.880Å within the chain and 3.197Å between chains. Due to the eclipsed nature of the extended metal chains two types of sodiums are noted: one located between the molybdenum ribbons and the second between the interchain oxide bridges. Each Na cation is trigonal prismatically coordinated by three inner and three ausser oxygens revealing a more traditional sodium substructure, a hexagonal net (Figure 1.6). The sodium ions offset from under the metal chains are located in quite distorted sites with sodium (Na1) to oxygen distances ranging from 2.291 to 2.664Å. The cations

(Na2) sandwiched by the metal ribbons reveal slightly more regular geometry with sodium to oxygen distances from 2.367 to 2.601Å.

DISCUSSION

One of the important features of these layered compounds is the clustering of Mo atoms within the metal dioxide slabs to form chains of condensed rhombuses. Employing the γ form as an example, it can be concluded from the formula, $Na_{0.51}MoO_2$, that each Mo atom has 2.49 electrons available for metal-metal bonding. If the short diagonal bonds (2.537(5)Å) are to be considered as normal electron pair bonds, each Mo must contribute one electron to each of these bonds. The remaining 0.49 electrons must then enter into the longer bonds (2.897(4)Å) parallel to the chain. Thus the long bonds would show a bond order of 0.245. This is in good agreement with the bond order, 0.251, calculated using the Pauling[18] relation:

$$d(obs.) = d_1 - 0.6 \log n$$

where n is the bond order and d_1 is a single bond distance set at the diagonal bond distance, 2.537Å. Equal spacing of the metal atoms along the chain suggests that the bonding is delocalized and the compound should exhibit good electrical conductivity along the chain axis, a. The Mo-Mo interchain distances, 3.200(5)Å, with a computed bond order of 0.07, indicates the interaction between neighboring ribbons is essentially nonexistent. Similarly, interlayer interaction should be even weaker, thus conductivity in both the other axial directions, b and c, is expected to be small.

The layered framework of the sodium molybdenum oxides stands in sharp contrast to the hollandite structures of $Ba_{1.14}Mo_8O_{16}$[6] and $K_2Mo_8O_{16}$[8] which also contain chains comprised of molybdenum rhomboidal clusters. In these compounds the chains are linked to yield channels in

which the counter cations are embedded. The metal chains are broken into discrete clusters and two types of chains are noted, one with distorted clusters and one with more regular units. Using the Ba compound as an example, 10 of the 18.28 metal electrons can be assigned to the "regular" clusters and the remaining 8.28 electrons to the distorted clusters leading to the formula: $Ba_{1.14}(Mo_4O_8)^{-2}(Mo_4O_8)^{-0.28}$. $Na_{0.51}MoO_2$ with essentially ten electrons for every Mo_4O_8 should be ideal for forming a hollandite structure with all regular rhomboidal clusters. The formation of a layered over a hollandite framework in $Na_{0.51}MoO_2$ provides a good example of how the resulting structure can be influenced by factors other than the metal electron count. To reiterate, electronically, $Na_{0.51}MoO_2$ might be expected to form a tunneled framework with discrete regular rhomboidal clusters. But the hollandite structure provides only two cubic cationic sites per every Mo_8O_{16} unit; $Na_{0.51}MoO_2$, reformulated as $Na_{\sim 4}Mo_8O_{16}$, requires four cationic sites for every Mo_8O_{16} repeat. Thus a new structure type is dictated.

The observation of infinite ribbons composed of distorted rhomboidal clusters over discrete regular rhombuses in the layered framework is not easy to explain. Burdett and Hughbanks[19] have reported the stabilization energy as a function of d-electron count of a distorted hexagonal layer with chains of condensed rhombuses versus discrete clusters. From their calculations, they conclude that the condensed chain shows the greatest relative stability for d electron counts from 2.0 to 2.5. The energy difference between the chain and the cluster structure for a $d^{2.5}$ material is about 9kcal per Mo_4O_8 cluster. Their calculations indicate that discrete clustering is most likely for d^3

systems which is contrary to the expectations resulting from normal 2-center 2-electron counting.

The layered structures of the sodium molybdenum oxides are remarkably similar to a series of transition metal molybdenum sulfides, MMo_2S_4 (M = V, Cr, Fe, Co)[20]. The sulfides show a layered structure with the Mo disulfide sheets sandwiched by transition metals. The Mo atoms are again shifted from ideal octahedral sites to form chains. But the Mo atoms, unlike that in the oxides, form chains of linked distorted rhomboidal clusters. This type of metal clustering is also observed in $ReSe_2$[21]. Both the Mo sulfides and the Re selenide are d^3 systems. Due to the higher electron to metal ratio found in the higher chalcogenides, one would expect a ribbon composed of regular rhombuses. Electronically, this difference in cluster condensation can be crudely explained by a model put forth by Burdett and Hughbanks[19].

In this model one begins with an ideal MoO_2 hexagonal layer. The Mo d_{xy}, d_{xz}, and d_{yz} orbitals are free for metal-metal bonding within the layer and also potentially available for Mo-O π interactions. Two assumptions are made: (1) that each d-orbital with t_{2g} symmetry interacts only with orbitals on neighboring metals with the same label; and (2) that the Mo-O π interactions are insignificant. As illustrated in Figure 1.7a, the Mo bonding in the Na_xMoO_2 series can be viewed as a distortion in which two subsystems, d_{xz} and d_{yz}, are paired while the third, d_{xy}, has been left unaltered. The expected electronic structure scheme is given in Figure 1.8a. Since it is assumed that each subsystem behaves as one dimensional in that half filled bands are expected to result from the pairing distortions, the d_{xz} and d_{yz} bands split and the Fermi level falls at the top of these bonding bands. From Figure 1.8a,

one can see that a $d^{2.5}$ system would be expected for the metal clustering seen in the Na-Mo-oxides. $Na_{0.51}MoO_2$ is a $d^{2.51}$ system, while $Na_{0.41}MoO_2$ has slightly less electrons and $Na_{0.66}MoO_2$ has more.

As depicted in Figure 1.7b, the pairing distortion leading to the metal bonding observed in MMo_2S_4 and $ReSe_2$ involves all three subsystems. Thus all three of the t_{2g} sub-bands are split as predicted for a d^3 system (Figure 1.8b). Even though extrapolation to chalcogenides is really inappropriate due to the greater metal-chalcogenide π interaction, this model can provide some understanding of the observed difference in metal clustering.

The comparison of the oxides to the heavier chalcogenides provides a good example of how the size of the anions can affect the structure. More specifically, matrix effects must play an important role in the extent of metal clustering. In close packed structures, the intralayer M-M distances of the interstitial atoms corresponds directly to the intralayer spacing of the framework atoms. The effective ionic radius for O^{2-} is 1.4Å[22], yielding an intralayer O-O spacing of 2.8Å. As dictated by the O-O distances, in the Na-Mo-oxides, the minimum "undistorted" Mo-Mo distance would be ~2.9Å. In contrast, an "undistorted" Mo-Mo distance of 3.6Å is noted in $CoMo_2S_4$[20] where the spacing of the sulfur atoms within a layer is about 3.7Å. For the oxides, the pairing distortion leads to quite short diagonal interactions of about 2.5Å, while the Mo clustering in the sulfide shows substantially longer distances between 2.75 and 2.99Å[20]. Thus, due to the larger size of S (and Se) over O, it is apparent that the metal atoms may not be able to approach each other close enough to yield a completely condensed ribbon.

While the size of the framework atoms may determine the extent of metal clustering in such layered compounds, the number of counter cations may be the controlling factor in the stacking pattern of the metal-anion bilayers. Each of the Na-Mo-oxides structures shows a different structural form with respect to the O-Mo-O layer stacking, each form related to the varied amount of sodium in the interlamellar space. A similar dependence of structural form on Na content is observed in the Na-Co bronzes[23-26].

During an electrochemical study of the Na_xCoO_2 system, Delmas et al.[23] observed four distinct layered phases over a range $0.82 \leq x \leq 1$. When the compositional variable x is 0.82, the material has a hexagonal structure with ABBCCA oxygen packing symbolized by Delmas et al. as P3. Na ions are located on trigonal prismatic sites while Co atoms occupy octahedral sites. As the concentration of the Na increases to x = 0.90, the hexagonal material distorts slightly to show a monoclinic structure (P'3). When the Na content reaches 0.95, the O-Co-O slabs slip in such a way to allow Na to enter octahedral sites. In this monoclinic form (O'3) no distinct layer-stacking sequence for oxygen can be defined. When the interlayer space becomes completely filled by Na ions, the beta angle opens up and the oxygens shift to allow for true cubic close packing, ABCABC. The hexagonal material, $NaCoO_2$, is isostructural with the prototype α-$NaFeO_2$[27].

The oxygen layering of the Na-Mo-oxides is like the Co bronzes in reverse (see Figure 1.8). The $Na_{0.66}MoO_2$ material has an P'3 structure type showing ABBCCA oxygen packing with Na in trigonal prismatic sites and Mo in octahedral sites.

The Na ions in the Co bronzes, $Na_{0.82}CoO_2$ and $Na_{0.90}CoO_2$, with

trigonal prismatic coordination show greater mobility than those in the cases where the Na ions are located in octahedral environments[28]. Similarly, the greater mobility of Na in trigonal prismatic sites of $Na_{0.66}MoO_2$ permits deintercalation in air to form the water stable α phase, $Na_{0.41}MoO_2$, which has Na in octahedral sites.

Focusing on the monoclinic cell projections in Figure 1.8, the structural change from $Na_{0.66}MoO_2$ to $Na_{0.41}MoO_2$ (α), results from a translation of the second MoO_2 slab by one half in the 001 direction which enables the Na atoms to move into octahedral coordination sites. Since the monoclinic α compound, $Na_{0.41}MoO_2$, has Na cations located in octahedral sites, it can be labeled as having an O'3 structure type. Like the O'3 type Co oxide, $Na_{0.95}CoO_2$, the α phase, $Na_{0.41}MoO_2$, shows no sequential oxygen packing.

The conversion to γ-$Na_{0.51}MoO_2$ from either of the other variants requires the breakage of Mo-O bonds. Again studying the monoclinic cell projections in Figure 1.8, the change from the high sodium phase, $Na_{0.66}MoO_2$ to γ-$Na_{0.51}MoO_2$ is basically a shift of the second layer of oxygens to the left by one half the c-axis. This cleavage of Mo-O bonds is probably the reason why the γ form, $Na_{0.51}MoO_2$, is not generated upon deintercalation of $Na_{0.66}MoO_2$.

The conversion of the α phase, $Na_{0.41}MoO_2$, to the γ structure, $Na_{0.51}MoO_2$, can be visualized by the slippage of the first O and Mo layers in opposite directions, O to the left and Mo to the right. The C-centering observed in the α-$Na_{0.41}MoO_2$ compound is destroyed by a slight displacement of the central layer of Na atoms. A small decrease in the unique angle yields an oxygen packing sequence of ABCDA in γ-$Na_{0.51}MoO_2$.

As discussed in the previous section, $Na_{0.66}MoO_2$ differs significantly from $Na_{0.41}MoO_2$ (α) and $Na_{0.51}MoO_2$ (γ) in regard to the Na sublattice. In the α and γ compounds, the Na ions are found in an unusual rectangular arrangement (see Figure 1.3). If all Na sites were fully occupied, this rectangular net would yield two nearest neighbors at 2.45Å, two next nearest neighbors at 2.89Å, and finally four neighbors at 3.8Å. Both the α and γ forms show a Na concentration around one half, which means that roughly every other site is vacant on the cationic net. Ordering of the Na ions to minimize repulsions would then yield Na-Na distances of 3.8Å. When the concentration of the alkali metal increases significantly above one half, the sites located at a distance of 2.45Å will be increasingly more occupied. Thus the hexagonal net (Figure 1.6) with nearest neighbor distances of 2.89Å should be more favorable which is in accord with the model for $Na_{0.66}MoO_2$.

Conclusion

This series of Na-Mo-oxides has provided a novel structural type, a two dimensional network, among the previously known structures observed for reduced molybdenum oxides. The basic framework of these phases consists of oxide layers alternating with sheets of Na and Mo atoms. Within the Mo layers, the metal atoms shift from ideal octahedral sites toward neighboring Mo atoms to form extended chains of fused rhomboidal clusters. This metal bonding is comparable to the discrete Mo rhombuses observed in the less electron rich systems of $Ba_{1.14}Mo_8O_{16}$[6] and $K_2Mo_8O_{16}$[8]; and the chains of linked distorted rhomboidal units in the

more electron rich systems of MMo_2S_4[20] and $ReSe_2$[21].

The concentration of sodium between the O-Mo-O slabs seems to influence the stacking of the slabs, similar to the effect of varied sodium content noted in the cobalt bronzes, Na_xCoO_2[23-26]. Structurally, from $Na_{0.41}MoO_2$ to $Na_{0.66}MoO_2$, the Na ions shift from octahedral to trigonal prismatic sites; and the oxygen packing changes from nonsequential to ABBCCA. In contrast, in the cobalt bronzes, from low to high Na concentration, the ternary cations move from trigonal prismatic to octahedral sites; and the oxygen layering shifts from ABBCCA through nonsequential to ABCABC. This distortion toward cubic close packing (ccp) is not excluded in the layered Mo-oxides. As detailed in the next two sections, exploration of the analogous Li system reveals a monoclinic material, $Li_{0.74}MoO_2$[29,30] with distorted ccp; and a hexagonal compound, $LiMoO_2$[31] with true ccp of oxygen atoms.

REFERENCES

1. Torardi, C. C.; McCarley, R. E. J. Am. Chem. Soc. 1979, 101, 3963.

2. McCarley, R. E. ACS Symp. Ser. 1983, 211, 273; Philos. Trans. R. Soc. London Ser. A 1982, 308, 141.

3. Carlson, C. D.; Edwards, P. A.; McCarley, R. E., unpublished results, Department of Chemistry, Iowa State University, Ames, Iowa, 1982.

4. McCarley, R. E.; Lii, K. -H.; Edwards, P. A.; Brough, L. F. J. Solid State Chem. 1985, 57, 17.

5. Lii, K. -H.; McCarley, R. E.; Sangsoo, K.; Jacobson, R. A. J. Solid State Chem. 1986, 64, 347.

6. Torardi, C. C.; McCarley, R. E. J. Solid State Chem. 1981, 37, 393.

7. Lii, K. -H., Ph.D. Dissertation, Iowa State University, Ames, Iowa, 1985, Section 1.

8. Torardi, C. C.; Calabrese, J. C. Inorg. Chem. 1984, 23, 3281.

9. Hubert, P. H. C. R. Acad. Sc. Paris 1966, 262, 1189.

10. Simon, A., private communication, Max Planck Institute for Solid State Research, Stuttgart, F. R. G.

11. Reau, J. M.; Fouassier, C.; Hagenmuller, P. Bull. Soc. Chim. 1970, 11, 3827.

12. Tarascon, J. M.; Hull, G. W. Solid State Ionics 1986, 22, 85.

13. Rohrbaugh, W. J.; Jacobson, R. A. Inorg. Chem. 1974, 13, 2535.

14. Jacobson, R. A. J. Appl. Crystallogr. 1976, 9, 115.

15. Hansen, H. P.; Herman, F.; Lea, J. D.; Skillman, S. Acta Crystallogr. 1964, 17, 1040.

16. Templeton, D. H. In "International Tables for X-ray Crystallography", 1st ed.; Macgillavry, C. H. and Rieck, G. D., Eds.; Kynoch Press: Birmingham, England, 1962; Vol. III, P. 215.

17. This Datex four-circle diffractometer was modified in Dr. R. A. Jacobson's laboratory. Stepping motors and encoders were attached and interfaced to a LSI/11 computer, which in turn was interfaced to a VAX11/730 computer. It is equipped with a scintillation counter and incorporates a graphite monochromator in the detection system.

18. Pauling, L. "The Nature of the Chemical Bond", 3rd Ed.; Cornell University Press, Ithaca, 1960, p. 400.

19. Burdett, J. K.; Hughbanks, T. Inorg. Chem. 1985, 24, 1741.

20. Guillevic, J.; Le Marouille, J. -Y.; Grandjean, D. Acta Crystallogr. 1974, B30, 111.

21. Alcock, N. W.; Kjekshus, A. Acta Chemica Scand. 1965, 19, 79.

22. Shannon, R. D. Acta Crystallogr. 1976, A32, 751.

23. Delmas, C.; Braconnier, J. J.; Fouassier, C.; Hagenmuller, P. Solid State Ionics 1981, 3/4, 165.

24. Delmas, C.; Fouassier, C.; Hagenmuller, P. Physica 1980, 99B, 81.

25. Fouassier, C.; Delmas, C.; Hagenmuller, P. Mat. Res. Bull. 1975, 10, 443.

26. Fouassier, C.; Matejka, G.; Reau, J. M.; Hagenmuller, P. J. Solid State Chem. 1973, 6, 532.

27. Goldsztaub, S. Compt. Rend. 1933, 196, 280.

28. Delmas, C.; Maazarz, A.; Fouassier, C.; Reau, J. M.; Hagenmuller, P. Mat. Res. Bull. 1979, 14, 329.

29. Aleandri, L. E.; Edwards, P. A.; McCarley, R. E., American Chemical Society Meeting, Chicago, Sept. 8-13 (1985).

30. Aleandri, L. E.; McCarley, R. E., American Chemical Society Meeting, New York, April 13-18 (1986).

31. Aleandri, L. E.; McCarley, R. E., submitted for publication in Inorg. Chem.

Table 1.1. The crystallographic data for $Na_{0.41}MoO_2$

crystal system	monoclinic
space group	C2/m
lattice constants	
a (Å)	12.448(7)
b (Å)	2.893(3)
c (Å)	4.934(3)
β (degree)	104.02(6)
Volume ($Å^3$)	172.4(2)
Z	4
density (calcd) (g/cm^3)	5.28
crystal dimensions (mm)	0.10 x 0.06 x 0.02
abs coeff (cm^{-1})	71.14
reflection absorp. corr. (hkl, 2θ, Tmax/Tmin)	$\bar{1}3\ \bar{1}\ 3$, 58.50, 1.43
diffractometer	AL[a]
radiation: MoKα (λ,Å)	0.71084
monochromator	graphite
scan type	ω-scan
scan half width (degree)	0.5
standard reflections:	
number monitored	3
frequency measured	every 75 reflns.
intensity variation	none
reflections measured	HKL, $\bar{H}$KL, $\bar{H}K\bar{L}$, H$\bar{K}\bar{L}$
max 2θ (degree)	60
reflections collected	1302
observed [I > 3σ(I)]	620
number unique reflns. with I > 3σ(I)	253
number parameters refined	30
R (%)[b]	4.5
R_w (%)[c]	5.6

[a] For details of the AL diffractometer, see reference 13.

[b] $R = \Sigma||F_o| - |F_c||/\Sigma|F_o|$.

[c] $R_w = [\Sigma w(|F_o|-|F_c|)^2/\Sigma w|F_o|^2]^{1/2}$; $w = 1/\sigma^2(|F_o|)$.

Table 1.2. Positional parameters for $Na_{0.41}MoO_2$

atom	multiplier	x	y	z	B(Å^2)[a]
Na1	0.098(6)	0.00	0.50	0.00	1.02
Na2	0.105(6)	0.00	0.50	0.50	1.25
Mo1	0.5	0.25438(4)	0.00	0.2135(1)	0.94
O1	0.5	0.1343(5)	0.00	0.837(1)	1.12
O2	0.5	0.3364(5)	0.00	0.640(1)	0.72

[a]The isotropic equivalent thermal parameter is defined as $B = 4/3\ [a^2\beta_{11} + b^2\beta_{22} + c^2\beta_{33} + 2ab(\cos\gamma)\beta_{12} + 2ac(\cos\beta)\beta_{13} + 2bc(\cos\alpha)\beta_{23}]$.

Table 1.3. Thermal parameters[a] for $Na_{0.41}MoO_2$

atom	B_{11}	B_{22}	B_{33}	B_{12}	B_{13}	B_{23}
Na1	0.2(3)	2.7(5)	0.9(4)	0.0	-1.3(1.2)	0.0
Na2	0.4(3)	3.3(6)	1.2(4)	0.0	0.3(1.2)	0.0
Mo1	1.01(4)	1.25(4)	0.54(4)	0.0	0.56(9)	0.0
O1	1.2(2)	1.2(2)	0.7(2)	0.0	-0.1(6)	0.0
O2	1.4(2)	0.9(1)	0.5(1)	0.0	1.3(6)	0.0

[a]The general thermal parameter expression used is $\exp[-1/4\ (B11h^2a^{*2} + B22k^2b^{*2} + \ldots + 2B23klb^*c^*)]$.

Table 1.4. Bond distances (Å) in $Na_{0.41}MoO_2$

Mo1 - Mo1	2.535(2)[a]	
	2.890(2)[a]	
	3.200(2)[b]	
Mo1 - O1[i]	2.058(5)	
	2.058(5)	
	2.083(7)	
Mo1 - O2[a]	2.070(5)	
	2.070(5)	
	2.108(6)	
Na1 - O1[i]	2.485(5)	(4X)
Na1 - O2[a]	2.357(8)	(2X)
Na2 - O1[i]	2.514(6)	(4X)
Na2 - O2[a]	2.302(7)	(2X)

[a]Intrachain distance.

[b]Interchain distance.

Table 1.5. The crystallographic data for $Na_{0.51}MoO_2$

crystal system	monoclinic
space group	$P2_1/c$
lattice constants	
a (Å)	2.897(4)
b (Å)	4.931(6)
c (Å)	12.433(15)
β (degree)	103.73(15)
Volume ($Å^3$)	172.5(3)
Z	4
density (calcd) (g/cm^3)	5.38
crystal dimensions (mm)	0.08 x 0.08 x 0.02
abs coeff (cm^{-1})	70.88
reflection absorp. corr. (hkl, 2θ, Tmax/Tmin)	0 $\bar{2}$ 0, 16.56, 2.35
diffractometer	Datex[a]
radiation: MoKα (λ,Å)	0.70966
monochromator	graphite
scan type	ω-scan
scan half width (degree)	0.6
standard reflections:	
number monitored	3
frequency measured	every 50 reflns.
intensity variation	none
reflections measured	HKL, $\bar{H}$KL, $\bar{H}K\bar{L}$, H$\bar{K}\bar{L}$
max 2θ (degree)	60
reflections collected	1328
observed [I > 3σ(I)]	606
number unique reflns. with I > 3σ(I)	233
number parameters refined	34
R (%)[b]	5.5
R_w (%)[c]	7.7

[a]For details of the Datex diffractometer, see reference 17.

[b]$R = \Sigma||F_o| - |F_c||/\Sigma|F_o|$.

[c]$R_w = [\Sigma w(|F_o|-|F_c|)^2/\Sigma w|F_o|^2]^{1/2}$; $w = 1/\sigma^2(|F_o|)$.

Table 1.6. Positional parameters for $Na_{0.51}MoO_2$

atom	multiplier	x	y	z	B(Å^2)[a]
Na1	0.51(3)	0.499(9)	0.661(5)	0.747(1)	1.7
Mo1	1.0	0.255(1)	0.2109(4)	0.0041(1)	0.98
O1	1.0	0.135(5)	0.588(3)	0.384(1)	0.61
O2	1.0	0.331(5)	0.911(4)	0.585(1)	1.0

[a]The isotropic equivalent thermal parameter is defined as $B = 4/3\ [a^2\beta_{11} + b^2\beta_{22} + c^2\beta_{33} + 2ab(\cos\gamma)\beta_{12} + 2ac(\cos\beta)\beta_{13} + 2bc(\cos\alpha)\beta_{23}]$.

Table 1.7. Thermal parameters[a] for $Na_{0.51}MoO_2$

atom	B_{11}	B_{22}	B_{33}	B_{12}	B_{13}	B_{23}
Na1	1.4(9)	2.6(1.2)	1.0(6)	0.0	2.1(2.2)	0.0
Mo1	1.08(8)	1.18(8)	0.84(6)	0.0	2.2(1)	0.0
O1	isotropic temperature factor (B): 0.6(2)					
O2	0.3(6)	1.8(8)	0.8(5)	0.0	1.4(1.8)	0.0

[a]The general thermal parameter expression used is $\exp[-1/4\ (B11h^2a^{*2} + B22k^2b^{*2} + \ldots + 2B23klb^*c^*)]$.

Table 1.8. Bond distances (Å) in $Na_{0.51}MoO_2$

Mo1 - Mo1	2.537(5)[a]
	2.897(4)[a]
	3.200(5)[b]
Mo1 - O1[i]	2.059(16)
	2.066(17)
	2.075(15)
Mo1 - O2[a]	2.047(18)
	2.067(18)
	2.106(21)
Na1 - O1[i]	2.487(30)
	2.486(28)
	2.511(29)
	2.522(28)
Na1 - O2[a]	2.318(28)
	2.366(28)

[a]Intrachain distance.

[b]Interchain distance.

Table 1.9. X-ray powder diffraction data for $Na_{0.41}MoO_2$

d-spacings (Å) observed	d-spacings (Å) calculated	intensities	h k l
6.072(9)	6.044	vs	2 0 0
4.803(5)	4.789	w	0 0 1
4.294(4)	4.288	w	-2 0 1
3.023(2)	3.022	m	4 0 0
2.485(1)	2.485	ms	-1 1 1
2.436(1)	2.435	m	-2 0 2
2.394(1)	2.394	m	0 0 2
2.365(1)	2.367	m	1 1 1
2.234(1)	2.235	ms	-3 1 1
2.147(1)	2.144	vvw	-4 0 2
2.0636(9)	2.0631	m	2 0 2
2.0163(9)	2.0147	vw	6 0 0
1.9989(9)	2.0007	w	3 1 1
1.8743(7)	1.8753	vvw	-1 1 2
1.8495(7)	1.8476	w	-5 1 1
1.8085(7)	1.8080	vw	-3 1 2
1.7669(6)	1.7646	vw	-6 0 2
1.6897(6)	1.6897	vvw	4 0 2
1.6441(5)	1.6441	vvw	-2 0 3
1.6293(5)	1.6310	vw	5 1 1
1.5953(5)	1.5965	vw	0 0 3
1.5781(5)	1.5767	vw	-4 0 3
1.5112(4)	1.5110	w	8 0 0
1.4433(4)	1.4450	wm	0 2 0
1.4225(4)	1.4227	vw	-1 1 3
1.4146(4)	1.4156	vw	-3 1 3
1.4037(4)	1.4053	vw	2 2 0
1.3384(3)	1.3378	vvw	-5 1 3
1.3024(3)	1.3036	vvw	4 2 0

Table 1.10. X-ray powder diffraction data for $Na_{0.51}MoO_2$

d-spacings (Å) observed	d-spacings (Å) calculated	intensities	h k l
6.045(10)	6.038	s	0 0 2
4.569(4)	4.565	wm	0 1 1
3.021(2)	3.019	w	0 0 4
2.467(1)	2.465	w	0 2 0
2.441(1)	2.447	m-b	-1 1 2
	2.444		1 1 0
2.282(1)	2.282	wm	0 2 2
2.014(1)	2.012	vvw	0 0 6
1.911(1)	1.909	vw	0 2 4
1.7910(8)	1.7914	vw	1 2 1
1.7356(8)	1.7397	w-b	-1 1 6
	1.7330		1 1 4
1.6304(7)	1.6285	w	0 3 1
1.4439(5)	1.4484	vw-b	-2 0 2
1.4193(5)	1.4200	vw-vb	-1 3 2
	1.4193		1 3 0
	1.4170		1 1 6
1.4040(6)	1.4071	vvw	2 0 0

Table 1.11. X-ray powder diffraction data for $Na_{0.66}MoO_2$

d-spacings (Å)		intensities		h k l
observed[a]	calculated	observed	calculated	
6.1	6.041	vs	100%	2 0 0
4.76	4.752	w	2%	0 0 1
4.35	4.394	w	3%	-2 0 1
3.02	3.020	ms	15%	4 0 0
2.465	2.464	m	5%	-2 0 2
	2.463		13%	0 1 1
2.415	2.409	m	19%	-2 1 1
2.37	2.376	m	9%	0 0 2
2.18	2.197	w	2%	-4 0 2
	2.171		6%	2 1 1
2.075	2.064	ms	24%	-4 1 1
2.012	2.023	m	10%	2 0 2
1.92$\bar{0}$	2.012	w	2%	6 0 0
1.870	1.872	w	2%	-2 1 2
	1.832		2%	0 1 2
	1.812		3%	-6 0 2
1.785	1.784	m	12%	4 1 1
	1.746		2%	-4 1 2
1.696	1.686	w	7%	-6 1 1
1.654	1.652	w	3%	4 0 2
1.510	1.510	m	4%	8 0 0

[a]Powder data taken from reference 9.

Table 1.12. Lattice parameters for layered sodium molybdenum oxides, Na_xMoO_2

compound	a, Å	b, Å	c, Å	β, °
$Na_{0.41}MoO_2$	12.464(3)	2.8867(4)	4.938(2)	104.01(4)[a]
	12.448(7)	2.893(3)	4.934(3)	104.02(6)[b]
$Na_{0.51}MoO_2$	2.892(3)	4.935(1)	12.445(12)	103.77(21)[a]
	2.897(4)	4.931(6)	12.433(15)	103.73(15)[b]
$Na_{0.66}MoO_2$	12.63(2)	2.896(9)	4.94(1)	106.7(1)[c]
	12.608	2.880	4.959	106.59[d]

[a]From powder x-ray diffraction data.

[b]From single crystal x-ray diffraction data.

[c]Indexed based on data obtained from reference 9.

[d]Parameters used in model.

Table 1.13. Positional parameters for $Na_{0.66}MoO_2$[a]

atom	multiplier	x	y	z	B(Å^2)
Mo	1.0	0.253	0.00	0.222	0.6
O1	1.0	0.169	0.50	0.354	0.97
O2	1.0	0.145	0.00	0.851	0.97
Na1	0.165	0.50	0.00	0.00	1.2
Na2	0.165	0.50	0.50	0.50	1.2

[a]Based on the nonstandard space group $P2_1/a$.

Table 1.14. Positional parameters for $Na_{0.66}MoO_2$[a]

atom	multiplier	x	y	z	B(Å^2)
Na1	0.66	0.25	0.50	0.59	1.20
Na2	0.66	0.25	0.00	0.09	1.20
Mo1	1.00	0.003	0.00	0.2145	0.60
Mo2	1.00	0.503	0.00	0.2145	0.60
O1	1.00	0.0827	0.00	0.6385	0.97
O2	1.00	0.1132	0.50	0.1708	0.97
O3	1.00	0.5827	0.00	0.6385	0.97
O4	1.00	0.6132	0.50	0.1708	0.97

[a]Based on the space group, $P2_1/m$.

Table 1.15. Bond distances (Å) in $Na_{0.66}MoO_2$

Mo1 - Mo1	2.552[a]	Mo2 - Mo2	2.552[a]
	2.880[a]		2.880[a]
	3.197[b]		3.197[b]
Mo1 - O1[a]	2.055	Mo2 - O3[a]	2.055
	2.055		2.055
	2.055		2.055
Mo1 - O2[i]	2.055	Mo2 - O4[i]	2.055
	2.055		2.055
	2.056		2.056
Na1 - O1	2.621	Na2 - O1	2.601
	2.621	- O2	2.367
- O2	2.291		2.367
- O3	2.664	- O3	2.591
- O4	2.299		2.591
	2.299	- O4	2.433

[a]Intrachain distance.

[b]Interchain distance.

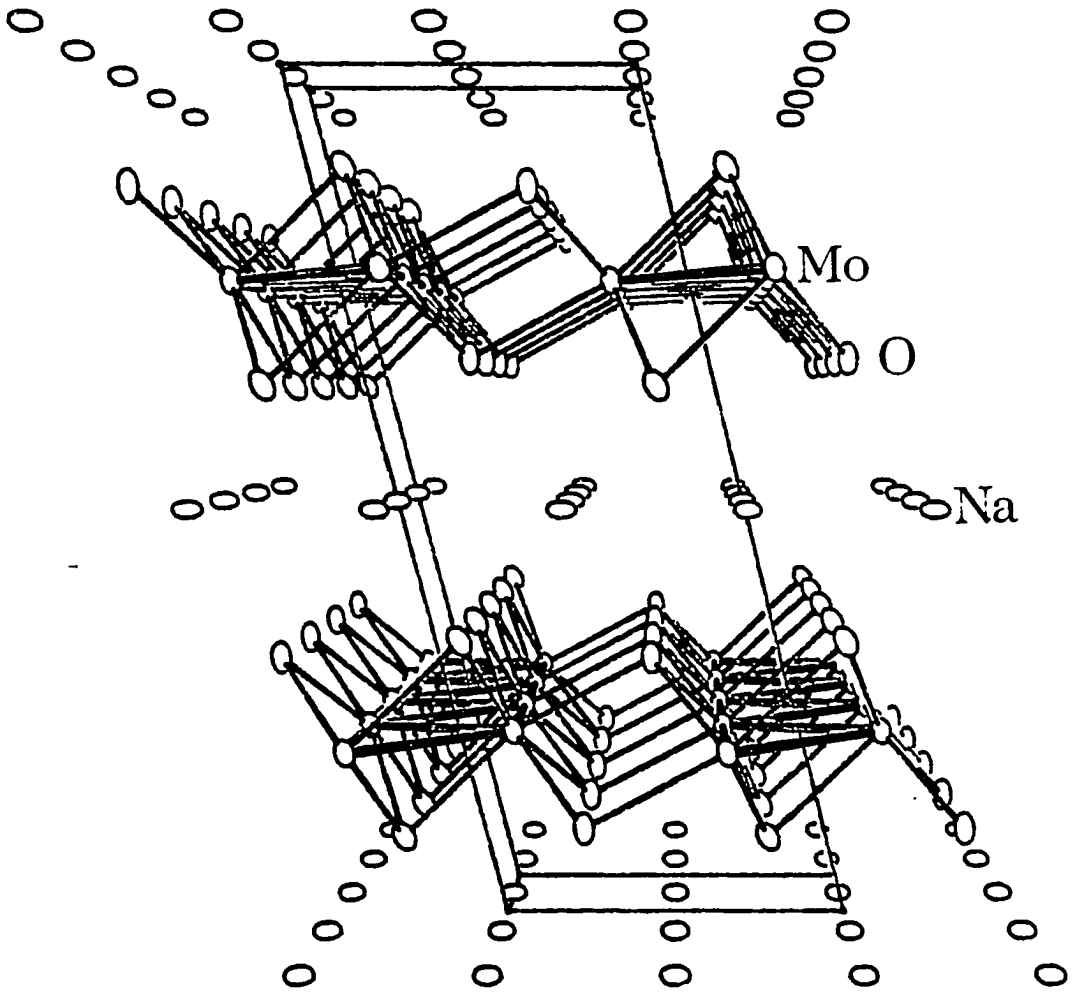

Fig. 1.1. Three dimensional view of the unit cell of the $Na_{0.41}MoO_2$ structure as seen along the b axis. The framework consists of Mo zig-zag ribbons bridged by oxygen atoms [d(Mo-O) = 2.058(5) to 2.108(6)Å] to form O-Mo-O slabs separated by layers of Na ions [d(Na-O)= 2.302(7) to 2.514(6)Å]

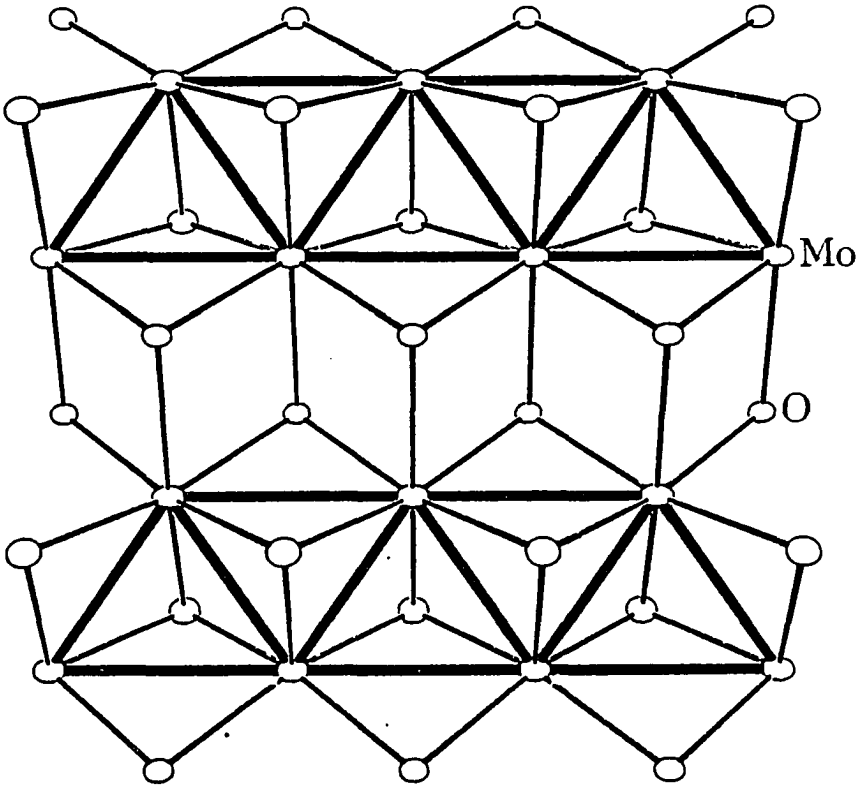

Fig. 1.2. View down the a axis of $Na_{0.41}MoO_2$ showing a O-Mo-O slab. The Mo atoms distort from a hexagonal array to generate metal ribbons with Mo-Mo distances of 2.890(2)Å along the chain, and 2.535(2)Å diagonally forming zig-zag bonds

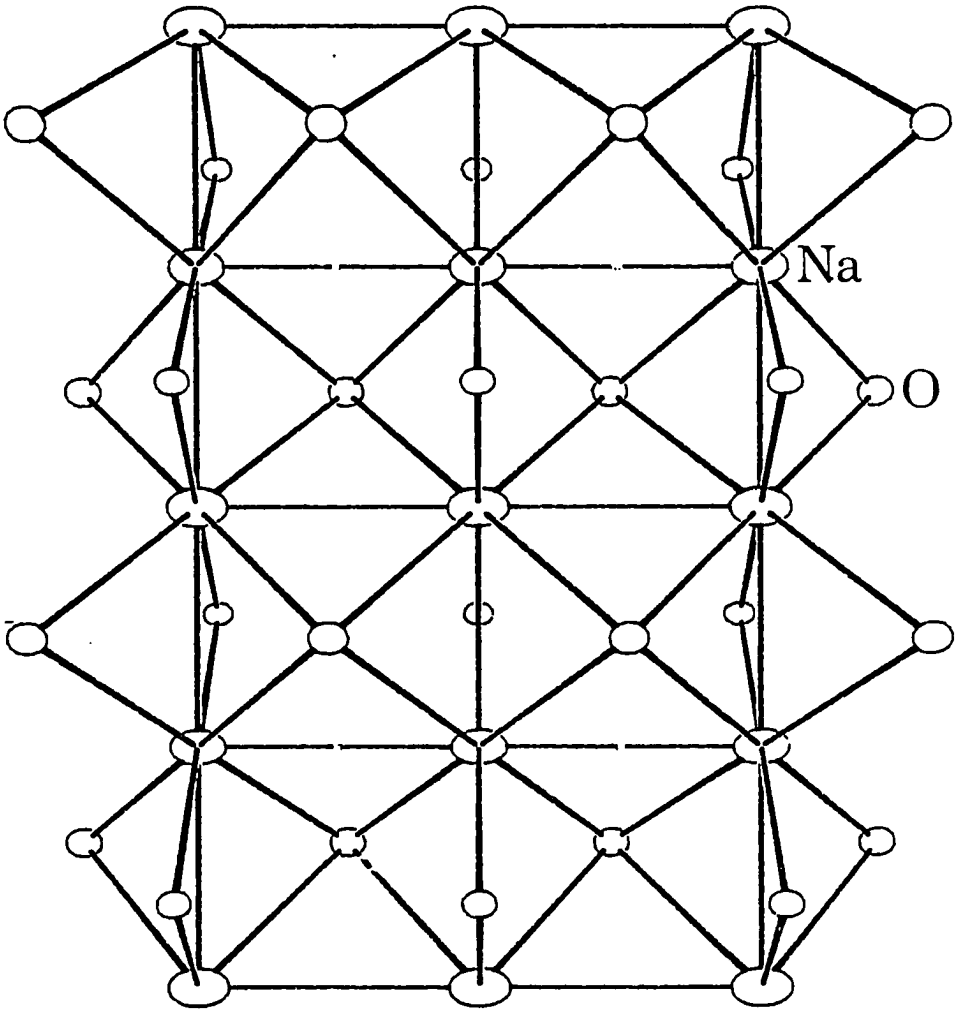

Fig. 1.3. View down the a axis of $Na_{0.41}MoO_2$ showing a O-Na-O slab. Each Na ion is found in a distorted oxygen octahedral site with the ternary cations arranged in a rectangular net. This unusual array yields two nearest Na neighbors at 2.45Å, two next nearest neighbors at 2.89Å and finally four neighbors at 3.8Å

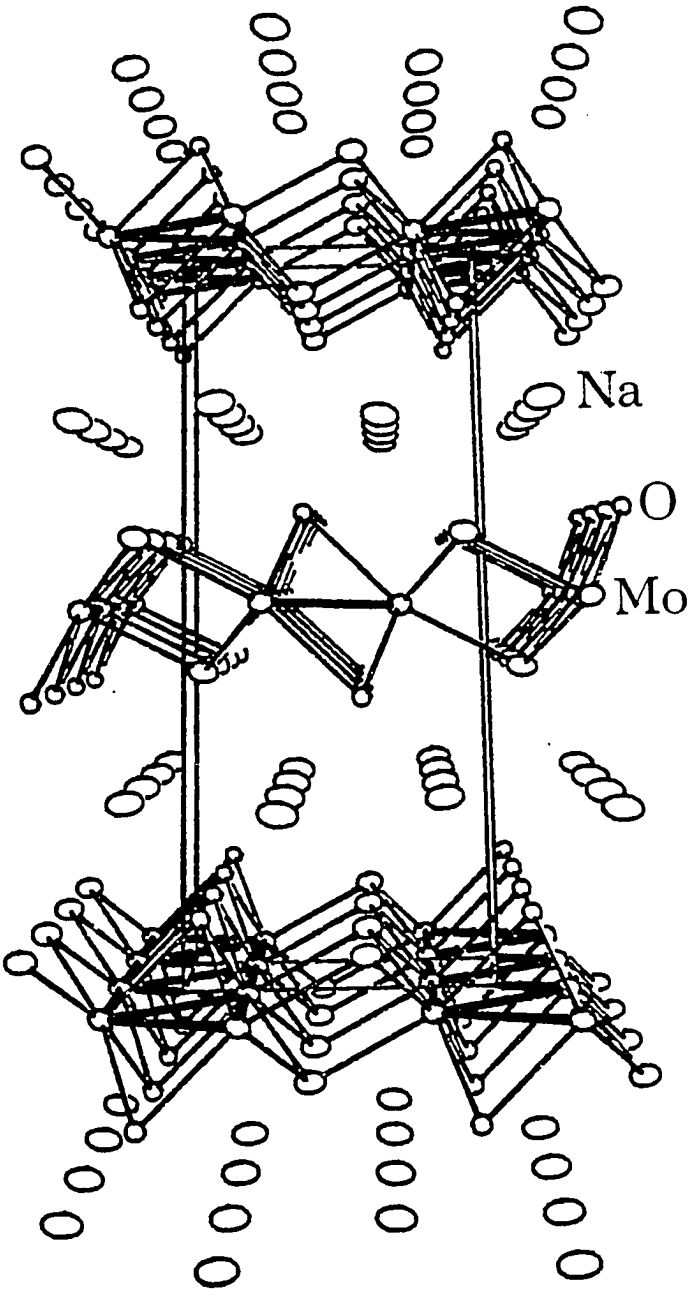

Fig. 1.4. Three dimensional view of the unit cell of the $Na_{0.51}MoO_2$ structure as seen along the a axis

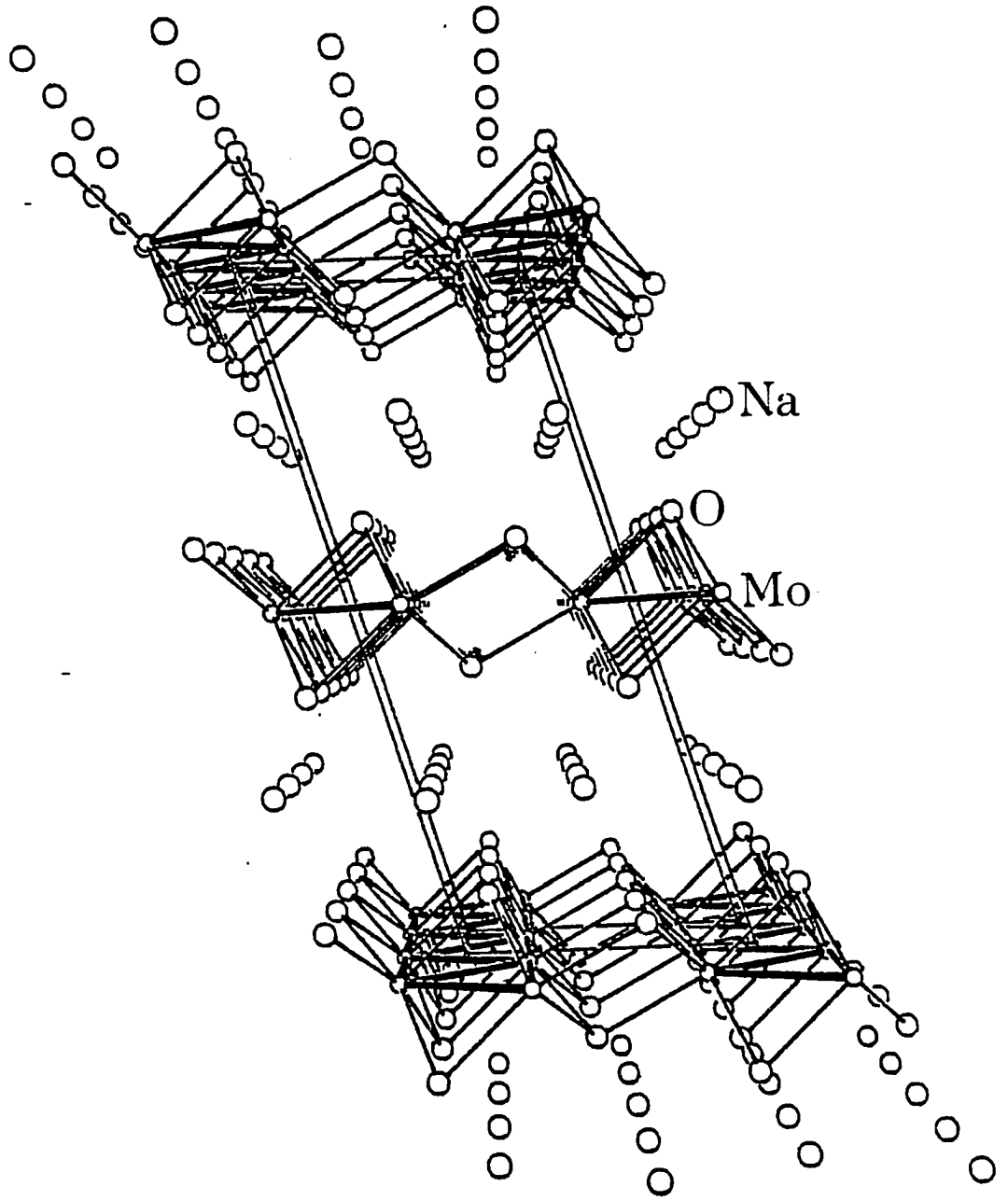

Fig. 1.5. Three dimensional view of the structural model proposed for $Na_{0.66}MoO_2$ looking down the b axis

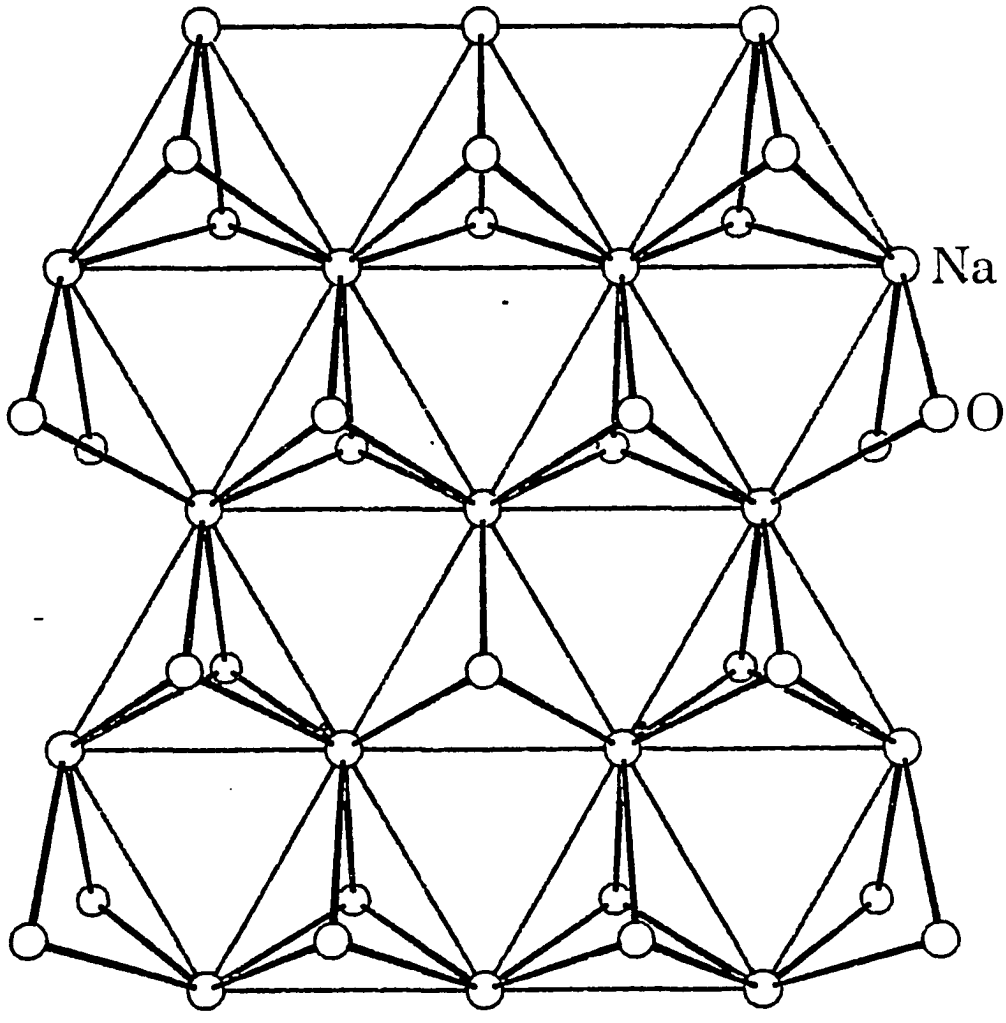

Fig. 1.6. View down the a axis of $Na_{0.66}MoO_2$ model showing a O-Na-O slab. Each Na cation is trigonal prismatically coordinated by oxygen atoms revealing a hexagonal Na substructure with Na-Na nearest neighbor distances of ~2.89Å

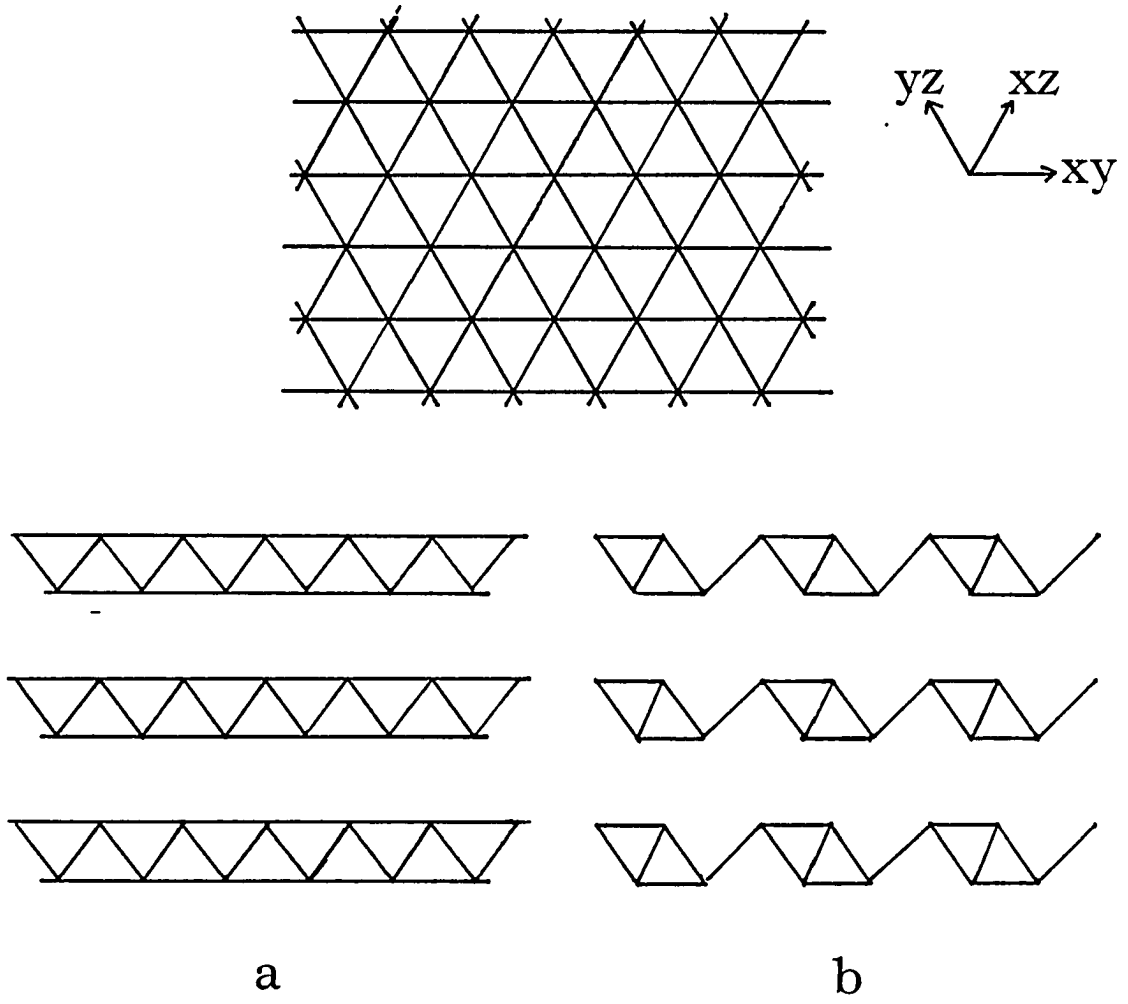

Fig. 1.7. Schematic representation of the metal-metal bonding within a hexagonal layer upon pairing distortions of the t_{2g} orbitals: a) An extended chain of fused rhomboidal units is generated by the pairing of the d_{xz} and d_{yz} subsystems. b) A linked chain of rhomboidal clusters is formed by the pairing of all three subsystems, d_{xy}, d_{xz}, and d_{yz}

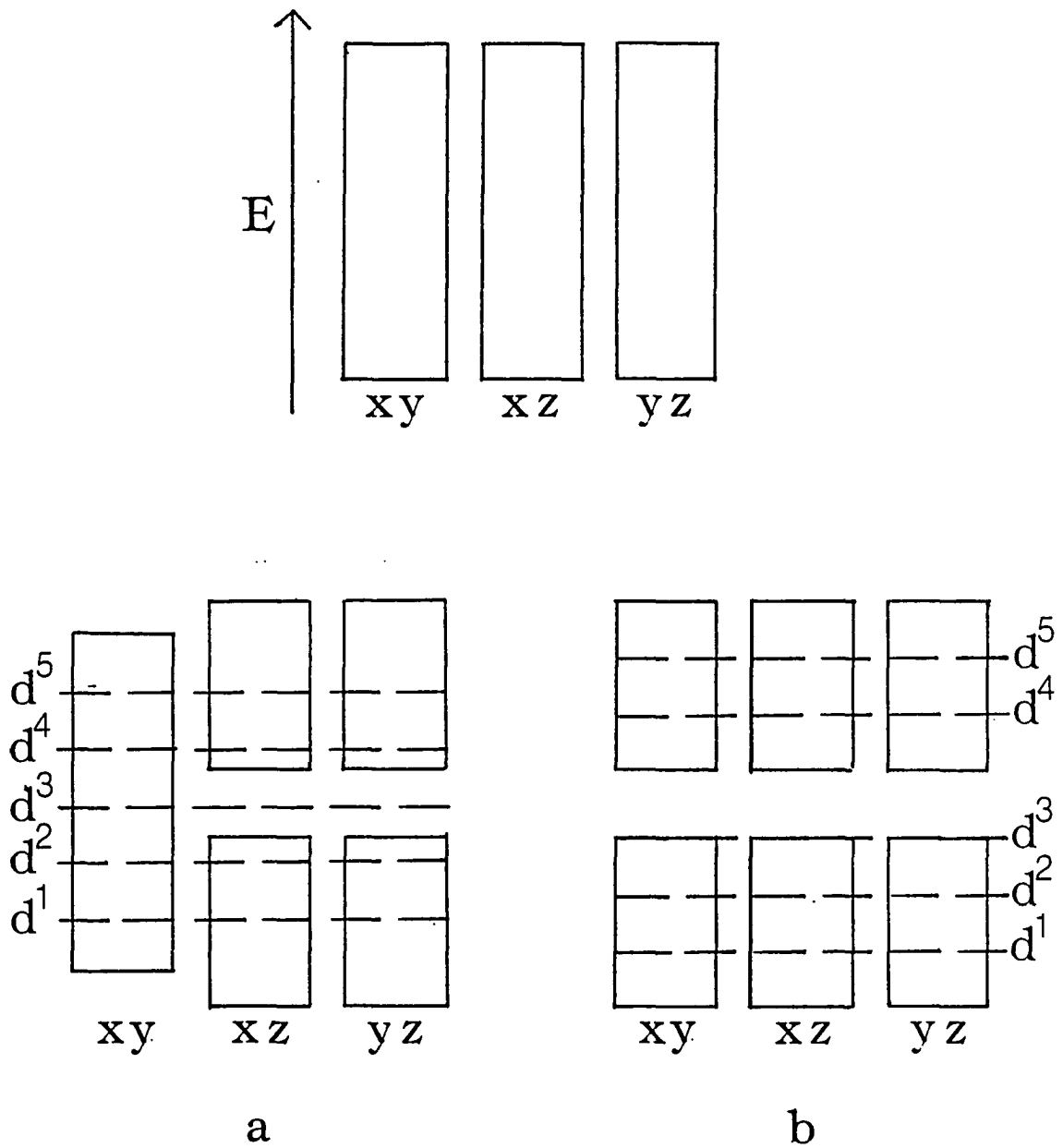

Fig. 1.8. Schematic representation of the expected band structures resulting from the Pierels distortions within a hexagonal metal layer: a) Upon the pairing of the d_{xz} and d_{yz} subsystems, the corresponding bands split and a $d^{2.5}$ system is expected. b) The pairing of all three subsystems, leads to the splitting of all the t_{2g} bands indicating a d^3 system

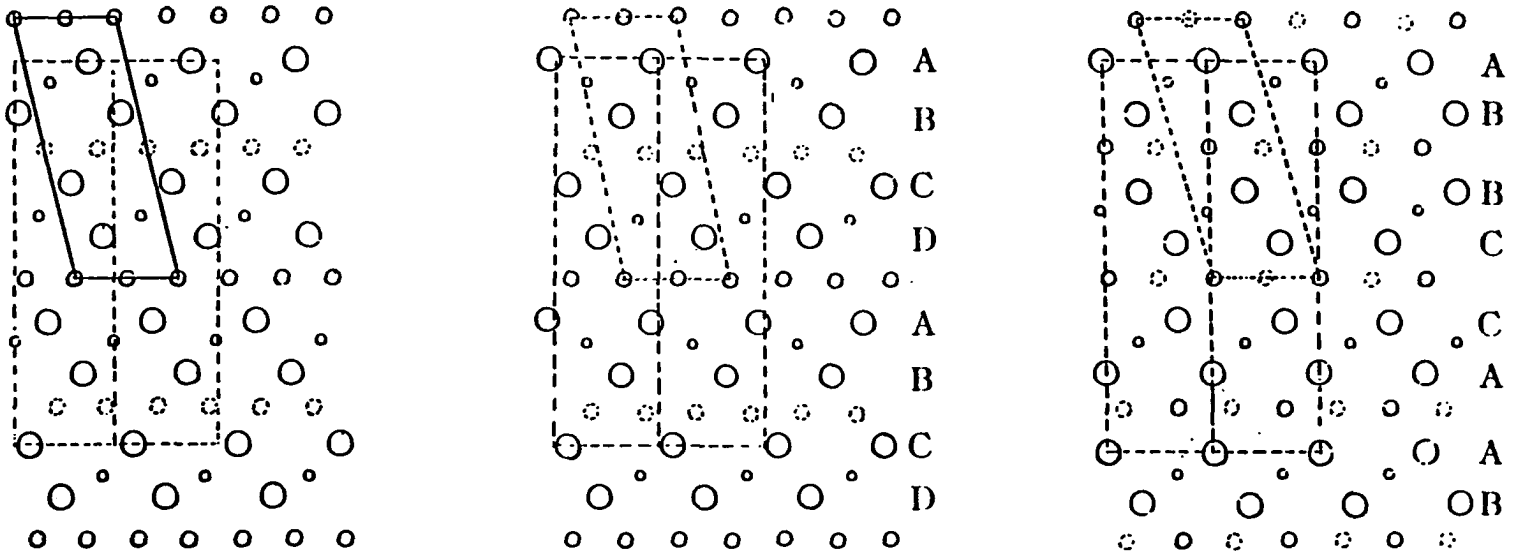

$Na_{0.41}MoO_2$ $Na_{0.51}MoO_2$ $Na_{0.66}MoO_2$

a	12.448(7)Å	12.675(15)Å	12.608(4)Å
b	2.892(3)Å	2.897(4)Å	2.880(5)Å
c	4.934(3)Å	4.931(6)Å	4.959(6)Å
β	104.02(6)°	101.21(15)°	106.59(11)°

Fig. 1.9. Projections of the Na_xMoO_2 phases illustrating the oxygen packing. The large circles represent O atoms, the medium size, Na ions, and the small circles, Mo atoms. The solid atoms are at y=0 and the dashed Na atoms are at y=1/2. The a-c plane of monoclinic cell in relation to the hexagonal setting is outline

SECTION 2. HEXAGONAL $LiMoO_2$ - A CLOSE-PACKED LAYERED STRUCTURE WITH INFINITE Mo-Mo BONDED SHEETS

ABSTRACT

A new compound, $LiMoO_2$, with hexagonal layered structure has been prepared by reaction of Li_2MoO_4 with Mo metal at 900°C for 21 days. Neutron powder diffraction Rietveld analysis shows that $LiMoO_2$ is isomorphous with α-$NaFeO_2$, space group $R\bar{3}m$, $a = 2.8663(1)$, $c = 15.4743(5)$Å, $Z = 3$. The structure consists of cubic close-packed oxide layers with Mo and Li atoms occupying octahedral sites between alternate layers. Each Mo atom is thus bonded to six other Mo atoms in a hexagonal sheet with d(Mo-Mo) = 2.8663(1)Å. The Mo-O and Li-O distances are 2.0520(9) and 2.146(1)Å, respectively. DOS and COOP curves from extended Hückel band calculations indicate that all Mo-Mo bonding states are filled within the O-Mo-O slabs.

INTRODUCTION

Among the various classes of host structures suitable for use as cathodes in batteries, layered dichalcogenides have been the most investigated. Layered oxide systems also may be potential hosts. In this laboratory, a series of layered Na-Mo-oxides has been prepared and characterized, viz. $Na_{0.45}MoO_2$, $Na_{0.51}MoO_2$, and $Na_{0.66}MoO_2$[1-5]. The structures of these compounds feature the presence of extended chains consisting of fused molybdenum rhomboidal clusters. The chains are sandwiched between close-packed layers of oxygen atoms to form three-layer O-Mo-O slabs. These O-Mo-O sheets are then separated by layers of sodium ions. Lithium ions, due to their smaller size and potentially greater mobility may be more promising with respect to application of such compounds as battery cathodes. Thus, the high temperature syntheses of Li-Mo-oxides were explored, yielding the analogous compound, $Li_{0.74}MoO_2$[2,3]. Tarascon and Hull[6], and Tarascon[7] have studied the electrochemical intercalation of both the sodium and lithium M_xMoO_2 systems and the work reveals that the Li_xMoO_2 system is indeed a promising cathode material for secondary lithium cells.

An important structural feature of the Na-Mo-oxides and $Li_{0.74}MoO_2$ is the extensive molybdenum bonding in the form of chains of condensed rhomboidal clusters. This mode of Mo-Mo bonding may be compared to the discrete Mo rhombuses observed in the less electron rich systems of $Ba_{1.14}Mo_8O_{16}$[8] and $K_2Mo_8O_{16}$[9]. Interestingly, studies of more electron rich systems with related layer structures, such as $CoMo_2S_4$[10] and $ReSe_2$[11], reveal the occurrence of chains consisting of distorted rhomboidal units interlinked in one dimension. Thus, beginning with a

layer of close-packed metal atoms, a range of clustering is possible from discrete units, to chains of linked units, to condensed ribbons, to a hexagonal sheet. In this paper, we report the synthesis and structural characterization of the end member of this series, $LiMoO_2$, revealing for Mo-Mo bonded compounds the unprecedented arrangement of an infinite hexagonal sheet.

EXPERIMENTAL AND RESULTS

Materials

Lithium molybdate (Alfa Products, purity 98.5%) was recrystallized from water, dried at 150°C under vacuum for 12h, and stored in a dry box. In synthetic efforts, handling of the hygroscopic lithium molybdate was confined solely to the inert atmosphere of N_2 of the dry box. Molybdenum tubing was obtained from Thermo-Electron Corporation (purity 99.97%), molybdenum powder from Aldrich (99.99%), and copper tubing from laboratory stock.

Synthesis

The title compound was first observed in the multiphase product obtained in the exploratory reaction between Li_2MoO_4 and Mo (1:1 molar ratio). The reaction mixture was ground in a mortar and sealed by electron beam welding into an evacuated Mo reaction vessel, which was then loaded into a high vacuum furnace and fired at 1500°C for two days. The product revealed unreacted lithium molybdate, black polycrystalline powder and a few chunky hexagonal prisms. The lithium molybdate was removed by washing with water. After drying, a Guinier powder pattern was taken of the product. The pattern indicated the presence of a new lithium molybdenum oxide which could be indexed based on the pattern observed for α-$NaFeO_2$[12]. This X-ray powder pattern also showed the lines of unreacted Mo metal.

Subsequent work showed that x-ray pure hexagonal layered material

could be prepared by oxidizing Mo metal in the presence of an excess of lithium molybdate. The reactants were thoroughly ground in a mortar, sealed in an evacuated copper vessel, and held at 900°C for 21 days. The polycrystalline product was powdered in a mortar and washed several times with deionized water to remove unreacted Li_2MoO_4; the solid was then dried under vacuum at 120°C.

X-ray Powder Diffraction Data

The Enraf Nonius Delft triple focusing Guinier camera was used with Cu $K\alpha_1$ radiation (λ = 1.54056Å) to obtain the powder diffraction and unit cell data. The diffraction lines of $LiMoO_2$ (Table 1.1) were indexed based on the reported pattern of α-$NaFeO_2$ yielding the hexagonal cell ($R\bar{3}m$ #166): a=b=2.8666(8), c=15.469(8)Å, and V=110.09(9)Å^3. Utilizing these cell constants and the atomic positions (Li on the 3b site; Mo on the 3a site; O on the 6c site with z=0.257) a calculated powder pattern of $LiMoO_2$ was generated. There was a good correlation between the observed and calculated intensites indicating that the model was correct. Subsequently, the structure was refined using neutron powder data as detailed below.

Neutron Powder Diffraction Data

Neutron powder diffraction data were collected on the General Purpose Powder Diffractometer (GPPD) at the Intense Pulsed Neutron Source (IPNS) at Argonne National Laboratory. IPNS uses a proton accelerator and synchrotron to produce high-energy neutrons by

bombardment of a spallation target (uranium). These neutrons are then moderated to lower energies before they are used for diffraction. The GPPD is equipped with time-of-flight detectors, of which there are two sets each at 30°, 45°, 60°, 75°, 90°, and 150°. Time-of-flight data were collected on a five gram sample loaded in a vanadium cell at 300K with an exposure time of 12 hours. The high resolution data obtained from the 150° detector bank were used in the Rietveld refinement. The diffractometer and the Rietveld refinement software are discussed in references 13-18.

The structure of $LiMoO_2$ was refined using the atomic positions determined in the model discussed above. The refinement involved 4013 data points, 95 reflections in the d space region of 0.657 to 2.579Å, and 22 parameters. The refined parameters included five background parameters, a scale factor, extinction, absorption, anisotropic peak broadening, lattice constants, positional and anisotropic thermal parameters on each atom, and the occupancy of lithium. Table 2.2 lists the final cell parameters (which correspond well with those calculated from the X-ray powder pattern) along with the residual factors, while Tables 2.3 and 2.4 give the positional and thermal parameters for each atom.

The spectrum showed broadening of certain peaks, [00ℓ] type, with respect to the others which could be caused by stacking defects along the c axis. This effect was taken into account by including anisotropic peak broadening along the c (stacking) axis[15b].

Figures 2.1 and 2.2 illustrate the low d space region of the Rietveld refinement. A close examination of the difference between the calculated and experimental profiles revealed extra reflections such as

those found between 1.10 and 1.15Å. These lines and other extra peaks correspond to the diffraction pattern of lithium molybdate. Due to the low concentration and the complex diffraction pattern of lithium molybdate, the structure could not be satisfactorily refined via multiphase refinements. Since this second compound was not taken into account, the background fitting led to a slight oscillatory function in the single phase refinement's difference plot which was not observed in the multiphase experiments. To achieve the best fit of the data, and to subsequently refine the Li occupancy, the oscillatory function based on all scattering data was fitted and removed from the background[16]. The Li occupancy converged to a value of 1.02(5) per MoO_2 unit.

Quantitative Analysis

A precipitation method was employed for the determination of percent molybdenum. Samples were decomposed in a basic solution and neutralized to methyl red using an acetic acid/sodium acetate buffer. Quantitative precipitation of $MoO_2(ONC_9H_6)_2$ was effected by addition of a solution of 8-hydroxyquinoline. The precipitate was filtered into previously tared fritted crucibles and dried at 140°C overnight. The oxidation state of the molybdenum was determined via a cerium titration. Samples were oxidized by a known excess of standardized Ce(IV) and the solution was back-titrated to a Fe(1,10 phenanthroline)$_3^{2}$ endpoint with a freshly standardized Fe(II) solution. From these data, the electron to Mo ratio was calculated. The percent lithium was determined by atomic absorption techniques. **Anal.** Found: Li, 5.66%; Mo, 64.96%; e^-/Mo, 2.48.

Since the samples were contaminated with lithium molybdate, the

following relationship was used to determine the Li content of the layered material and the amount of lithium molybdate in the mixture:

$$(1-x)Li_2MoO_4 + xLi_yMoO_2 = 1$$

where x equals the mol fraction of Li_yMoO_2 and (1-x) equals the mol fraction of Li_2MoO_4. This relationship yields the equations:

$$Li/Mo = 1.205 = 2(1-x) + xy;$$

$$e^-/Mo = 2.48 = (1-x)0 + x(2+y)$$

which can be solved to give:

$$x = 0.82$$

$$y = 1.03.$$

Thus the sample consists of

$$0.18Li_2MoO_4 + 0.82Li_{1.03}MoO_2$$

and the formula for the hexagonal compound may be taken as $LiMoO_2$.

DISCUSSION

The layered structure of $LiMoO_2$ can be viewed in Figure 2.3. As discussed above, the material is isostructural with α-$NaFeO_2$ with an oxygen packing sequence of ABCABC with Mo and Li occupying octahedral coordination sites between alternate layers. During the structural determination, the Li multiplier was refined to a value of 1.02(5) per MoO_2 unit indicating that every octahedral site between the O-Mo-O slabs is occupied by a lithium cation.

The change in layering from the monoclinic compound, $Li_{0.74}MoO_2$ [C2/m a=10.647(6), b=2.881(1), c=4.953(2)Å, β=99.64(5)°], to that observed in $LiMoO_2$ is the result of the slippage of the MoO_2 slabs via a small decrease in the monoclinic β angle. The corresponding cell dimensions for $LiMoO_2$ in the monoclinic setting are a=10.448, b=2.8663, c=4.9645Å, β=99.10°.

Structurally, the most important feature of the title compound is the mode of Mo-Mo bonding. As shown in Figure 2.4a, the Mo atoms are found in a hexagonal close-packed layer with Mo-Mo bond distances of 2.8663(1)Å. In contrast, as shown in Figure 2.4b, the metal atoms in $Li_{0.74}MoO_2$ are distorted from an ideal hexagonal array toward neighboring Mo atoms to form infinite chains having two parallel rows of Mo atoms with bond distances of 2.881(1)Å between adjacent Mo atoms of the same row, and 2.549(2)Å between Mo atoms of adjoining rows, generating the zig-zag bonds within the chains.

Extended Hückel calculations performed in this laboratory and those reported by Burdett and Hughbanks[19] indicate that the distorted monoclinic form is energetically slightly more stable than the ideal

hexagonal arrangement. Computations were done on a O-Mo-O slab utilizing the observed atomic positions from the Rietveld refinement for the hexagonal structure, and the single crystal refinement of $Li_{0.74}MoO_2$ for the chain structure, with the Mo and O functions taken from reference 20. The energy difference between the monoclinic and hexagonal frameworks, each with d^3 electron population on Mo, is only 0.08eV. Because the extended Hückel calculations are not adequate to account for all important interactions, this small energy difference in favor of the monoclinic structure, with infinite chain formation, could be incorrect. The long reaction time, 21 days, at 900°C for preparation of the hexagonal structure, indeed indicates that the latter structure is the more stable for $LiMoO_2$ with the d^3 electron population. No evidence such as supercell reflections was found in neutron diffraction data which would signal long range clustering of Mo atoms in $LiMoO_2$. However, the oscillatory function noted in the background of the single phase refinement may be indicative of diffuse scattering resulting from short-range ordering of molybdenum atoms.

The density of states (DOS) curve (Figure 2.5a) obtained via extended Hückel calculations clearly shows a high density of states at the Fermi level suggesting that $LiMoO_2$ should be a metallic conductor. The resistivity of this material has not yet been measured due to the lack of success in obtaining single crystals.

In reviewing the comparative orbital overlap population (COOP) curves (Figure 2.6), it can be noted that for a d^3 system, Mo-Mo antibonding states are occupied in the distorted monoclinic structure whereas in the hexagonal structure the metal bonding states are totally full and the antibonding levels empty. This contrast in the occupancy

of the metal antibonding states may be the reason why the hexagonal structure is observed. The COOP curve raises the question of what would happen to the metal-metal bonding as the lithium content is lowered? It is expected that as the bonding levels are emptied, the Mo sheet would rearrange to form Mo ribbons or some other type of clustering favored by the lower electron to Mo ratio. Presently, more detailed work is being carried out with respect to the structural changes of the hexagonal phase upon delithiation and ion exchange. The results of this investigation will be forthcoming.

Acknowledgement

We thank J. Faber Jr., J. Richardson Jr., and R. Hitterman of Argonne National Laboratory for providing valuable assistance and advice during the collection and Rietveld refinement of the neutron data.

REFERENCES

1. McCarley, R. E.; Lii, K. -H.; Edwards, P. A.; Brough, L. F. J. Solid State Chem. 1985, 57, 17.

2. Aleandri, L. E.; Edwards, P. A.; McCarley, R. E., American Chemical Society Meeting, Chicago, Sept. 8-13 (1985).

3. Aleandri, L. E.; McCarley, R. E., American Chemical Society Meeting, New York, April 13-18 (1986).

4. $Na_{0.66}MoO_2$ was initially reported as $Na_2Mo_3O_6$ in: (a) Hubert, P. H. C. R. Acad. Sc. Paris 1966, 262, 1189. and (b) Reau, J. M.; Fouassier, C.; Hagenmuller, P. Bull. Soc. Chim. 1970, 11, 3827. The structure based on X-ray powder diffraction data is given in reference 5.

5. Aleandri, L. E., Ph.D. Dissertation, Iowa State University, Ames, Iowa, 1987, Section 1.

6. Tarascon, J. M.; Hull, G. W. Solid State Ionics 1986, 22, 85.

7. Tarascon, J. M., submitted for publication in Solid State Ionics.

8. Torardi, C. C.; McCarley, R. E. J. Solid State Chem. 1981, 37, 393.

9. Torardi, C. C.; Calabrese, J. C. Inorg. Chem. 1984, 23, 3281.

10. Guillevic, J.; Le Marouille, J. -Y.; Grandjean, D. Acta Cryst. 1974, B30, 111.

11. Alcock, N. W.; Kjekshus, A. Acta Chemica Scand. 1965, 19, 79.

12. Goldsztaub, S. Compt. Rend. 1933, 196, 280.

13. IPNS Progress Report; Argonne National Laboratory: Argonne, IL, 1981-1983, pp. 2-40.

14. Rietveld, H. M. J. Appl. Crystallogr. 1969, 2, 65.

15. a. Rotella, F. J. Users Manual for Rietveld Analysis of Time-of-Flight Neutron Diffraction Data at IPNS; Argonne National Laboratory: Argonne, IL, 1983. b. Rotella, F. J. Notes on the Rietveld Analysis of Time-of-Flight Neutron Diffraction Powder Data from Multiple Phase Samples using TPRMPH2 and TLSMPH2; Argonne National Laboratory: Argonne, IL, 1985.

16. Richardson Jr., J. W.; Faber Jr., J. In "Advances in X-Ray Analysis", Vol. 29; Plenum Press: New York, 1985; pp. 143-152.

17. Jorgensen, J. D.; Rotella, F. J. J. Appl. Crystallogr. 1982, 15, 27.

18. Von Dreele, R. B.; Jorgensen, J. D.; Windsor, C. G. J. Appl. Crystallogr. 1982, 15, 581.

19. Burdett, J. K.; Hughbanks, T. Inorg. Chem. 1985, 24, 1741.

20. Hughbanks, T.; Hoffmann, R. J. Am. Chem. Soc. 1983, 195, 3537.

Table 2.1. The observed and calculated X-ray powder diffraction data for $LiMoO_2$

d-spacing (Å)[a]	intensity[b]	h k l	d-spacing (Å)[c]	intensity[c]
5.168(6)	s	0 0 3	5.156	100.0
2.579(1)	w	0 0 6	2.578	7.1
2.450(1)	ms	1 0 1	2.451	36.9
3.363(1)	m	0 1 2	2.363	16.5
2.0893(9)	ms	1 0 4	2.0891	42.5
1.9371(7)	w	0 1 5	1.9362	17.0
		0 0 9	1.7187	3.7
1.6509(5)	wm	1 0 7	1.6506	14.2
1.5265(4)	wm	0 1 8	1.5254	16.6
1.4343(4)	wm	1 1 0	1.4333	14.1
1.3826(3)	wm	1 1 3	1.3809	16.7
		1 0 10	1.3128	5.3
		0 0 12	1.2890	3.6
1.2525(2)	vw	1 1 6	1.2527	9.1
1.2359(2)	w	0 2 1	1.2373	6.3
1.2231(2)	w	0 1 11	1.2236	7.5

[a] Values observed from Guinier X-ray powder pattern indexed to give hexagonal cell: $R\bar{3}m$, a=b=2.8666(8), c=15.469(8)Å.

[b] Relative intensities indicated by s, strong; m, medium; w, weak; vw, very weak.

[c] Values based on calculated powder pattern with hexagonal cell: $R\bar{3}m$, a=b=2.8666, c=15.469Å, Li @ 0 0 1/2, Mo @ 0 0 0, and O @ 0 0 0.257.

Table 2.2. The crystallographic data for $LiMoO_2$[a]

---

crystal system: trigonal

space group: $R\bar{3}m$

a = 2.8663(1)Å

c = 15.4743(5)Å

V = 110.097(3)Å^3

Z = 3

d(calc.) = 6.10g/cm^3

diffractometer: GPPD

no. of data points: 4013

no. of reflections: 95

d space region: 0.657Å < d < 2.57Å

no. of parameters refined: 22

expected R^b = 3.64%

profile R^c = 3.45%

weighted R^d = 3.10%

intensity R^e = 8.76%

---

[a]For details on Rietveld refinement of the neutron diffraction data see the text.

[b]$R_e = \sqrt{(N(\text{degrees of freedom}))/\Sigma w Y_o^2}$; $w = 1/\sigma^2(Y_o)$.

[c]$R = \Sigma|Y_o - (Y_c*\text{scale})|/\Sigma|Y_o|$.

[d]$R_w = \sqrt{\{\Sigma[w(Y_o - (Y_c*\text{scale}))^2]/\Sigma w(Y_o)^2\}}$.

[e]$R_i = \Sigma|I_o - (I_c*\text{scale})|/\Sigma|I_o|$.

Table 2.3. Positional parameters for $LiMoO_2$

atom	sym. position	x	y	z	B($Å^2$)[a]
Li	3b ($\bar{3}$m)	0	0	1/2	3.22(3)
Mo	3a ($\bar{3}$m)	0	0	0	1.916(4)
O	6c (3m)	0	0	0.25481(9)	1.013(3)

[a]The isotropic equivalent thermal parameter is defined as $B = 4/3\ [2a^2\beta_{11} + c^2\beta_{33} + 2a^2(\cos 120^o)\beta_{12}]$.

Table 2.4. Anisotropic thermal parameters[a] for $LiMoO_2$

atom	B_{11}	$B_{22}=B_{11}$	B_{33}	$B_{12}=B_{11}/2$	B_{13}	B_{23}
Li1	2.0(2)	2.0(2)	5.6(6)	1.0(1)	0	0
Mo1	2.24(5)	2.24(5)	1.25(8)	1.12(2)	0	0
O1	0.40(4)	0.40(4)	2.22(8)	0.2(2)	0	0

[a]The general thermal parameter expression used is $\exp[-1/4\ (B_{11}h^2a^{*2} + B_{22}k^2b^{*2} + \ldots + 2B_{23}klb^*c^*)]$.

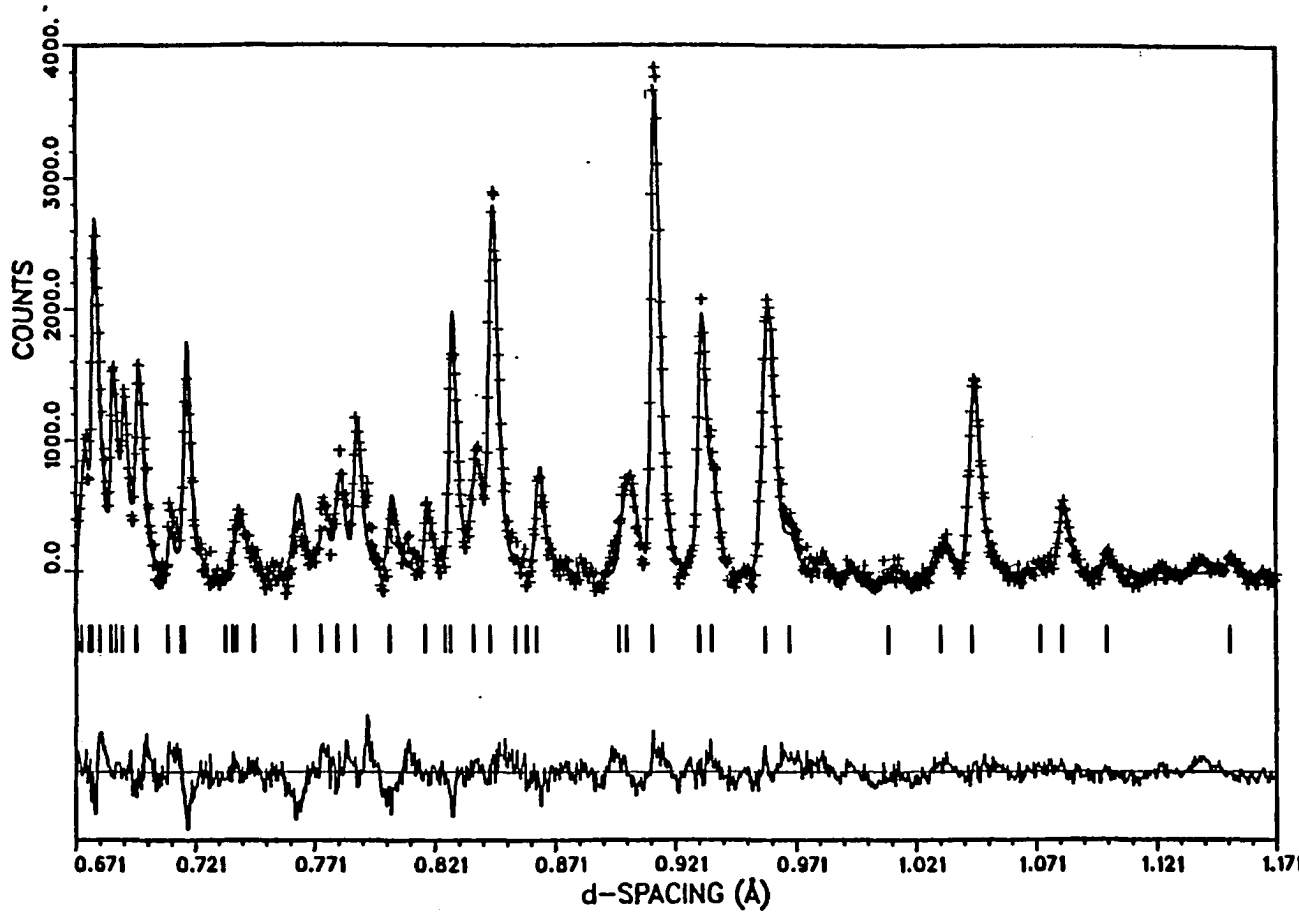

Fig. 2.1. Profile refinement of the low d space portion of the 150° bank neutron diffraction data ranging from 0.671 to 1.171Å. The observed data are indicated by crosses and the calculated data by a solid line. Marks directly beneath the pattern indicate positions of reflections. A difference curve appears at the bottom

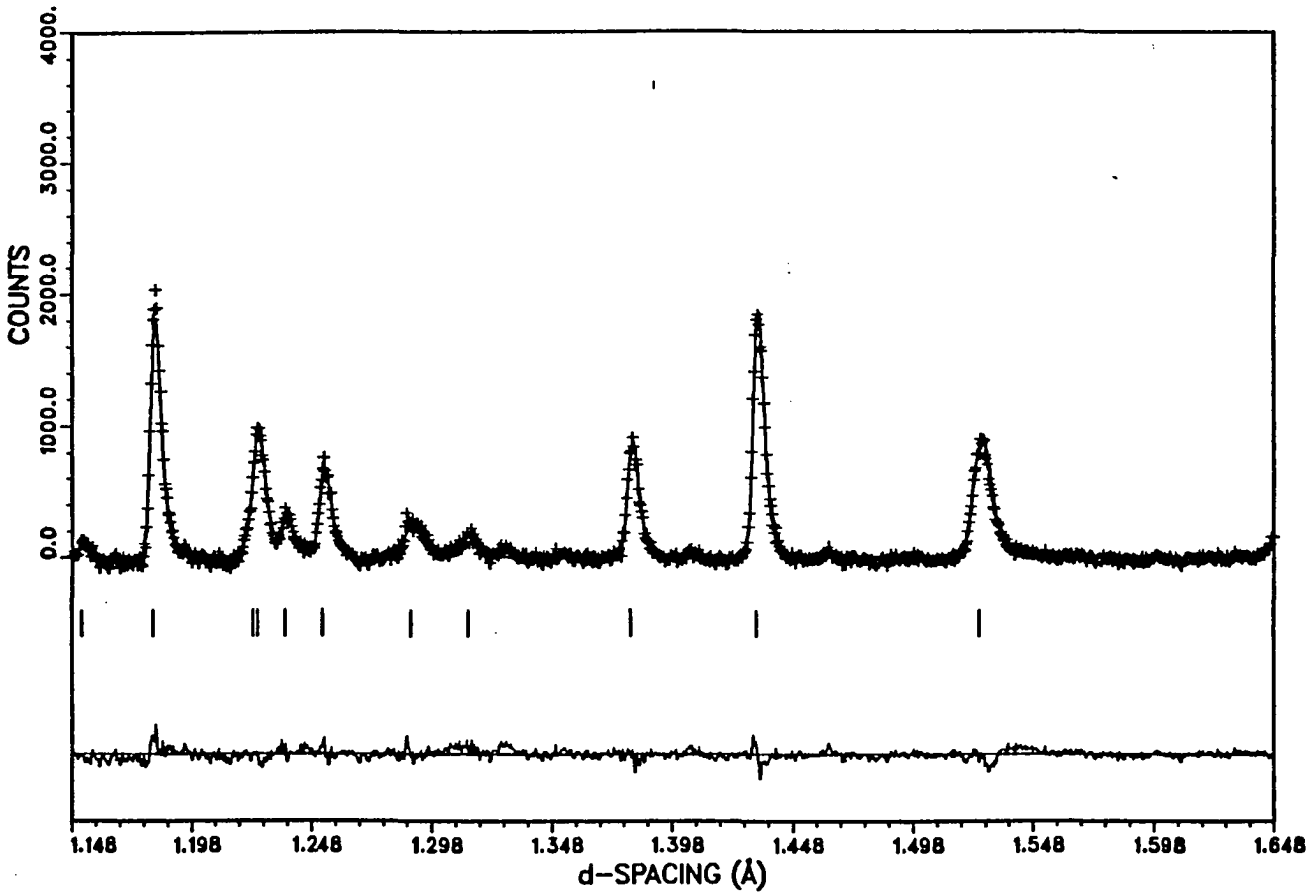

Fig 2.2. Profile refinement of the d space portion of the 150°C bank neutron diffraction data ranging from 1.148 to 1.648Å

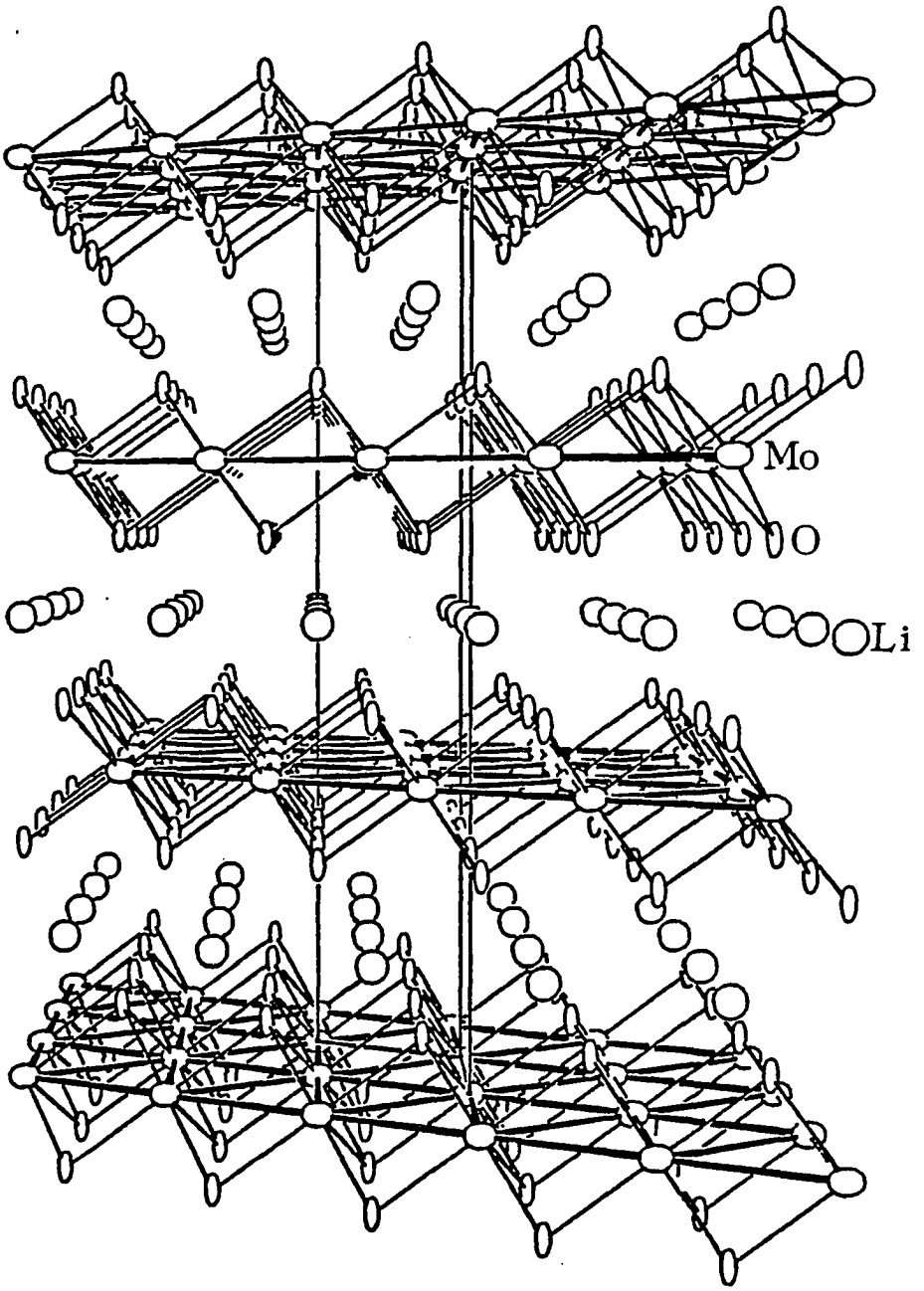

Fig. 2.3. Three dimensional view of the unit cell of the $LiMoO_2$ structure as seen along the a axis. The framework consists of Mo sheets [d(Mo-Mo) = 2.8663(1)Å] bridged by oxygen atoms [d(Mo-O) = 2.0520(9)Å] to form O-Mo-O slabs separated by layers of Li ions [d(Li-O) = 2.146(1)Å]

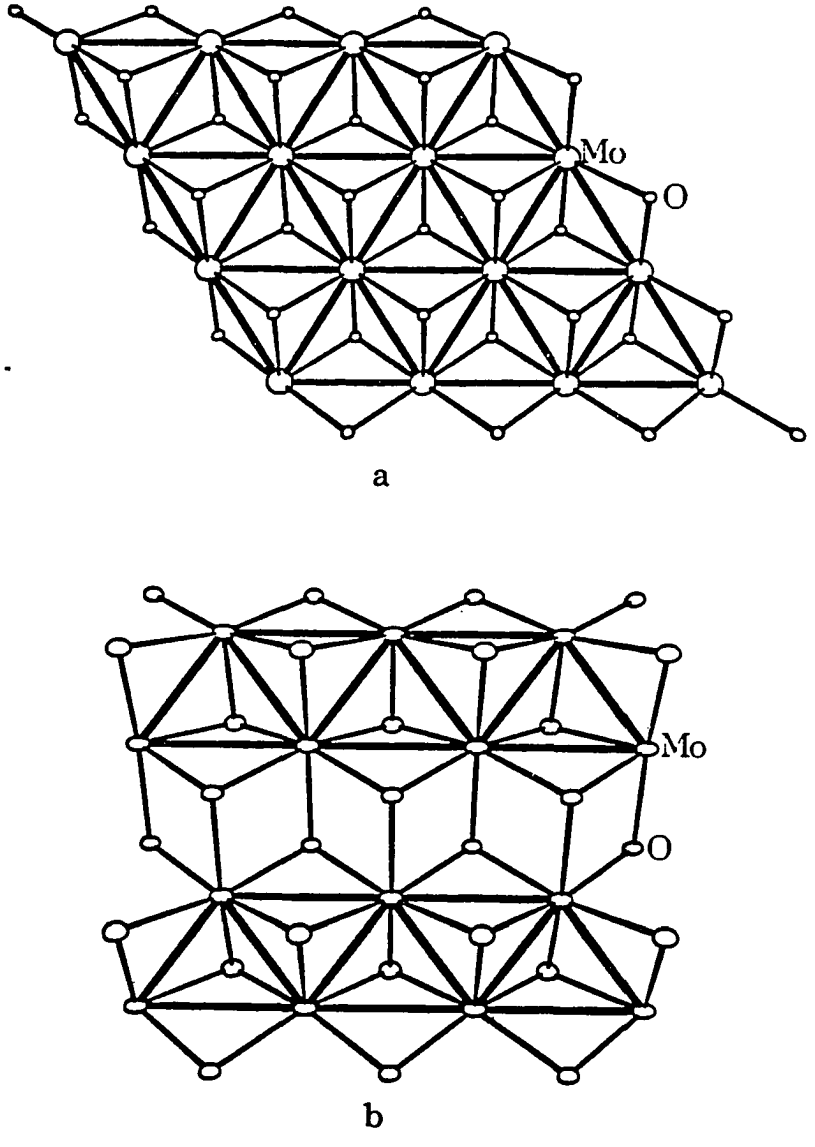

Fig. 2.4. A single O-Mo-O slab in $LiMoO_2$ and $Li_{0.74}MoO_2$ detailing the Mo bonding with heavy lines and the Mo-O interactions with lighter lines: (a) In $LiMoO_2$, the Mo atoms form an infinite hexagonal sheet with bonding distances of 2.8663(1)Å. (b) In $Li_{0.74}MoO_2$, the Mo atoms distort from a hexagonal array to generate metal ribbons with Mo-Mo distances of 2.881(1)Å along the chain, and 2.549(2)Å diagonally forming zig-zag bonds

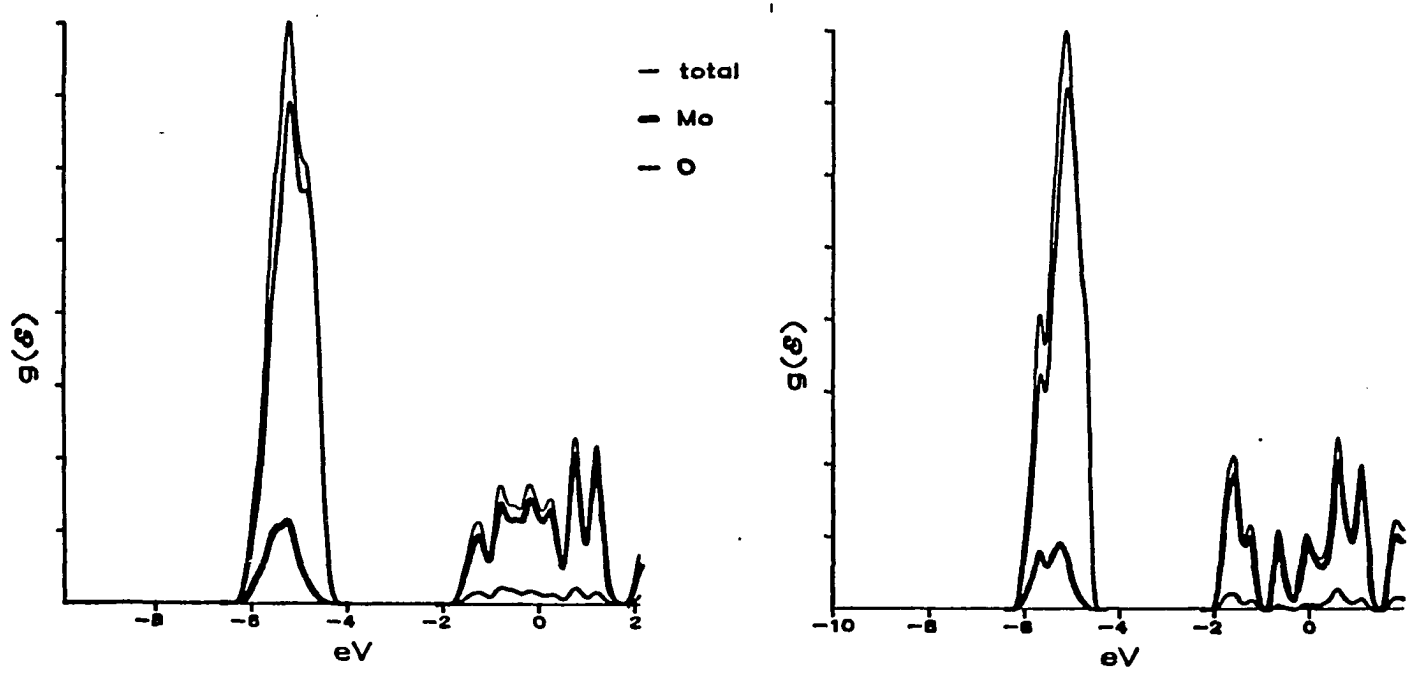

Fig. 2.5. The density of states (DOS) curve for the structural modifications of $LiMoO_2$ (d^3 systems): (a) the hexagonal structure with a Mo bonded sheet; (b) the monoclinic framework with chains comprised of condensed rhomboidal units. The heavy curve indicates Mo states and the lighter curve indicates the O contribution

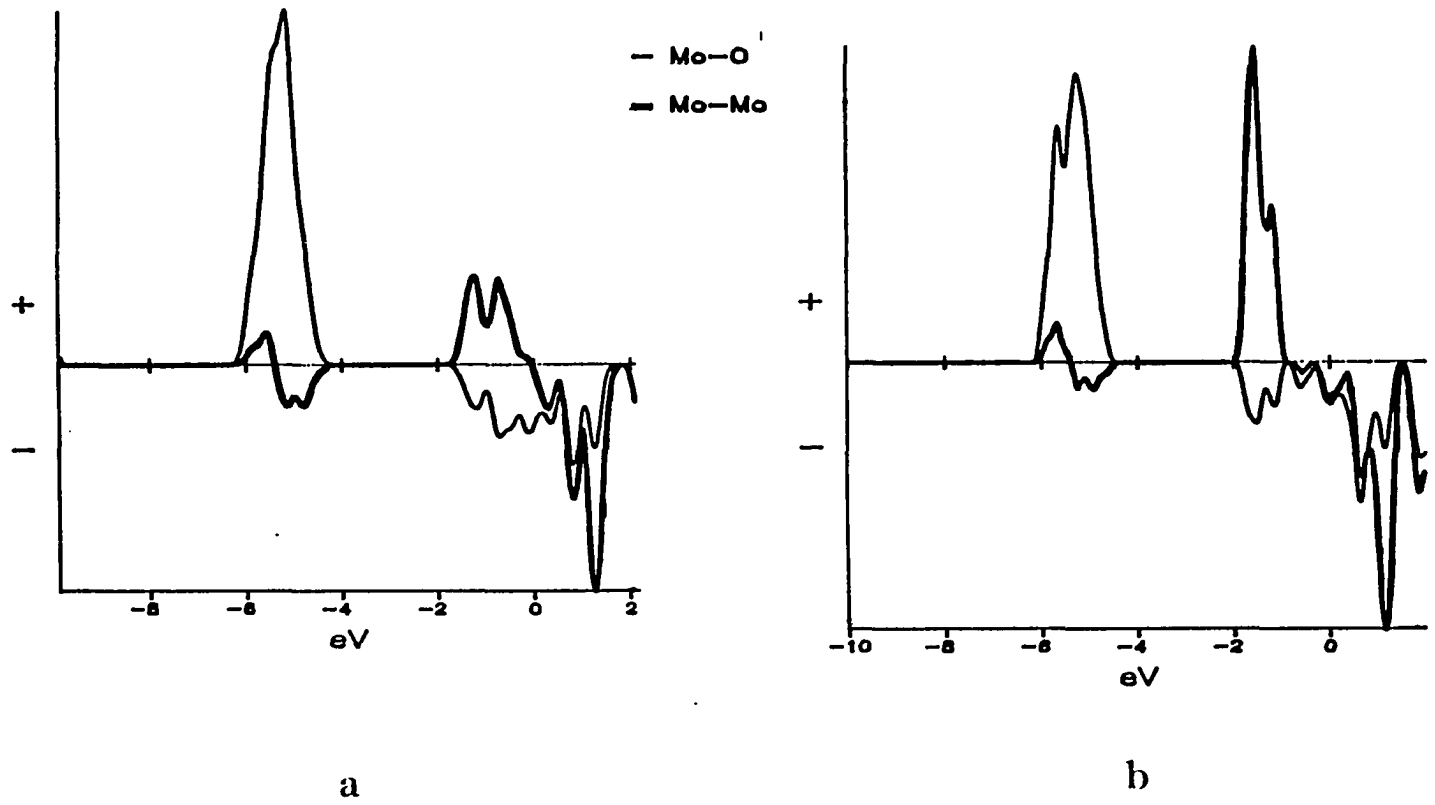

Fig. 2.6. The comparative orbital overlap population (COOP) curves for the structural modifications of $LiMoO_2$ (d^3 systems): (a) the hexagonal structure with a Mo bonded sheet; (b) the monoclinic framework with chains comprised of condensed rhomboidal units. The heavy curve represents the Mo-Mo states while the light curve corresponds to Mo-O levels

SECTION 3. THE TRANSFORMATION OF HEXAGONAL $LiMoO_2$ TO MONOCLINIC Li_xMoO_2.

INTRODUCTION

In a previous paper, we reported the synthesis and structural characterization of h-$LiMoO_2$, a material with hexagonal symmetry[1]. This compound is isostructural with α-$NaFeO_2$[2], revealing a layered framework with oxygen found in a cubic close-packed (ccp) array with Mo and Li atoms occupying octahedral sites in alternate layers.

The synthesis and structure of a different phase with the same stoichiometry has been studied by Murphy et al.[3], and Cox et al.[4]. This material, symbolized here as r-$LiMoO_2$, is prepared by lithiation of MoO_2[3]. The vacant distorted octahedral sites in the rutile-related structure become inhabited by Li^+ ions. The resulting framework can be viewed as a NiAs type derivative with the oxide lattice in the rutile host moving quite close to a hexagonal close-packed (hcp) arrangement[4]. It can be envisioned that the hcp framework can distort through an intermediate structure[5] to a ccp framework to form h-$LiMoO_2$. Here we report the novel synthesis of h-$LiMoO_2$ starting with the lithium inserted MoO_2.

The Mo bonding observed in h-$LiMoO_2$ is unprecedented: an infinitely bonded hexagonal sheet. The absence of distortion in this metal layer towards the type of Mo clustering (a zig-zag ribbon) observed in the related monoclinic layered compounds, Na_xMoO_2[6-10], is quite surprising. But results of extended Hückel calculations indicate that for a d^3 system, Mo-Mo antibonding states are occupied in the distorted monoclinic structure whereas in the hexagonal form the metal bonding levels are totally full and the antibonding levels empty. It is expected that as the Mo bonding states are emptied via oxidation by

delithiation, the Mo sheet would rearrange to form Mo ribbons or some other type of clustering favored by the lower electron to Mo ratio.

In this paper, we detail such a structural transition of the hexagonal structure in h-$LiMoO_2$ to a monoclinic framework with infinite Mo bonded zig-zag chains, along with the complete x-ray single crystal analysis of the monoclinic layered compound, $Li_{0.74}MoO_2$.

EXPERIMENTAL AND RESULTS

Materials

Lithium molybdate (Alfa Products, 98.5%) was recrystallized, dried at 150°C under vacuum for 12h, and stored in a dry box. In synthetic efforts, handling of lithium molybdate was confined solely to the inert atmosphere of the dry box. Molybdenum dioxide was obtained from Alfa Products (99%), molybdenum powder from Aldrich Chemical Co. (99.99%), elemental lithium and iodine from Fisher Scientific Co., 2.4M n-butyllithium in n-hexane from Alfa Products, molybdenum tubing from Thermo-Electron Corporation (99.97%), and copper tubing from laboratory stock. The salts, zinc chloride and calcium chloride, supplied by Fisher Scientific Co., were dried overnight at 150°C under vacuum and stored in a dry box.

Analytical Procedures

The elemental analyses reported in this paper were carried out by Schwarzhopf Microanalytical Laboratory, Inc. Percent lithium and zinc were determined by atomic absorption techniques with an error of $\pm$0.03%. The percent Mo content was analyzed by gravimetric precipitation of $PbMoO_4$ with a typical error of $\pm$0.03%.

Syntheses

h-$LiMoO_2$

As described in the previous paper x-ray pure samples of h-$LiMoO_2$ can be prepared by oxidizing Mo metal in the presence of an excess of lithium molybdate.[1] The reactants were thoroughly ground in a mortar, sealed in an evacuated copper tube, and held at 900°C for 21 days. The polycrystalline product was powdered in a mortar and washed several times with deionized water to remove unreacted lithium molybdate; the solid was then dried under vacuum at 120°C overnight. A Guinier x-ray powder diffraction pattern of the product showed only the lines of h-$LiMoO_2$. When samples were washed with deionized water over long periods of time or with slight warming, the Guinier powder pattern changed with the appearance of a previously unobserved line at the d-spacing of 7.22Å. In order to avoid this apparent instability of h-$LiMoO_2$ to such vigorous water washing, a different preparation was attempted. This route involved the conversion of lithium inserted rutile molybdenum dioxide (r-$LiMoO_2$) to h-$LiMoO_2$ at high temperatures. First, as described by Murphy et al.[3], rutile MoO_2 was lithiated by employing a saturated n-BuLi/n-hexane solution with stirring under argon gas at 69°C or room temperature. The r-$LiMoO_2$ was filtered, washed with hexane, dried, and stored in a dry box. The material was ground in a mortar and cold welded into an evacuated copper vessel. The reaction was then fired at 900°C for 3 to 11 days. As discussed below, the h-$LiMoO_2$ product generated in this manner revealed somewhat broader x-ray diffraction lines than those observed for the material produced in the reaction between Li_2MoO_4 and Mo. For the sake of clarity the hexagonal

layered material prepared through the conversion of r-$LiMoO_2$ at high temperatures will be distinguished as h'-$LiMoO_2$. The composition of h'-$LiMoO_2$ was verified by quantitative analysis and was consistent with a fully lithiated interlayer space.

Anal. Calcd. for h'-$LiMoO_2$: Li, 5.14%; Mo, 71.13%;

Found: Li, 5.08%; Mo, 69.47%.

Ion exchange reactions

In order to isolate layered materials with +2 counter ions, exchange reactions with molten $ZnCl_2$ and $CaCl_2$ were conducted. With respect to the zinc reactions, h-$LiMoO_2$ (or h'-$LiMoO_2$) ground together with a 11 (or 6) fold excess of $ZnCl_2$ was sealed in an evacuated copper vessel and fired at 300°C for 4 days. The resulting products were washed with water to remove the excess $ZnCl_2$ reactant and LiCl product; then the solid was rinsed with acetone and dried under vacuum. Guinier x-ray powder diffraction patterns of the products showed lines that could be indexed based on the hexagonal layered structure (see x-ray powder diffraction data).

Although, the powder patterns indicated the presence of only hexagonal layered compound, the quantitative analysis of both samples yielded puzzling data. In the case of the exchanged reaction with h-$LiMoO_2$, a final composition of $Li_{0.28}Zn_{0.54}MoO_{3.48}$ (**Anal.** Found: Li, 1.05%; Zn, 18.70%; Mo, 50.74%) was found while for h'-$LiMoO_2$, the data (**Anal.** Found: Li, 2.11%; Zn, 16.49%; Mo, 55.69%) gave the formula, $Li_{0.52}Zn_{0.43}MoO_{2.76}$. The data suggest that the resulting layered compounds may be hydrated, thus giving high oxygen content, or the products may be oxidizing during the water washing as evidenced by the

gray color of the washed samples.

The reaction between excess $CaCl_2$ and h-$LiMoO_2$ conducted in a copper tube at 800°C for 4 days yielded a mixture of products. The 16-fold excess $CaCl_2$ reactant and the resulting LiCl were removed by washing with water. The Guinier diffraction pattern of the dried gray-black solid revealed lines for $CaMoO_4$, Mo, and a monoclinic layered product. It appears that the reaction conditions necessary to obtain molten $CaCl_2$; i.e., firing temperature of 800°C, is too extreme. Due to the presence of Mo metal and the molybdate, quantitative analysis on the layered phase could not be obtained. However, as detailed below, the diffraction pattern was indexed to yield a monoclinic cell.

Delithiation

By employing I_2, a h-$LiMoO_2$ sample was delithiated; the solid was stirred in a solution of acetonitrile in the presence of excess I_2. After 6 days, the mixture was filtered and extracted. The Guinier powder pattern suggested the preparation of a layered material with a hexagonal c-axis decreased significantly from the initial h-$LiMoO_2$ (14.79 versus 15.4743Å). Quantitative analysis gave a very low percent Mo content indicating that all the LiI was not removed. The delithiation reaction was repeated starting with h'-$LiMoO_2$. A sample of h'-$LiMoO_2$ was reacted with excess I_2 in acetonitrile for 3 days followed by washing with six aliquots of fresh acetonitrile to insure complete removal of LiI and I_2. The final product gave a x-ray diffraction pattern essentially the same as the starting layered material. The extent of delithiation was determined through quantitative analysis.

Anal. Calcd. for $Li_{0.33}MoO_2$: Li, 1.76%; Mo, 73.67%;

Found: Li, 1.74%; Mo, 71.62%.

The h'-$LiMoO_2$ seems to be more reactive with respect to delithiation in air than the oxide synthesized via the high temperature reaction between Li_2MoO_4 and Mo metal. A sample of h'-$LiMoO_2$ was found to be oxidized to Li_2MoO_4 after sitting in air for approximately 8 weeks. The Guinier powder pattern gave lines for Li_2MoO_4, one very weak line for h'-$LiMoO_2$, and a line at about 7.3Å. This oxidized mixture was still black, while Li_2MoO_4 is white. The molybdate was removed by washing with deionized water. The black solid was rinsed with acetone and dried under vacuum. The diffraction pattern taken with a long exposure time (8 hours) verified the absence of Li_2MoO_4 and h'-$LiMoO_2$ and showed lines for a new phase with a peak at 7.20Å possessing the strongest intensity. (Recall that after extensive washing with warm water, the Guinier powder pattern of h-$LiMoO_2$ shows a line at 7.22Å.) Chemical analysis showed that the washed material has Li/Mo ratio of 0.42:1.0 (**Anal.** Found: Li, 2.07%; Mo, 67.95%).

m'-Li_xMoO_2 & m-$Li_{0.74}MoO_2$

The h'-$LiMoO_2$ also reveals an interesting transformation into a monoclinic layered variant. h'-$LiMoO_2$ partially delithiated by exposure to air or washing in water and reannealed at 900°C for 3 to 7 days yields products which give sharp diffraction patterns for a monoclinic structure, m'-Li_xMoO_2. Material obtained from air exposed h'-$LiMoO_2$ (washed with water prior to quantitative analysis) revealed a decrease in Li content, $Li_{0.89}MoO_2$.

Anal. Calcd. for $Li_{0.89}MoO_2$: Li, 4.60%; Mo, 71.53%;

Found: Li, 4.59%; Mo, 70.98%.

While the compound prepared from water washed h'-$LiMoO_2$ gave an even lower Li to Mo ratio of 0.75:1.0.

Anal. Calcd. for $Li_{0.75}MoO_2$: Li, 3.90%; Mo, 72.05%;

Found: Li, 3.80%; Mo, 70.07%.

The analyses indicate a slightly higher oxygen content than expected. This may reflect inaccuracy of the data in regard to the oxygen content which is determined by difference.

The monoclinic form can also be synthesized via other solid state reactions. m-Li_xMoO_2 was first obtained via the reduction of molybdenum dioxide by elemental lithium. Finely ground molybdenum dioxide was sealed along with a piece of lithium metal in the mol ratio of 2:1 in an evacuated copper vessel. The cold-welded metal tube was then sealed inside a quartz jacket and fired at 900°C for 5 days. The resulting product was reground, loaded into a new copper vessel, and fired for five more days at 900°C. The Guinier x-ray powder pattern revealed lines that could be indexed based on the structure of α-$Na_{0.41}MoO_2$[10] plus diffraction lines of Mo metal.

In attempts to prepare single crystals of this compound, reactions with a 1:1 molar ratio of lithium molybdate to molybdenum metal were conducted utilizing molybdenum containers. The first preparation was heated at 1300°C for 3 days. The Guinier powder pattern of the final product revealed a diffraction pattern belonging to a new phase along with only a weak 100% line for the desired oxide, m-Li_xMoO_2. A second reaction fired at lower temperature, 1100°C, but for a longer period, 10 days, yielded single crystals. A tablet shaped plate cut from an

irregular shaped piece was used for the single crystal structural analysis which showed a layered framework with monoclinic symmetry (see below). The x-ray powder pattern for the second reaction surprisingly did not show any lines for the layered compound but revealed the presence of the new phase seen in the reaction fired at 1300°C.

Like the layered Na_xMoO_2 system[7-10], m-Li_xMoO_2 can be prepared by oxidizing the reduced compound, $NaMo_4O_6$, with alkali metal molybdate, Li_2MoO_4, at 900°C for seven to sixteen days. Unlike the Na system, pure samples of the layered phase could not be isolated; invariably MoO_2 was found in the final product.

A pure sample of the monoclinic compound was accidentally achieved by a reaction intended to prepare h-$LiMoO_2$: the oxidation of Mo metal by excess Li_2MoO_4, seemingly contaminated with H_2O admitted through a small leak in the cold-welded seal of the Cu reaction vessel. After firing at 900°C for 21 days, large black platelets had grown out of the improperly sealed end of the Cu tube. The inner quartz jacket was attacked by the alkali molybdate. The contents of the vessel after water washing, yielded a well-crystallized x-ray pure sample of the monoclinic compound. Analysis of this material gave a final formula of $Li_{0.74}MoO_2$ for the monoclinic phase.

Anal. Calcd. for $Li_{0.74}MoO_2$: Li, 3.86%; Mo, 72.09%

Found: Li, 3.90%; Mo, 72.38%.

Miscellaneous Li-Mo-Oxides

Overall the Li-Mo-O ternary system is quite complex. In synthetic work, the particular compound obtained is very dependent on firing temperature. The new uncharacterized material referred to above seems

to be stable between reaction temperatures from 1000°C to 1300°C. Preparations conducted in this laboratory[11,12] in this temperature range also show this phase. For example, this unknown Li-Mo-oxide is the major product of the reaction between lithium molybdate, zinc oxide, and Mo metal (3:4:3 molar ratio, respectively) fired at 1100°C for 3.5 days and then 1300°C for 3 days[11]. Between 1300°C and 1450°C, $LiMo_8O_{10}$[13] becomes more stable and is consistently the major product. At even higher temperatures, such as 1500°C, the unknown material and $LiMo_8O_{10}$ are not observed; but the presence of the hexagonal layered material is noted.

X-ray Single Crystal Analysis for $Li_{0.74}MoO_2$

A black tablet-shaped plate with dimensions 0.14mm X 0.04mm X 0.01mm, cut from an irregular-shaped piece isolated in the reaction between Li_2MoO_4 and Mo at 1100°C, was used for film work and subsequent structure determination. The oscillation and Weissenberg photographs yielded the following lattice constants: a = 4.70, b = 2.87, c = 5.05Å, and β = 100°. X-ray data collection was accomplished by employing the Datex four circle diffractometer[14]. Using six orientation reflections from ω-oscillation photographs, the following preliminary unit cell dimensions were determined through an automatic indexing program[15]: a = 4.935, b = 2.878, c = 5.481Å, and β = 106.93°. The axial oscillation photographs were in accord with the above cell. However, the indexed powder diffraction pattern of this material indicated that the axis perpendicular to the layers should be doubled from 5.481 to 10.969Å. The presence of observed reflections with odd l indices in the cell with

c = 10.969Å indicated that the c-dimension is truly doubled. The details of data collection are summarized in Table 3.1. Final unit cell parameters and their estimated standard deviations listed in Table 3.1 were obtained by a least squares refinement of 2θ values of 20 independent reflections randomly distributed in reciprocal space having $24^o < 2\theta < 36^o$.

Lorentz, polarization, and empirical absorption corrections were applied to the data. Scattering factors[16] for neutral atoms were used throughout the analysis. Both the real and imaginary components of anomalous dispersion[17] were included for molybdenum atoms. Examination of the intensity set revealed there was an h + k + l = 2n condition for hkl reflections. Thus the nonstandard space group, I2/m (no. 12), was utilized for the structural refinement.

The molybdenum atom position was located by Patterson techniques The least-squares refinement of the positional parameters of the metal atom led to R = 16.0% and R_w = 25.1%. The locations of the oxygen atoms were subsequently inferred from an electron density map. Following refinement of the oxygen positions, an electron difference map revealed the position of the lithium cations in octahedral sites between the oxygen layers. Due to the small size and the weak scattering ability of lithium, the multipliers of the cations were not refined. Refinement of positional parameters, anisotropic temperature factors for Mo and O, and isotropic temperature factors for Li converged at R = 6.0% and R_w = 7.2%. The maximum residual electron density on the difference map was $2e^-/Å^3$. Tables 3.2 and 3.3 list the atomic positional and thermal parameters, respectively. Selected interatomic distances are recorded in Table 3.4. The structure can also be described with a C-centered

cell (C2/m) with the dimensions: a = 10.647(6), b = 2.881(1), c = 4.953(2)Å, and β =99.64(5)°.

X-ray Powder Diffraction Data

The Enraf Nonius Delft triple focusing Guinier camera was used with Cu $K\alpha_1$ radiation (λ = 1.54056Å) to obtain the powder diffraction and unit cell data. National Bureau of Standards silicon powder was mixed with all samples as an internal standard.

h'-$LiMoO_2$

As mentioned above the powder diffraction pattern for h'-$LiMoO_2$ samples prepared via r-$LiMoO_2$ showed broader diffraction lines than the oxide synthesized by the reactions between Li_2MoO_4 and Mo metal. The line broadening may be due in part to the extremely fine particle size of the sample and partially due to structural disorder. As recorded in Table 3.5, this route also yielded samples which consistently show a longer c-axis, 15.57(1) versus 15.4743(5)Å. The reason for this increase in the axis perpendicular to the layers is not clearly understood. However it may reflect an increase in the Mo-O bond distance over neutron diffraction analyzed h-$LiMoO_2$, which revealed an exceptionally short Mo-O bond distance of 2.0520(9)Å[1]. The Mo-O bond distance increases to 2.062Å if the Li-O distance [2.146(1)Å][1] observed in h-$LiMoO_2$ is maintained. Table 3.6 gives a comparison of the observed d-spacings of the h'-$LiMoO_2$ with those calculated based on the refined structure.

Ion exchange products

The compound, $Zn_xLi_{1-2x}MoO_2$, generated from h-$LiMoO_2$ was indexed on the basis of a hexagonal unit cell, which yields a longer c axis of 15.75(1)Å, in comparison to h-$LiMoO_2$ with c = 15.4743(5)Å. The observed diffraction lines and refined lattice parameters are given in Table 3.7. The zinc exchanged material derived from h'-$LiMoO_2$ also yielded a powder diffraction pattern characteristic of the hexagonal framework with the refined cell constants of a = 2.8682(6) and c = 15.95(1)Å (Table 3.8).

The product of the exchanged reaction between h-$LiMoO_2$ and $CaCl_2$ can be indexed on the basis of a monoclinic unit cell. The axis perpendicular to the slabs is expanded from 10.965(6)Å (for m-$Li_{0.74}MoO_2$) to 11.80(1)Å owing to the greater effective ionic radii of Ca^{+2} over Li^+, 1.00 versus 0.76Å[18]. Table 3.9 lists only the reflections attributed to the $Ca_xLi_{1-2x}MoO_2$ product while the lines of $CaMoO_4$ and Mo were removed.

Delithiation products

The x-ray diffraction pattern (Table 3.10) for the product of the reaction between h-$LiMoO_2$ and I_2 showed a dramatic shift of the 003 line from 5.168Å for starting material to about 4.959Å which indicates that the c-axis contracted to 14.87(1)Å.

The diffraction lines for the delithiation product starting with h'-$LiMoO_2$ are broad like those observed for h'-$LiMoO_2$. Surprisingly, the material does not show a contraction along the c-axis similar to that observed above. As noted in Table 3.11, lattice parameters refined to the values of a = 2.889(1) and c = 15.51(6)Å for a hexagonal cell.

Table 3.12 lists the d-spacings noted in the Guinier powder pattern of the oxidized h'-$LiMoO_2$ after removing Li_2MoO_4 by washing with H_2O.

m-Li_xMoO_2

All the powder patterns of the monoclinic layered samples, m-Li_xMoO_2, synthesized either by traditional solid state reactions or by the transformation of h'-$LiMoO_2$ can be indexed based on the structure determined by single crystal x-ray analysis. The least squares refined monoclinic cell parameters are recorded in Table 3.5, while the observed versus calculated d-spacings for m-$Li_{0.74}MoO_2$ are listed in Table 3.13.

Miscellaneous Li-Mo-oxides

Table 3.14 lists the common diffraction lines noted for the uncharacterized lithium molybdenum oxide observed in products of four reactions fired between 1000 and 1300°C. Overall, the diffraction lines are much more intense and sharp than those observed for the layered compounds. The powder pattern of this material is reminiscent of that noted for $LiMo_8O_{10}$[11]. $LiMo_8O_{10}$ shows very strong to strong intensities at d-spacings, 5.694Å, 2.387Å, 2.068Å, 2.065Å, and 1.461Å; while the unknown material reveals very strong reflections at 2.38Å, 2.06Å, and 1.46Å. These two materials may be structurally related, with the new compound having a slight variation of the $LiMo_8O_{10}$ framework.

The diffraction pattern of the material obtained from the reaction of Li_2MoO_4 and Mo at 1500°C is recorded in Table 3.15. The final product after water washing contained Mo metal whose characteristic diffraction lines are omitted from the Table 3.15. This pattern can be indexed on the basis of a hexagonal unit cell [a = 2.863(1) and c = 15.40(1)Å] with a shorter layered axis than that noted for h-$LiMoO_2$ [c = 15.4743(5)Å][1].

DISCUSSION

Cox et al.[4] have studied the structure of the lithium inserted MoO_2. The rutile framework (Figure 3.1a) upon lithiation changes to a structure best described as a distorted NiAs type with hexagonal close-packed oxygen atoms with Li and Mo occupying octahedral sites as illustrated in Figure 3.1b.

The subsequent high temperature transformation to the cubic close-packed layered framework (h'-$LiMoO_2$) requires several atomic displacement steps. The first step is a cooperative jump to nearest-neighbor sites of half the cation array as indicated by the arrows in Figure 3.1b. This diffusion of cations yields a CdI_2 structural type where the Li^+ ion sites share faces with the MoO_6 octahedra (Figure 3.1c). Presumably because of the electrostatic repulsion between Li^+ and Mo^{3+}, the anionic sublattice converts to cubic close packing (Figure 3.1e) where the metal ions in the octahedral sites share only edges via an intermediate structure proposed by Dâvid et al.[5]

As shown in Figure 3.1d, this transition framework possesses quite distorted alkali metal octahedral sites and a nonclose-packed oxygen arrangement. Interestingly, this intermediate layered array is seen in the related Na-Mo-oxide, α-$Na_{0.41}MoO_2$. This oxide shows the same basic packing but with corrugated oxide layers arising from the distortion due to the molybdenum clustering (Figure 3.2).

With respect to the transformation of one structure type to another, David et al. discussed the change of rutile framework of β-MnO_2 into a spinel structure ($LiMn_2O_4$) upon lithiation[19]. The zinc exchanged h-$LiMoO_2$ may provide an ideal starting reactant for the preparation of

spinel $ZnMo_2O_4$. The necessary structural changes, as illustrated in Figure 3.3, involve the diffusion of every fourth Mo atom into vacant octahedral sites within the zinc layers, subsequent migration of the neighboring zinc ions into tetrahedral sites, and a following movement of the near Mo atoms to enter adjacent empty sites. An attempt to effect this framework change (h-$Zn_{0.5}MoO_2$ to spinel $ZnMo_2O_4$) was conducted by heating a sample at 1250°C in a Mo reaction vessel. During firing of the reaction, Mo metal was extracted from the reaction container to yield the Mo rich phase, $ZnMo_8O_{10}$[13]. Further work at higher temperatures with Pt inner jackets to prevent the addition of Mo metal to the reaction system may be fruitful.

The high temperature transformation of the partially delithiated h'-Li_xMoO_2 to m'-Li_xMoO_2 is a displacive type resulting from the clustering of Mo atoms within the hexagonal layer, and possibly the ordering of Li ions in the partially occupied Li layers.

In comparing the ORTEP drawings of the hexagonal and monoclinic layered frameworks in Figures 3.4 and 3.5, one can see that the structures are similar except for the formation of Mo ribbons in m-Li_xMoO_2. Figure 3.6 better illustrates the distortion within the metal layer. The ribbons formed by the Mo zig-zag bonds are achieved by a displacement of metal atoms toward neighboring atoms along one direction within the plane. The Mo atoms do not shift in the perpendicular direction corresponding to the a-axis of h-$LiMoO_2$ and the b-axis of m-Li_xMoO_2. The lack of movement in this direction is evidenced by the observation that the monoclinic b-axis [2.866(4)Å] remains equal to the a-axis [2.867(1)Å] of the initial h'-$LiMoO_2$ sample. It should be noted that m-Li_xMoO_2 samples prepared by other synthetic

routes show a slightly longer b-axis [2.880Å]

This Mo clustering along with a slight distortion of the anionic lattice probably occurs continuously, typical of a second order transition. The crystal-structure change involves a group ($R\bar{3}m$) to subgroup (C2/m) transition in fulfillment of the first condition of Landau's theory of second order phase transitions. However such transitions involve a change of symmetry from a low temperature, low symmetry structure to a high temperature, high symmetry framework. The observed transformation is just the opposite: low temperature, hexagonal cell to high temperature, monoclinic lattice.

The transformation of the hexagonal to monoclinic layered framework requires a change in stoichiometry which also indicates that the change can not be a second order phase transition. As indicated by extended Hückel calculations, the fully lithiated hexagonal compound appears to be electronically favored over the monoclinic variant. The ideal cubic close-packed framework of the hexagonal structure may also be stabilized with respect to the distorted packing in the monoclinic structure by the presence of a completely loaded interlamellar space. But a metastable hexagonal material is generated upon the oxidation of the Mo net through delithiation. Thus the observed structure change from h'-Li_xMoO_2 to m'-Li_xMoO_2 at high temperature is best described as a transition of a metastable lattice into the thermodynamically favored state.

The reactivities of h-$LiMoO_2$ and h'-$LiMoO_2$ are quite different. The layered compound prepared via the high temperature reaction between Li_2MoO_4 and Mo metal can be washed with water for short periods of time without extraction of lithium from the Mo-oxide framework. Whereas h'-$LiMoO_2$ is easily partially delithiated by water washings and

subsequently converted to the monoclinic form at high temperatures. The resulting monoclinic phase shows a Li/Mo ratio of 0.75 indicating the hexagonal material was delithiated to h'-$Li_{0.75}MoO_2$. The greater reactivity of h'-$LiMoO_2$ over h-$LiMoO_2$ may be due to presence of structural disorder indicated by broad x-ray diffraction lines and greater Li mobility suggested by the increased layer spacing.

The hexagonal framework is maintained upon ion exchange reactions with zinc chloride. In material obtained from both types of hexagonal $LiMoO_2$, an approximate 2% increase in the layered axis is noted from 15.4743(5) to 15.75(1)Å for h-$LiMoO_2$; and 15.57(1) to 15.95(1)Å for h'-$LiMoO_2$. By simple comparison of the six-coordinate effective ionic radii for Li^+ and Zn^{+2} (0.76 versus 0.74Å)[18], one would expect the zinc-exchanged material to show the same or a slightly smaller c-axis. However, the interslab distance is dependent on the competition between attractive forces (Zn^{2+} <--> O^{2-}) and repulsive interactions (O^{2-} <--> O^{2-}). As the number of counter cations decreases within the interlameller space, the attractive forces should decrease with respect to repulsive ones, causing the layers to expand. Thus the observed expansion may be the result of the formation of vacancies in octahedral sites between the Mo-dioxide slabs. This characteristic increase in the layer spacing was noted during the deintercalation of $NaCoO_2$ (5.19 to 5.56Å)[20] and $LiCoO_2$ (4.68 to 4.77Å)[20,21] to form $Na_{0.5}CoO_2$ and $Li_{0.5}CoO_2$, respectively.

The ion exchange reaction with $CaCl_2$ was conducted at a higher temperature than the zinc chloride reaction giving a greater potential for rearrangement of the Mo bonding. The reaction yielded a layered compound with a monoclinic framework along with $CaMoO_4$ and Mo metal. In

comparison to the lattice parameters for m-$Li_{0.74}MoO_2$, the layered axis for the Ca exchanged material is significantly longer, 11.80(1) versus 10.647(6)Å. Using the cell parameters for m-$Li_{0.74}MoO_2$, a Li-O-Mo-O repeat is computed to be 5.248Å; substituting Ca^{+2} for Li^+, a Ca-O-Mo-O repeat should equal 5.728Å. The refined lattice constants for the exchanged material, [a = 11.80(1); b = 2.866(2), c = 4.956(5)Å; and β = 98.39°], give a repeat distance of 5.836Å for a Ca-O-Mo-O slab. Thus the Ca exchanged compound shows a slightly greater layering distance than expected. Similar to the zinc exchanged products, the layering repeat (5.836Å for Ca-O-Mo-O) is about 2% greater than expected (5.728Å) owing to the formation of vacancies between the O-Mo-O slabs.

The results of the delithiation reactions employing I_2 at room temperature are in contrast to those obtained for the deintercalation of $NaCoO_2$ and $LiCoO_2$. For both h-$Li_{1-x}MoO_2$ and h'-$Li_{1-x}MoO_2$, the hexagonal structure is maintained but with a decrease in the layer spacing. The delithiated h-$Li_{1-x}MoO_2$ phase showed a greater change in the axis perpendicular to the layers [15.4743 to 14.87(1)Å] than the delithiated h'-$Li_{1-x}MoO_2$ [15.57(1) to 15.51(6)Å]. It appears that the net sum of the attractive and repulsive forces for the delithiated products is different than the sum for the ion exchange products, with a greater net attraction between the layers. The extent of contraction may simply reflect the extent of delithiation. Both compounds show an increase in the Mo-Mo distances from 2.867(1) to 2.889(1)Å for h'-$LiMoO_2$ and from 2.8663(1) to 2.9033(3)Å for h-$LiMoO_2$. The difference in the metal to metal distances in the two delithiated samples suggests that h-$Li_{1-x}MoO_2$ is more oxidized, thereby contains less lithium, than h'-$Li_{1-x}MoO_2$. For the zinc and calcium exchanged products, the oxidation state of the Mo

should be the same. Thus the attractive O^{2-} to Mo^{3+} interactions in the ion exchanged products should not significantly differ from that in the initial lithium phase. However, this attractive Mo to O interaction may be an important factor in the decrease in the interlayer distance observed for the delithiated products. A contraction of the layers could be accomplished through a greater O^{2-}-$Mo^{(3+x)+}$ attractive interaction and subsequent temperance of O^{2-}-O^{2-} repulsion effects.

At low temperature in the presence of moisture and air, the metastable partially delithiated h'-Li_xMoO_2 is sensitive to further deintercalation and oxidation. It appears that h'-Li_xMoO_2 reacts with O_2 to generate lithium molybdate and a further deintercalated layered framework. The formation of Li_2MoO_4 is easily detected by x-ray diffraction while the presence of the hexagonal phase is not confirmed. Instead a new series of lines is observed with the highest d-spacing diffraction line at 7.20(1)Å. It is believed that this diffraction pattern corresponds to a hydrated layered network. This hypothesis is supported by the observation that after extensive washing with warm water, the Guinier powder pattern of h-$LiMoO_2$ shows a line at 7.22Å. Also, Tarascon[22] observed that the monoclinic compound, m-$Li_{0.67}MoO_2$, could be hydrated to m-$Li_{0.67}(H_2O)_{0.48}MoO_2$, with an increase in the axis perpendicular to the MoO_2 layers from 10.666(1) to 14.60(2)Å. Thus, a $Li(H_2O)$-O-Mo-O slab repeat is approximately 7.30Å, which corresponds well with the highest d-spacing noted for the oxidized h'-Li_xMoO_2 sample. The analytical data reported in the experimental section can be interpretated to give the formula, $Li_{0.42}(H_2O)_{0.57}MoO_2$

Anal. Calc. for $Li_{0.42}(H_2O)_{0.57}MoO_2$: Li, 2.07%; Mo, 67.98%; O+H, 29.95%;
Found: Li, 2.07%; Mo, 67.95%; O+H, 29.97%.

Conclusion

The conversion of lithium inserted MoO_2 to a hexagonal layered material, $LiMoO_2$, and the preparation of a monoclinic structure from the delithiated hexagonal framework, provide examples of nontraditional routes to solid state compounds. The hexagonal layered phase may present a promising starting material into systems with other structures: As detailed in the discussion section, a fully Zn-exchanged sample, $Zn_{0.5}MoO_2$, might be easily transformed into a spinel structure, $ZnMo_2O_4$, which so far has not been obtained by direct high temperature synthesis. A hydrogen exchanged compound, $HMoO_2$, with the formation of H_2O could lead to the isolation of a Mo^{+3} oxide, Mo_2O_3. A fully delithiated material would give a new form of MoO_2 with great potential for intercalation chemistry.

The reactivity of the hexagonal layered material, h'-$LiMoO_2$, obtained via r-$LiMoO_2$, is much greater than that of h-$LiMoO_2$, which was prepared by traditional high temperature reaction between Li_2MoO_4 and Mo metal. This difference may be due to the presence of structural disorder and greater Li mobility in h'-$LiMoO_2$.

In accord with the results of extended Hückel calculations, the metal bonding and layered lattice should distort upon oxidation of the Mo sheet through delithiation. However, the metastable hexagonal framework of h-Li_xMoO_2 and h'-Li_xMoO_2 is maintained at low temperature (in a nonoxidizing atmosphere). In the case of h'-Li_xMoO_2, the transformation of the metastable lattice into the favored state, m'-Li_xMoO_2, is observed at 900°C.

In the presence of an oxidizing atmosphere, such as moist air, the

h'-Li_xMoO_2 decomposes to form Li_2MoO_4 and what appears to be a hydrated layered framework.

REFERENCES

1. Aleandri, L. E.; McCarley, R. E., submitted for publication in Inorg. Chem.

2. Goldsztaub, S. Compt. Rend. 1933, 196, 280.

3. Murphy, D. W.; Di Salvo, F. J.; Carides, J. N.; Waszczak, J .V. Mat. Res. Bull. 1978, 13, 1395.

4. Cox, D. E.; Cava, R. J.; McWhan, D. B.; Murphy, D. W. J. Phys. Chem. Solids 1982, 43, 657.

5. David, W. I. F; Bruce, P. G.; Goodenough, J. B. J. Solid State Chem. 1983, 50, 235.

6. McCarley, R. E.; Lii, K. -H.; Edwards, P. A.; Brough, L. F. J. Solid State Chem. 1985, 57, 17.

7. Aleandri, L. E.; Edwards, P. A.; McCarley, R. E., American Chemical Society Meeting, Chicago, Sept. 8-13 (1985).

8. Aleandri, L. E.; McCarley, R. E., American Chemical Society Meeting, New York, April 13-18 (1986).

9. $Na_{0.66}MoO_2$ was initially reported as $Na_2Mo_3O_6$ in: (a) Hubert, P. H. C. R. Acad. Sc. Paris 1966, 262, 1189. and (b) Reau, J. M.; Fouassier, C.; Hagenmuller, P. Bull. Soc. Chim. 1970, 11, 3827. The structure based on X-ray powder diffraction data is given in reference 10.

10. Aleandri, L. E., Ph.D. Dissertation, Iowa State University, Ames, Iowa, 1987, Section 1.

11. Brough, L. F.; McCarley, R. E. unpublished research, Department of Chemistry, Iowa State University, Ames, Iowa, 1982.

12. Lii, K. -H.; McCarley, R. E. unpublished research, Department of Chemistry, Iowa State University, Ames, Iowa, 1985.

13. Lii, K. -H.; McCarley, R. E.; Sangsoo, K.; Jacobson, R. A. J. Solid State Chem. 1986, 64, 347.

14. This Datex four-circle diffractometer was modified in Dr. R. A. Jacobson's laboratory. Stepping motors and encoders were attached and interfaced to a LSI/11 computer, which in turn was interfaced to a VAX11/730 computer. It is equipped with a scintillation counter and incorporates a graphite monochromator in the detection system.

15. Jacobson, R. A. J. Appl. Crystallogr. 1976, 9, 115.

16. Hansen, H. P.; Herman, F.; Lea, J. D.; Skillman, S. Acta Crystallogr. 1964, 17, 1040.

17. Templeton, D. H. In "International Tables for X-ray Crystallography", 1st ed.; Macgillavry, C. H. and Rieck, G. D., Eds.; Kynoch Press: Birmingham, England, 1962; Vol. III, P. 215.

18. Shannon, R. D. Acta Crystallogr. 1976, A32, 751.

19. David, W. I. F.; Thackeray, M. M.; Bruce, P. G.; Goodenough, J. B. Mat. Res. Bull. 1984, 19, 99.

20. Kikkawa, S.; Miyazaki, S.; Koizumi, M. J. Solid State Chem. 1986, 62, 35.

21. Mendiboure, A.; Delmas, C.; Hagenmuller, P. Mat. Res. Bull. 1984, 19, 1383.

22. Tarascon, J. M., submitted for publication in Solid State Ionics.

Table 3.1. The crystallographic data for $Li_{0.74}MoO_2$

crystal system	monoclinic
space group	I2/m
lattice constants	
a (Å)	4.953(2)
b (Å)	2.881(1)
c (Å)	10.965(6)
β (degree)	106.80(4)
Volume ($Å^3$)	149.8(1)
Z	4
density (calcd) (g/cm^3)	5.87
crystal dimensions (mm)	0.14 x 0.04 x 0.01
abs coeff (cm^{-1})	80.1
reflection absorp. corr. (hkl, 2θ, Tmax/Tmin)	0 2 0, 28.50, 2.23
diffractometer	Datex[a]
radiation: MoKα (λ,Å)	0.70966
monochromator	graphite
scan type	ω-scan
scan-half width (degree)	0.6
standard reflections:	
number monitored	3
frequency measured	every 50 reflns.
intensity variation	none
reflections measured	HKL, $\bar{H}$KL, H$\bar{K}$L, HK$\bar{L}$
max 2θ (degree)	60
reflections collected	1167
observed [$I > 3\sigma(I)$]	469
number unique reflns. with $I > 3\sigma(I)$	218
number parameters refined	27
R (%)[b]	6.0
R_w (%)[c]	7.2

[a] For details of the Datex diffractometer, see reference 14.

[b] $R = \Sigma||F_o| - |F_c||/\Sigma|F_o|$.

[c] $R_w = [\Sigma w(|F_o|-|F_c|)^2/\Sigma w|F_o|^2$; $w = 1/\sigma^2(|F_o|)]^{1/2}$.

Table 3.2. Positional parameters for $Li_{0.74}MoO_2$

atom	multiplier	x	y	z	B(Å^2)[a]
Li1	0.1875	0.50	0.50	0.00	4.81
Li2	0.1875	0.00	0.00	0.00	3.27
Mo1	0.5	0.4603(3)	0.00	0.2470(1)	0.83
O1	0.5	0.2452(26)	0.00	0.3839(12)	0.83
O2	0.5	0.7694(25)	0.00	0.1461(12)	0.59

[a]The isotropic equivalent thermal parameter is defined as $B = 4/3\ [a^2\beta_{11} + b^2\beta_{22} + c^2\beta_{33} + 2ab(\cos\gamma)\beta_{12} + 2ac(\cos\beta)\beta_{13} + 2bc(\cos\alpha)\beta_{23}]$.

Table 3.3. Thermal parameters[a] for $Li_{0.74}MoO_2$

atom	B_{11}	B_{22}	B_{33}	B_{12}	B_{13}	B_{23}
Li1	isotropic temperature factor (B): 4.8(2.8)					
Li2	isotropic temperature factor (B): 3.2(2.3)					
Mo1	0.58(5)	0.97(6)	0.83(5)	0.0	0.1(1)	0.0
O1	0.5(4)	0.8(5)	1.2(5)	0.0	1.0(1.0)	0.0
O2	0.5(4)	0.2(4)	1.0(4)	0.0	0.4(1.2)	0.0

[a]The general thermal parameter expression used is $\exp[-1/4\ (B_{11}h^2a^{*2} + B_{22}k^2b^{*2} + \ldots + 2B_{23}klb^*c^*)]$.

Table 3.4. Bond distances (Å) in $Li_{0.74}MoO_2$

Mo1 - Mo1	2.549(2)[a]	
	2.881(1)[a]	
	3.194(3)[b]	
Mo1 - O1[i]	2.082(15)	
	2.087(11)	
	2.087(11)	
Mo1 - O2[a]	2.081(10)	
	2.081(10)	
	2.132(14)	
Li1 - O1[i]	1.993(15)	(2X)
Li1 - O2[a]	2.279(11)	(4X)
Li2 - O1[i]	2.080(11)	(4X)
Li2 - O2[a]	2.220(15)	(2X)

[a]Intrachain distance.

[b]Interchain distance.

Table 3.5. Lattice parameters for layered lithium molybdenum oxides, Li_xMoO_2

compound	a, Å	b, Å	c, Å	α, deg.	β, deg.	γ, deg.
h-$LiMoO_2$	2.8663(1)		15.4743(5)	90.0	90.0	120.0[a]
	2.8666(8)		15.469(8)	90.0	90.0	120.0[b]
h'-$LiMoO_2$	2.867(1)		15.57(1)	90.0	90.0	120.0[b]
m-$Li_{0.74}MoO_2$	10.647(6)	2.881(1)	4.953(2)	90.0	99.64(5)	90.0[c]
	10.652(4)	2.8790(4)	4.9483(9)	90.0	99.53(2)	90.0[b]
m'-Li_xMoO_2	10.60(1)	2.866(4)	4.96(1)	90.0	99.5(1)	90.0[b]

[a]From powder neutron diffraction data.

[b]From powder x-ray diffraction data.

[c]From single crystal x-ray diffraction data.

Table 3.6. X-ray powder diffraction data for h'-$LiMoO_2$

d-spacings (Å) observed	d-spacings (Å) calculated[a]	intensities	h k l
5.177(6)	5.158	vs	0 0 3
2.602(1)	2.579	w	0 0 6
2.444(1)	2.450	ms	1 0 1
2.359(1)	2.363	m	0 1 2
2.0888(9)	2.0891	ms	1 0 4
1.9390(8)	1.9363	wm	0 1 5
1.6575(5)	1.6508	wm	1 0 7
1.5324(5)	1.5257	wm	0 1 8
1.4344(4)	1.4331	m	1 1 0
1.3826(3)	1.3808	m	1 1 3

[a]Guinier x-ray diffraction pattern computed using the positional and thermal parameters obtained during the refinement of the neutron diffraction data.

Table 3.7. X-ray powder diffraction data for h-$Zn_xLi_{1-2x}MoO_2$[a]

d-spacings	intensities	h k l
5.266(6)	s	0 0 3
2.634(1)	vw	0 0 6
2.454(1)	ms	1 0 1
2.370(1)	m	0 1 2
2.1031(9)	ms	1 0 4
1.6656(5)	w	1 0 7
1.5436(4)	w	0 1 8
1.4349(3)	m	1 1 0
1.3828(3)	w	1 1 3

[a]Refined hexagonal cell parameters are a = 2.868(1) and c = 15.75(1)Å.

Table 3.8. X-ray powder diffraction data for h'-$Zn_xLi_{1-2x}MoO_2$[a]

d-spacings	intensities	h k l
5.295(8)	s	0 0 3
2.660(1)	vw	0 0 6
2.455(1)	m	1 0 1
2.369(1)	wm	0 1 2
2.108(1)	m	1 0 4
1.4343(5)	w	1 1 0

[a]Refined hexagonal cell parameters are a = 2.8682(6) and c = 15.95(1)Å

Table 3.9. X-ray powder diffracton data for m-$Ca_xLi_{1-2x}MoO_2$[a]

d-spacings	intensities	h k l
5.827(7)	s	2 0 0
2.912(1)	w	4 0 0
2.466(1)	m	-1 1 1
2.448(1)	m	0 0 2
2.397(1)	m	-2 0 2
		1 1 1
2.1651(9)	m	-3 1 1
2.1533(9)	m	2 0 2
1.9889(8)	vw	3 1 1
1.7653(6)	w	-5 1 1
1.6426(5)	w	5 1 1
1.6332(5)	wm	0 0 3
1.4332(3)	wm	0 2 0
1.3901(3)	w	2 2 0
1.3529(3)	w	-6 0 3
1.3376(3)	w	7 1 1

[a]Refined monoclinic cell parameters are a = 11.80(1), b = 2.866(2), c = 4.956(5)Å, and β = 98.39(9)°.

Table 3.10. X-ray powder diffraction data for h-$Li_{1-x}MoO_2$[a]

d-spacings	intensities	h k l
4.959(5)	s	0 0 3
2.478(1)	ms	0 0 6, 1 0 1
2.383(1)	wm	0 1 2
2.0825(9)	m	1 0 4
1.4516(4)	w	1 1 0

[a]Refined hexagonal cell parameters are a = 2.9033(3) and c = 14.87(1)Å.

Table 3.11. X-ray powder diffraction data for h'-$Li_{0.33}MoO_2$[a]

d-spacings	intensities	h k l
5.230(6)	s	0 0 3
2.466(1)	ms	1 0 1
2.381(1)	ms	0 1 2
2.1016(8)	ms	1 0 4
1.4457(4)	m	1 1 0
1.3905(3)	w	1 1 3

[a]Refined hexagonal cell parameters are a = 2.889(1) and c = 15.51(6)Å.

Table 3.12. X-ray powder diffraction data for "h'-$Li_{0.42}(H_2O)_{0.57}MoO_2$"

d-dpacings	intensities
7.20(1)	s
3.599(3)	m
2.491(1)	w
2.439(1)	m
2.161(1)	w
2.092(1)	vvw
1.2814(3)	w

Table 3.13. X-ray powder diffraction data for m-$Li_{0.74}MoO_2$

d-spacings (Å) observed[a]	d-spacings (Å) calculated[b]	intensities	h k l
5.250(6)	5.248	vs	2 0 0
4.876(5)	4.883	w	0 0 1
3.912(3)	3.917	vw	-2 0 1
2.624(1)	2.624	w	4 0 0
2.460(1)	2.462	ms	-1 1 1
2.441(1)	2.441	ms	0 0 2
2.368(1)	2.370	ms	-2 0 2
2.1083(9)	2.1105	m	-3 1 1
2.0860(9)	2.0842	m	2 0 2
1.9489(7)	1.9473	w	3 1 1
1.8741(7)	1.8756	wm	-1 1 2
1.7940(6)	1.7949	vw	1 1 2
1.7375(6)	1.7495	vw	6 0 0
1.6752(5)	1.6745	vw	-5 1 1
1.6320(5)	1.6340	w	-2 0 3
1.6264(5)	1.6276	w	0 0 3
1.5394(4)	1.5393	w	5 1 1
1.4399(4)	1.4405	m	0 2 0
1.4312(3)	1.4323	wm	-1 1 3
1.3888(3)	1.3891	w	2 2 0
1.3841(3)	1.3850	w	-3 1 3
1.3780(3)	1.3780	w	1 1 3
1.2394(2)	1.2406	wm	0 2 2
	1.2376		7 1 1
1.2298(2)	1.2310	w	-2 2 2

[a]From powder x-ray diffraction data of the product of the reaction between Li_2MoO_4 and Mo metal.

[b]Guinier x-ray diffraction pattern computed using the positional and thermal parameters obtained during the x-ray single crystal study.

Table 3.14. X-ray powder diffraction data for $Li_xMo_yO_z$[a]

d-spacings	intensities
8.01	s
7.49	m
4.75	m
4.40	m
3.98	vw
3.18	vw
3.09	w
2.925	w
2.83	wm
2.49	w
2.38	vs
2.30	w
2.26	wm
2.19	wm
2.06	vs
1.93	w
1.88	w
1.87	m
1.45	vs

[a]This list is comprised of the d-spacings observed in the powder patterns of the products of the following reactions:

$$Li_2MoO_4 + Mo \xrightarrow[1100C\ 10d.]{}$$

$$Li_2MoO_4 + Mo \xrightarrow[1300C\ 2.7d.]{}$$

$$3Li_2MoO_4 + 4ZnO + 3Mo \xrightarrow[1100C\ 3.5d.\ \&\ 1300C\ 3d.]{} \qquad (11)$$

$$2Li_2MoO_4 + MoO_3 + Mo\ strips \xrightarrow[1000C\ 7d.]{} \qquad (12).$$

Table 3.15. X-ray powder diffraction data for h-Li_xMoO_2[a] obtained in reaction fired at 1500°C

d-spacings	intensities	h k l
5.134(6)	s	0 0 3
2.452(1)	sm	1 0 1
2.360(1)	ms	0 1 2
2.0827(9)	ms	1 0 4
1.5175(4)	w	0 1 8
1.4327(4)	m	1 1 0
1.3790(3)	m	1 1 3
1.2844(3)	mb	0 0 12

[a]Refined hexagonal cell parameters are a = 2.863(1) and c = 15.40(1)Å.

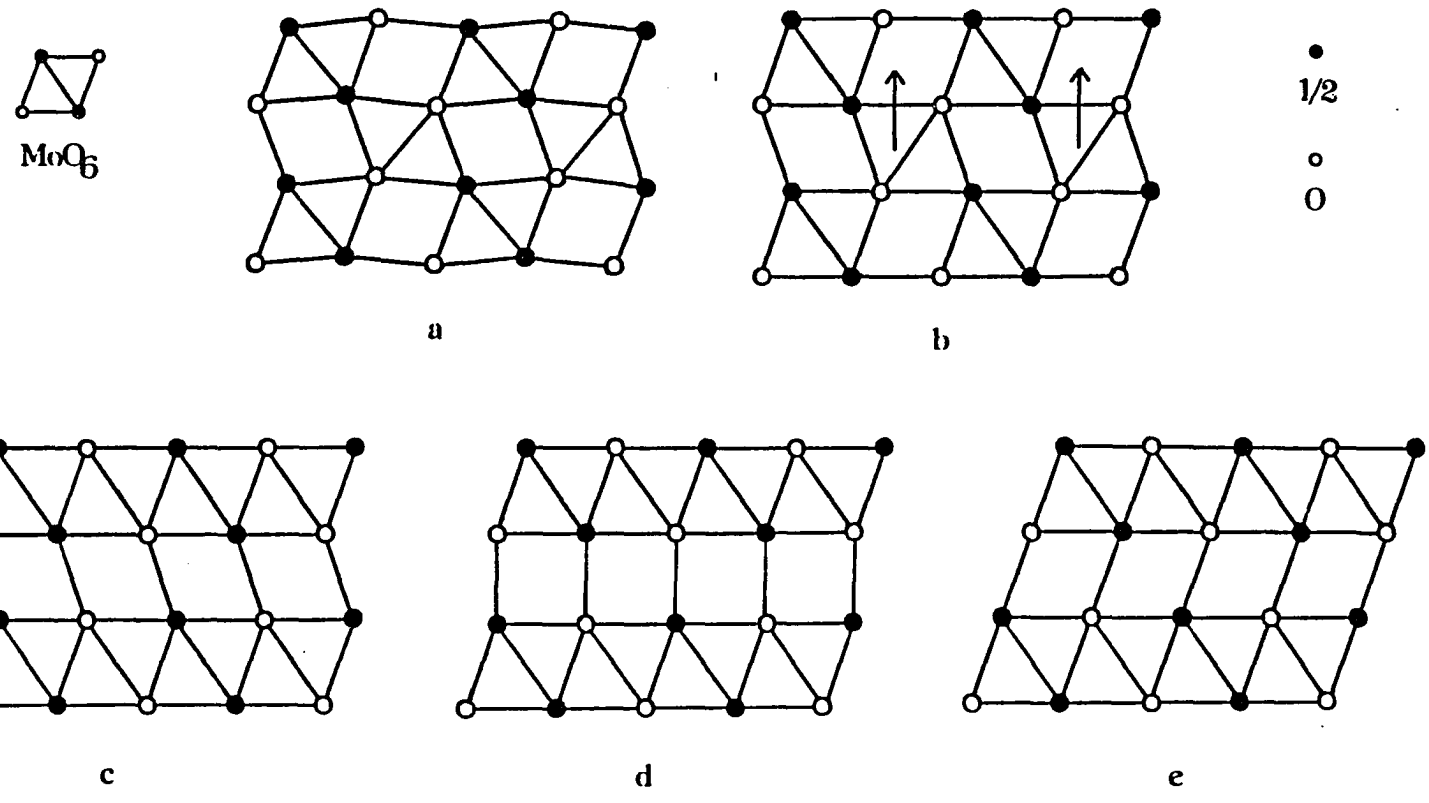

Fig. 3.1. The structural change seen upon the lithiation of MoO_2[4] and the proposed sequence of framework distortions necessary for the transformation of r-$LiMoO_2$ to h'-$LiMoO_2$: a) rutile-related MoO_2 structure; b) distorted NiAs structure type of r-$LiMoO_2$ with the solid arrows showing the movement of Mo atoms needed to obtain the CdI_2 layered network. c) CdI_2 framework; d) proposed intermediate lattice between CdI_2 and $CdCl_2$[5]; e) $CdCl_2$ structure type seen in h'-$LiMoO_2$

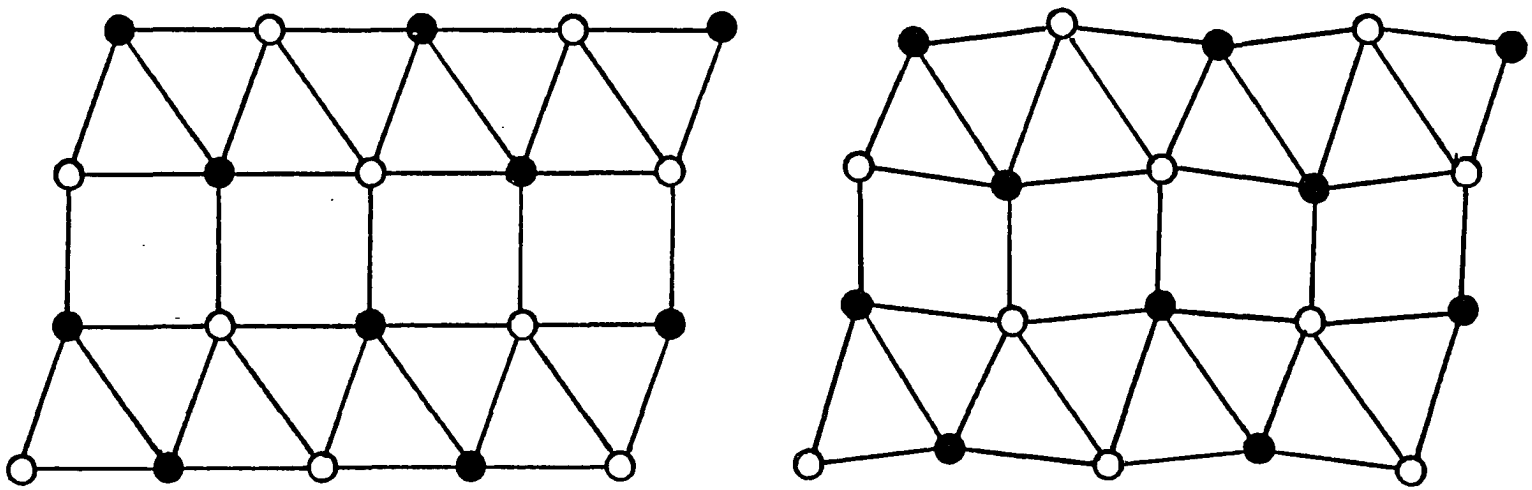

Fig. 3.2. The oxygen packing of the proposed transition structure between CdI_2 and $CdCl_2$ layered networks[5] in comparison to the oxygen layering observed for α-$Na_{0.41}MoO_2$[10]

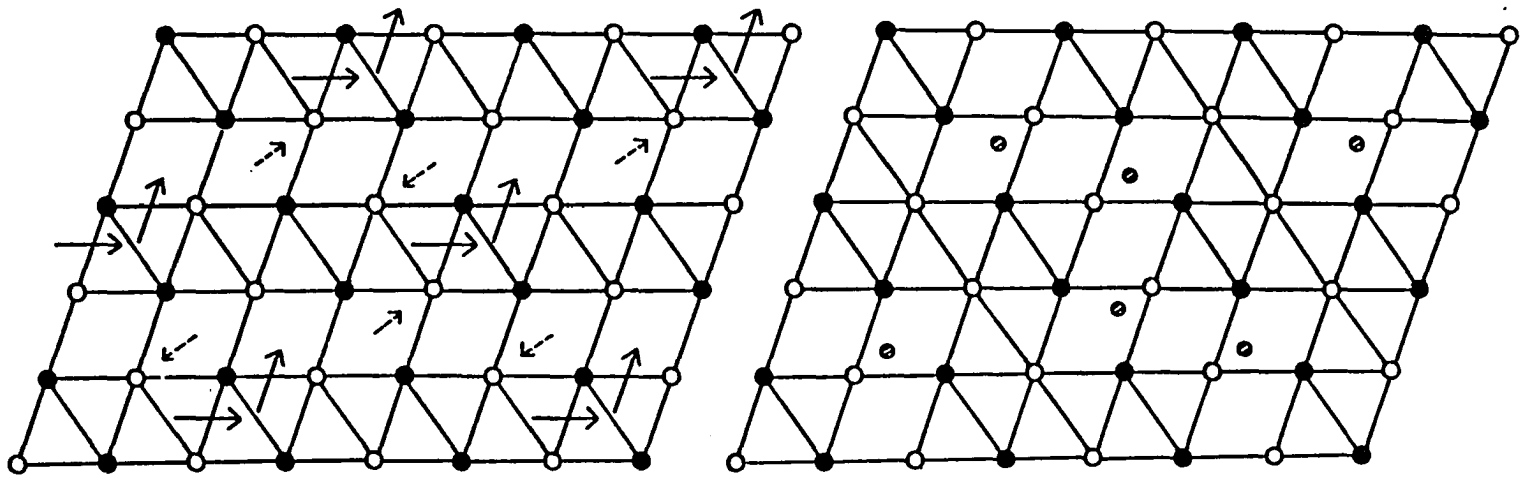

Fig. 3.3. The structural changes envisioned to allow for the transformation of a Zn exchanged layered compound, $Zn_{0.50}MoO_2$, illustrated in (a) to the spinel structure diagrammed in (b). The cross-hatched circles indicate Zn ions in tetrahedral sites at 1/4 and 3/4

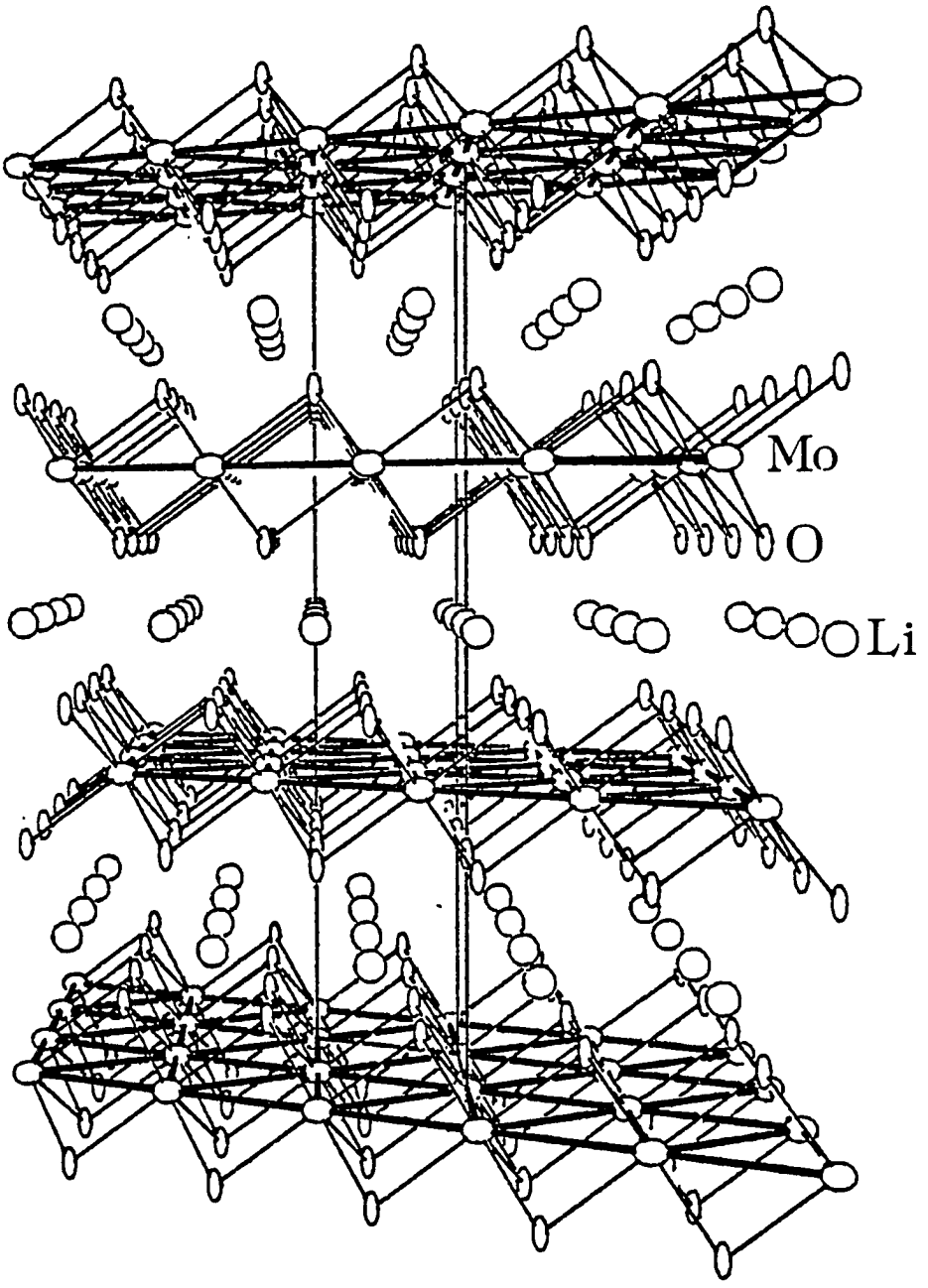

Fig. 3.4. Three dimensional view of the unit cell of the h-$LiMoO_2$ structure as seen along the a axis. The framework consists of Mo sheets [d(Mo-Mo) = 2.8663(1)Å] bridged by oxygen atoms [d(Mo-O) = 2.0520(9)Å] to form O-Mo-O slabs separated by layers of Li ions [d(Li-O) = 2.146(1)Å]

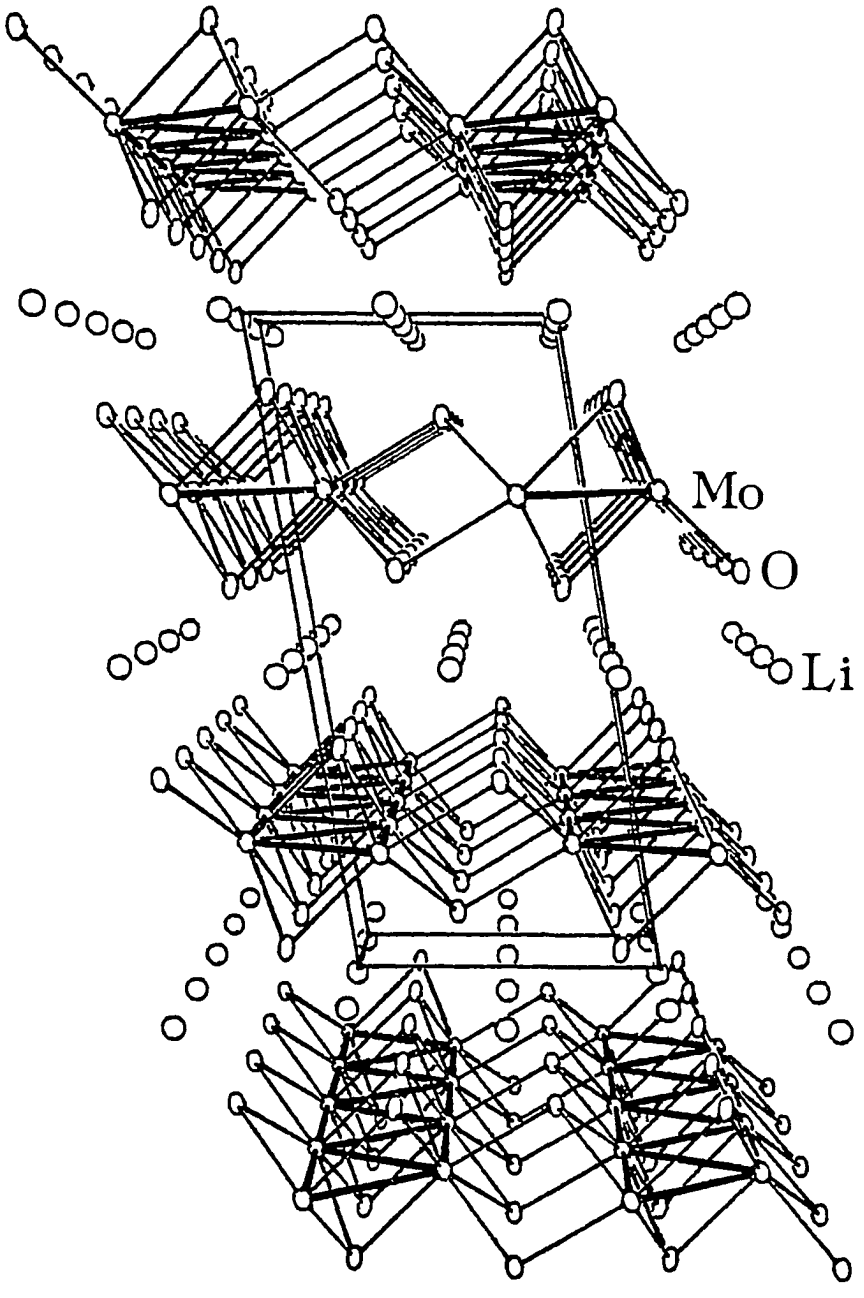

Fig. 3.5. Three dimensional view of the C-centered unit cell of the m-$Li_{0.74}MoO_2$ structure as seen along the b axis. The framework consists of Mo zig-zag ribbons bridged by oxygen atoms [d(Mo-O) = 2.081(10) to 2.132(14)Å] to form O-Mo-O slabs separated by layers of Li ions [d(Li-O)= 1.993(15) to 2.279(11)Å]

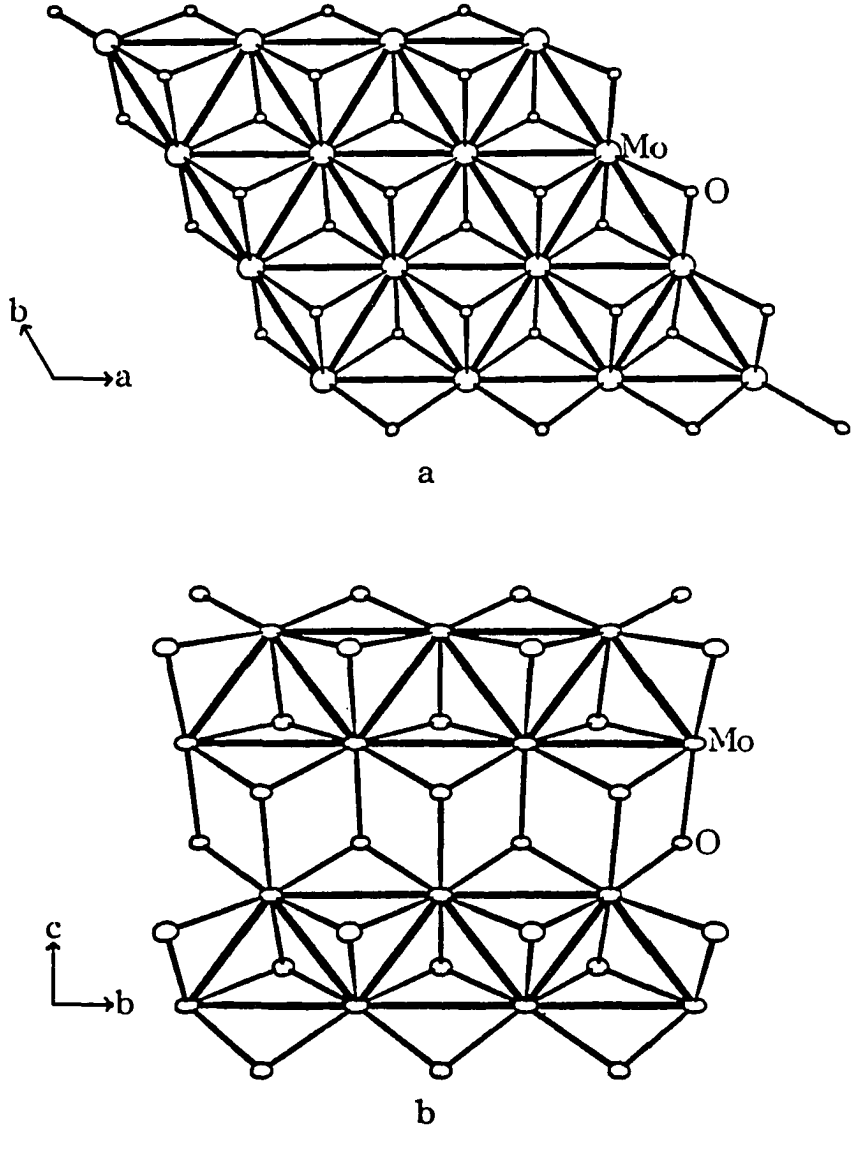

Fig. 3.6. A single O-Mo-O slab in h-$LiMoO_2$ and m-$Li_{0.74}MoO_2$ detailing the Mo bonding with heavy lines and the Mo-O interactions with lighter lines: (a) In h-$LiMoO_2$, the Mo atoms form an infinite metal bonded hexagonal sheet. (b) In m-Li_xMoO_2, the Mo atoms shift in the [100] direction of the C-centered cell toward neighboring atoms to generate zig-zag metal ribbons

SECTION 4. THE SYNTHESIS AND PARTIAL STRUCTURAL CHARACTERIZATION OF A REDUCED POTASSIUM MOLYBDENUM OXIDE

INTRODUCTION

Infinite chains of trans edge-shared Mo octahedra are a characteristic feature of many reduced ternary or quaternary Mo oxides including $NaMo_4O_6$[1], $Sc_{0.75}Zn_{1.25}Mo_4O_7$[2], $Mn_{1.5}Mo_8O_{11}$[3], $Ca_{5.45}Mo_{18}O_{32}$[4], and $LiMo_8O_{10}$[5].

Metal octahedra are also the basic structural units in the metal-rich lanthanide halide and ternary Mo chalcogenide systems. With respect to the former, the condensation of the M_6 units extends well beyond single chains from twin-chains to ultimately layers[6,7]. Due to the structural similarity between the reduced molybdates and the metal-rich lanthanide halides, the clustering of Mo_6 octahedra towards twin-chains or slabs in the oxide system is possible. However, so far, no examples are known.

In the Mo chalcogenide system, a series of compounds showing the segregation of the infinite metal cluster chain into finite segments has been found. This series, $M_xMo_{6n}Ch_{6n+2}$ where n represents the number of face-shared octahedral cluster units, shows condensation of Mo_6Ch_8 units from discrete clusters[8] through intermediate "oligomers"[9,10] to infinite chains[11,12].

With isolation of $In_{11}Mo_{40}O_{62}$ by Professor Simon's group[13], the cutting of the Mo octahedral chain in the oxide system was accomplished. This compound contains "oligomeric" units of 4 and 5 trans edge-shared Mo_6 octahedra. A new oligomeric series which consists of Mo_4O_8 "butterfly" cluster building blocks[12] was achieved with the synthesis of the novel compound, $NdMo_8O_{14}$[14].

This section will summarize the synthesis and partial structural

characterization of a novel K-Mo-oxide showing similar lattice parameters and structural features to those seen in $In_{11}Mo_{40}O_{62}$ and $NdMo_8O_{14}$.

EXPERIMENTAL

Materials

Potassium molybdate was prepared by the reaction of KOH (Fisher Certified A.C.S.) with a stoichiometric quantity of MoO_3 (Fisher Certified A.C.S.) in deionized water. The molybdate solution was filtered, its volume reduced by heating, and the precipitate collected on a glass frit. The product was finally dried at 120°C and stored in a dry box. Molybdenum powder was obtained from Aldrich Chemical Co. (99.99%); molybdenum tubing from Thermo-Electron Corp. (99.97%); and molybdenum sheet from Rembar Co. (99.95%).

Synthesis

Charlie Torardi first reported the preparation of a novel oxide with the tentative formula of $K_{2+x}Mo_{12}O_{19}$ by the reaction between MoO_2 and K_2MoO_4 in an evacuated Mo tube at 1100°C[15]. In the present work, the synthesis of this material was explored further by employing higher firing temperatures. A typical reaction mixture consisted of stoichiometric amounts of MoO_3, Mo metal, and a two-fold excess of K_2MoO_4 ground together within a dry box to achieve the composition wanted in the final product, $K_{2.5}Mo_{12}O_{19}$. Since the melting point of K_2MoO_4 is at 919°C, an excess of the molybdate was used to provide a liquid matrix to facilitate crystal growth. Reactions were fired at 1500°C for three days, or 1300°C for 5 days, employing Mo reaction vessels. The reaction mixture was washed with water to remove the

excess K_2MoO_4. The well crystallized products yielded Guinier x-ray diffraction patterns similar to that obtained by Charlie Torardi[15] as discussed below. One reaction conducted at 1300°C contained single crystals large enough for x-ray single crystal data collection as detailed in the next section.

X-ray Single Crystal Data

The black crystals obtained showed a variety of shapes: intergrown hexagonal plates; hexagonal pyramids; and truncated hexagonal bipyramids. Pyramidal crystals were selected for preliminary film work and subsequent data collection. Even though crystals with well defined edges and shapes were selected, most of the specimens examined were twinned. Owing to difficulty with crystal orientation, complete film work was not obtained on the few single crystals mounted. However, two lattice parameters were confirmed to be 9.27Å and 40.7Å which correspond well with Torardi's indexed hexagonal cell, a = 40.5 and c = 9.30Å[15]. Three crystals determined to be single by oscillation photographs could not be indexed by a random reflection search or by utilizing film coordinates of reflections with the Enraf Nonius CAD-4 diffractometer. Finally, a truncated hexagonal bipyramidal crystal with the dimensions 0.06 x 0.08 x 0.06mm was indexed by employing 25 random reflections in space to yield the following cell constants:

9.914(2), 9.327(1), 20.850(9)

90.00(2), 103.70(3), 90.00(1)

This cell was then transformed to an orthorhombic setting:

9.914(2), 40.51(2), 9.327(1)

89.99(2), 90.00(1), 90.04(3)

Axial photographs of the orthorhombic cell showed a mirror plane along the c-axis but not along the a or b axes indicating that the orthorhombic setting was incorrect. Thus the lower symmetry monoclinic cell was used for the data collection. Details of the data collection are summarized in Table 4.1.

X-ray Powder Diffraction Data

An Enraf Nonius Delft triple focusing Guinier x-ray powder diffraction camera was used with Cu $K\alpha_1$ radiation (λ = 1.5405Å) to obtain d-spacings. National Bureau of Standards silicon powder was mixed with all samples as an internal standard. The observed versus calculated d-spacings are listed in Table 4.2. The diffraction pattern could be indexed based on cell dimensions determined by the single crystal data. The cell parameters computed by a least-squared method using the 21 strongest diffraction lines are a = 9.925(6), b = 9.333(4), c = 20.86(1), β = 103.81(7)^{o}.

RESULTS AND DISCUSSION

The lattice parameters for the K-Mo-oxide (monoclinic and orthorhombic setting) are quite similar to those found for $In_{11}Mo_{40}O_{62}$ and $NdMo_8O_{14}$ as listed in Table 4.3. Projections of the Mo clustering seen in the In and Nd oxides are given in Figure 4.1a and b. From these illustrations, one can see that the 3-fold axis of an individual Mo_6 octahedral unit is aligned along the short axis (9.526Å for $In_{11}Mo_{40}O_{62}$ and 9.191Å for $NdMo_8O_{14}$) and the segmented "chains" are aligned perpendicular to the axis approximately equal to 10Å (9.895Å for $In_{11}Mo_{40}O_{62}$ and 9.996Å for $NdMo_8O_{14}$). The length of the third axis given in multiples of a typical Mo-Mo distance (~2.8Å) reflects the length of the discrete clusters. For the In compound, the a-axis is 10 x 2.8878Å. Within the unit cell, along this axis, 9 Mo octahedral units are found with 2 interchain spacings equivalent to one-half of an octahedral unit each. The Nd compound shows a long axis equal to 4 x 2.78Å, with a sum of 3 Mo octahedra and two intercluster spaces along this axis.

Thus, focusing on the orthorhombic setting for the potassium compound, one can see that the long axis, 40.48Å, is equivalent to 14 x 2.89Å. With respect to the orthorhombic cell (9.921, 9.332, 40.48Å) the 0,0,0 and 1/2,0,1/2 positions are at the origin and 0,0,1, respectively, for the monoclinic cell. Thus this orthorhomic cell must be B-centered. One can generate a model to incorporate two "1/2 Mo octahedra" interchain spacings and 13 Mo octahedra as seen in Figure 4.2. This model belongs to the "butterfly" oligomeric series. Using the general formula $M_xMo_{4n}O_{6n+2}$, where n is equal to the number of Mo_4 butterfly

units, the model with n = 7 gives the formula $K_xMo_{28}O_{44}$ which is close to twice the stoichiometry assigned by Charlie Torardi, $K_{2+x}Mo_{12}O_{19}$[15], and essentially the same O/Mo ratio.

Extrapolation of this model to the monoclinic setting dictates an acentric space group, Pa. The primitive cell was confirmed by the absence of extinctions for general hkl reflections. However, the subset 0k0 revealed a k = 2n + 1 extinction, indicating a 2-fold screw along the b-axis and a centric space group. Results of the statistical analysis given by the SHELXS-86 direct methods program[16] also indicated a centric system. The intensity data of the h0l reflection subset showed both h = 2n + 1 and l = 2n + 1 extinctions. Based on all these conditions the $P2_1/n$ space group was applied for a structure solution.

Direct method (SHELXS-86) solutions showed chains of Mo octahedral cluster units with the expected orientation (the 3-fold axis of a single octahedral unit along the short b axis). Refinement of various solutions with 9 to 13 Mo atoms yielded residuals no less than 52%.

In the next step, the l = 2n condition was ignored leaving only an a-glide. This symmetry element would be in accord with the above model. Using the space group $P2_1/a$, SHELXS-86 led to the location of 11 Mo atoms forming a Mo_{22} cluster with the same orientation and arrangement within the cell as the model above except with equivalent chain ends. However, this structure could not be refined with a R factor lower than 30% by varying isotropic thermal parameters and adding potassium atoms to appropriate sites.

Other models based on SHELXS-86 solutions, such as a segment containing four Mo_6 octahedra, also refined to R factors around thirty percent but no lower. At this point the zone residuals were examined,

but the R factors for the observed reflections revealed no special pattern. However, the examination of intensity data showed that the EOO and EEO class of reflections were absent which indicates a definite problem with the data set.

At this stage, it is probably best to examine other crystals and obtain a new data set. The difficulty in finding single crystals of this compound may be pointing to problems in crystallization or intergrowth. Similar to $In_{11}Mo_{40}O_{62}$, the structure may be composed of segmented chains of varied length. But unlike the structure of the In compound, the clusters in the potassium compound may not be well ordered. Microprobe analyses on a series of crystals may provide some information on the variation of composition from one crystal to the next. Intergrowth structural features could be detected by electron microscopy. "Recrystallization" through a vapor transport reaction using Cl_2 or I_2 as a transport agent, could yield better crystals for the x-ray structural analysis.

Conclusion

Further synthetic and structural work on a novel potassium compound, $K_{2+x}Mo_{12}O_{19}$, first reported by Charlie Torardi[15] has shown that is reminiscent of the Mo-oxides, $In_{11}Mo_{40}O_{62}$[13] and $NdMo_8O_{14}$[14] which contain discrete clusters derived from Mo octahedral units. A close correspondence in lattice parameters of the three compounds enable the formulation of a model structure with the composition, $K_xMo_{28}O_{44}$. This is close to twice the stoichiometry established by Charlie Torardi[15]. Unfortunately, the crystal structure could not be solved, possibly stemming from intergrowth problems.

REFERENCES

1. Torardi, C. C.; McCarley, R. E. J. Am. Chem. Soc. 1979, 101, 3963.

2. McCarley, R. E. ACS Symp. Ser. 1983, 211, 273; Philos. Trans. R. Soc. London Ser. A 1982, 308, 141.

3. Carlson, C. D.; Edwards, P. A.; McCarley, R. E., unpublished results, Department of Chemistry, Iowa State University, Ames, Iowa, 1982.

4. McCarley, R. E.; Lii, K. -H.; Edwards, P. A.; Brough, L. F. J. Solid State Chem. 1985, 57, 17.

5. Lii, K. -H.; McCarley, R. E.; Sangsoo, K.; Jacobson, R. A. J. Solid State Chem. 1986, 64, 347.

6. Simon. A. Angew. Chem. Int. Ed. Engl. 1981, 20, 1.

7. Simon, A. J. Solid State Chem. 1985, 57, 2.

8. Chevrel, R.; Sergent, M.; Prigent, J. Mat. Res. Bull. 1974, 9, 1487.

9. Potel, M; Chevrel, R.; Sergent, M.; Decroux, M.; Fischer, Ø. C. R. Acad. Sci., Ser. C 1979, 288, 429.

10. Honle, W.; von Schnering, H. G.; Lipka, A.; Yvon, A. J. Less-Common Met. 1980, 71, 135.

11. Gougeon, P.; Padiou, J.; Le Marouille, J. Y.; Potel, M.; Sergent, M. J. Solid State Chem. 1984, 51, 218.

12. Chevrel, R.; Gougeon, P.; Potel, M.; Sergent, M. J. Solid State Chem. 1985, 57, 25.

13. Mattausch, Hj.; Simon, A.; Peters, E.-M. Inorg. Chem. 1986, 25, 3428.

14. Gougeon, P.; McCarley, R. E. unpublished results, Ames Laboratory, Iowa State University, Ames, Iowa, 1985.

15. Torardi, C. C., Ph.D. Dissertation, Iowa State University, Ames, Iowa 1981, Section 5.

16. Sheldrick, G. M., Institut fur Anorganische Chemie der Universitat, Gottingen, F.R.G.

Table 4.1. The crystallographic data for "$K_{2+x}Mo_{12}O_{19}$"

crystal system	monoclinic
space group	$P2_1/a$
lattice constants	
a (Å)	9.920(4)
b (Å)	9.331(1)
c (Å)	20.83(1)
β (°)	103.78(5)
Volume ($Å^3$)	1873.5(5)
crystal dimensions (mm)	0.06 x 0.08 x 0.06
empirical absorption correction (Tmax/Tmin)	1.279
diffractometer	Enraf Nonius CAD-4
radiation: MoK$\bar{\alpha}$ (λ,Å)	0.71069
monochromator	graphite
scan type	ω/2θ
scan half width (degree)	0.85 + 0.34tanθ
standard reflections:	
number monitored	3
frequency measured	every 250 reflns.
intensity variation	none
reflections measured	HKL, HK$\bar{L}$, $\bar{H}$KL, $\bar{H}$K$\bar{L}$
max 2θ (degree)	55
reflections collected	8560
observed [I > 3σ(I)]	3254
number unique reflns. with I > 3σ(I)	996
residual factors for averaging	
based on I	0.030
based on F_{obs}	0.025

Table 4.2. X-ray powder diffraction data for "$K_{2+5}Mo_{12}O_{19}$"[a]

d-spacings (Å) observed	d-spacings (Å) calculated[a]	intensities	h k l
6.73(1)	6.700	ms	-1 1 1, 1 1 0
6.098(9)	6.070	w	-1 1 2, 1 1 1
3.111(2)	3.108	wm	-3 1 2, -3 1 1
2.961(2)	2.960	ms	-1 3 1, 1 3 0
2.832(1)	2.830	w	1 1 6
2.692(1)	2.692	m	-3 2 2, -3 2 1
2.507(1)	2.506	wm	-1 2 7, 1 2 6
2.479(1)	2.480	w	-4 0 2
2.421(1)	2.413	w	-2 1 8
2.413(1)	2.412	wm	2 1 6
2.397(1)	2.397	w	-4 1 2
2.334(1)	2.333	w	0 4 0
2.279(1)	2.274	m	-1 2 8, 1 2 7
2.210(1)	2.209	w	0 4 3
2.077(1)	2.077	vw	-2 3 7
2.0444(9)	2.0402	w	-3 1 9, 3 1 6
1.9522(8)	1.9537	wm	4 1 4
1.9481(8)	1.9476	wm	-2 3 8, 2 3 6
1.9404(8)	1.9392	wm	-4 3 2
1.9081(8)	1.9080	w	-3 2 9
1.8324(7)	1.8322	w	-1 5 1, 1 5 0
1.8255(7)	1.8250	w	-2 3 9

[a]Refined monoclinic cell parameters a = 9.925(6), b = 9.333(4), c = 20.86(1)Å, and β = 103.81(7)°.

Table 4.3. Lattice parameters for some reduced ternary Mo-oxides

compound	a, Å	b, Å	c, Å	a, deg.	β, deg.	γ, deg.
$K_{2+x}Mo_{12}O_{19}$	9.921(4)	9.332(1)	20.84(1)	90.0	103.78(5)	90.0
	9.921	9.332	40.48	90.0	90.0	90.0
$In_{11}Mo_{40}O_{62}$	28.878(9)	9.526(3)	9.895(2)	90.0	90.0	90.0[13]
$NdMo_8O_{14}$	9.191(1)	9.996(1)	11.121(1)	90.0	90.0	90.0[14]

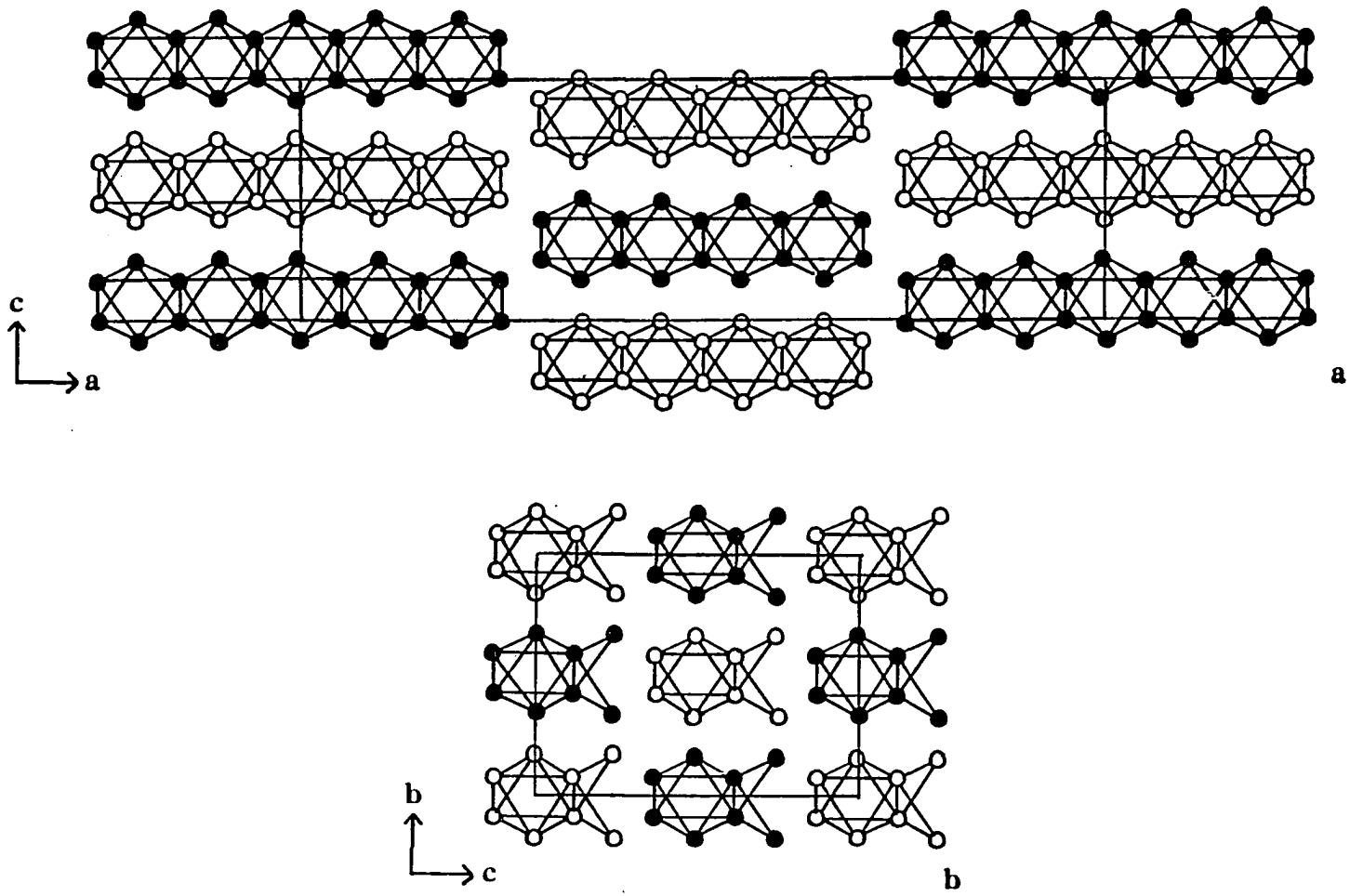

Fig. 4.1. Projections illustrating the Mo clustering observed in (a) $In_{11}Mo_{40}O_{62}$[13]; and (b)$NdMo_8O_{14}$[14]. The solid colored chains are 1/2 above the other chains in the cell along the axis perpendicular to the page

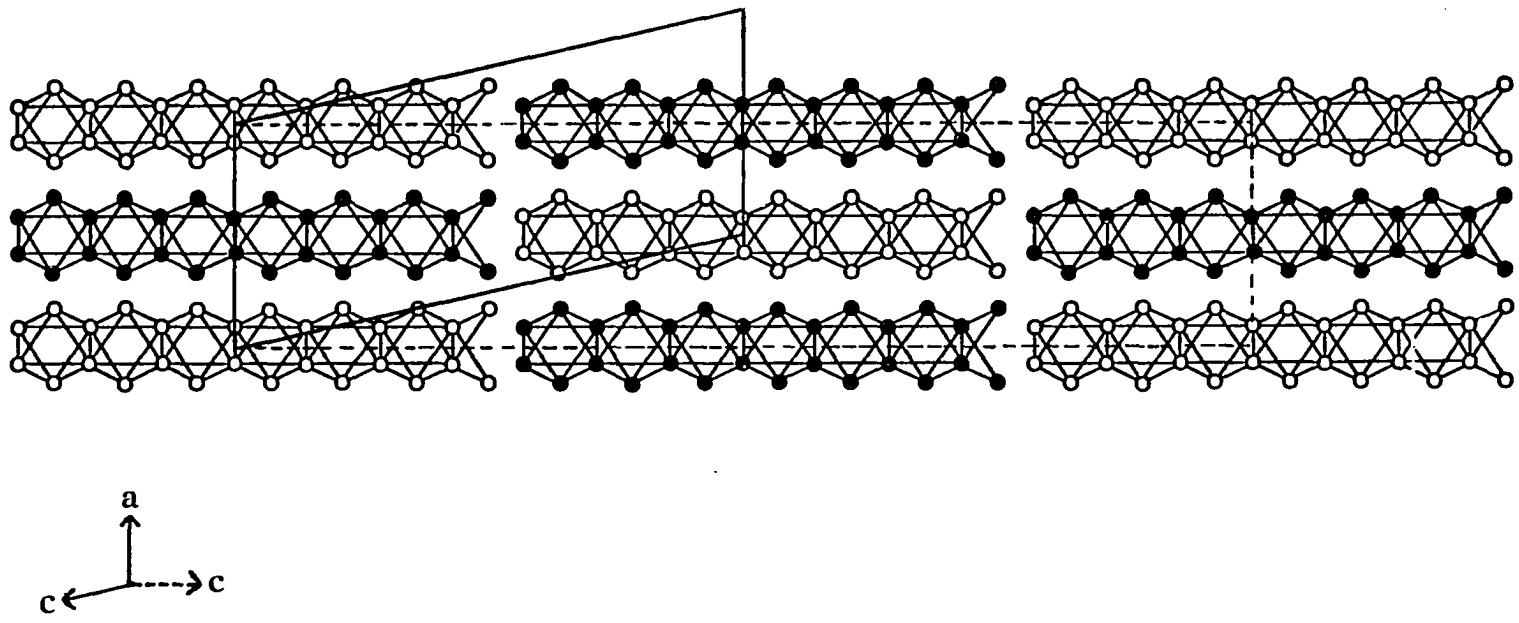

Fig. 4.2. Projection showing the Mo bonding seen in a structural model proposed for $K_{2+x}Mo_{12}O_{19}$. The dashed line represents the orthorhombic setting while the solid line marks the monoclinic cell

CONCLUSION

Synthetic exploration of the reduced molybdenum oxide $Na_2Mo_3O_6$, reported by Hubert[11] in 1966, led to the characterization of a series of layered Na-Mo-oxide, Na_xMoO_2. These compounds have provided a novel structure type, a two dimensional network, among the previously known structures observed for reduced molybdenum oxides. The basic framework of these phases consists of oxide layers alternating with sheets of Na and Mo atoms. Within the Mo layers, the metal atoms shift from ideal octahedral sites toward neighboring Mo atoms to form extended chains of fused rhomboidal clusters.

The layered framework of the Na-Mo-oxides stands in sharp contrast to the tunneled structure of $Ba_{1.14}MoO_8O_{16}$[6] and $K_2Mo_8O_{16}$[8] which also contain chains comprised of discrete, distorted Mo rhomboidal clusters. $Na_{0.51}MoO_2$ with essentially ten electrons for every Mo_4O_8 unit should be ideal for forming a hollandite structure with regular rhomboidal Mo clusters. But the hollandite framework provides only two cubic cationic sites per every Mo_8O_{16} unit; $Na_{0.51}MoO_2$, reformulated as $Na_{\sim 4}Mo_8O_{16}$, requires four cationic sites for every Mo_8O_{16} repeat. Thus a new structure type is dictated.

Typically, the most important factor affecting the structures of low oxidation state Mo-oxides is the extent to which Mo is reduced. In general, increasing the number of valence electrons on the Mo atom with simultaneous decrease in the O/Mo ratio leads to larger metal clusters[7]. The formation of a layered network instead of a hollandite framework in Na_xMoO_2 provides a good example of how the resulting structure can be influenced by factors other than the metal electron count, such as the

ternary cation to Mo ratio.

The size of the counter cations (or even the packing anions) may also play a role in the determining the final network and metal clustering. For instance, the structure and Mo bonding in the ternary Mo sulfide, $CoMo_2S_4$[12], is remarkably similar to that observed in layered Na-Mo-oxides. But the Mo atoms, unlike those in the oxides, form chains of linked distorted rhomboidal clusters. Since $CoMo_2S_4$ shows a higher electron to metal ratio compared to the Na_xMoO_2 series, one would have expected a condensed metal ribbon composed of regular rhombuses. Electronically, the contrast in metal clustering may be explained by the band splitting observed upon the pairing distortions seen in a hexagonal layer[13,14]. But the size and electronegativity of the packing anion, S^{2-}, may be more important. Due to the lower electronegativity of S^{2-} than O^{2-}, greater Mo-S π interaction should be observed, thus limiting the extent of Mo bonding. Also, due to the larger size of S^{2-} over O^{2-}, the Mo atoms may not be able to approach each other close enough to form a completely condensed ribbon.

While the size of the framework atoms may determine the extent of metal clustering within a layer, the number of ternary cations may be an influencing factor in the stacking pattern of the metal-anion bilayers. Each of the Na-Mo-oxide structures shows a different structural form with respect to oxygen packing, and like the Na-Co bronzes[15-18], this is believed to be related to the varied amount of sodium in the interlamellar space. The oxygen layering, from $Na_{0.41}MoO_2$ to $Na_{0.66}MoO_2$, changes from nonsequential through ABCD to ABBCCA. As the concentration of the ternary cations increases significantly above one half, the Na ions shift from octahedral to trigonal prismatic sites, and

from a rectangular to a hexagonal net.

The related layered Li-Mo-oxides also show a alkali metal hexagonal sublattice. But due to the smaller size of this counter cation, the coordination of the cation, the subsequent oxygen packing, and even the reactivity of the Li_xMoO_2 compounds is different from those in the corresponding Na_xMoO_2 series. With respect to composition, the monoclinic compound, m-$Li_{0.74}MoO_2$, is the closest to $Na_{0.66}MoO_2$. Except for the hexagonal alkali metal sublattice, the layered networks of m-$Li_{0.74}MoO_2$ and $Na_{0.66}MoO_2$ are quite contrasting. In $Na_{0.66}MoO_2$, the ternary cations are located in trigonal prismatic sites with ABBCCA oxygen packing. Whereas in m-$Li_{0.74}MoO_2$, the Li cations are found in octahedral coordination sites, and the oxygen layering shifts towards cubic close packing.

The reactivity of the corresponding Li and Na monoclinic layered compounds is also disparate. $Na_{0.66}MoO_2$ deintercalates in moist air to form the water stable phase, $Na_{0.41}MoO_2$ (plus NaOH and H_2) while the high content monoclinic Li form does not delithiate in moist air to form a higher oxidized layered variant. The change in coordination geometry about the alkali metal can account for this observation. It was noted in the Co bronze system, that counter cations located in trigonal prismatic sites are much more mobile than those in octahedral enviroments[19]. Thus the stability of m-$Li_{0.74}MoO_2$, $Na_{0.41}MoO_2$, and $Na_{0.51}MoO_2$ to deintercalation in moist air or water appears to be related to the octahedral coordination about the ternary cation.

The ideal cubic close-packed framework of the hexagonal structure of $LiMoO_2$ may be stabilized by the presence of a fully loaded interlamellar space. But, the metal electron count, which gives

completely filled Mo-Mo bonding states, may be a more important factor in the observation of a hexagonal framework with a bonded metal sheet (over a distorted framework with metal chains) for $LiMoO_2$. In the ion exchange reaction with $ZnCl_2$, which presumably maintained the same electron count on the Mo atoms while decreasing the number of cations in the interlamellar space, the hexagonal structure and the Mo-Mo bonded sheet were preserved. However, the formation of vacancies while keeping the same electron count could affect the structure, given enough energy to allow for distortion within the Mo layer. Assuming that the Ca exchanged material is $Ca_{0.5}MoO_2$, electronically one would expect a hexagonal structure with infinite Mo bonded sheets with distances around 2.866Å. But the exchange reaction was conducted at 800°C, a firing temperature high enough to allow structural transformation. Indeed, the resulting layered compound showed a monoclinic cell which points to the formation of Mo ribbons consisting of condensed rhomboidal units. Interestingly, the Mo-Mo bond distance along the chain direction (determined by the length of the monoclinic b-axis) is still 2.866(2)Å. The hexagonal framework of $LiMoO_2$ with the unusual Mo bonding is assuredly destabilized through the oxidation of the Mo bonded layer upon deintercalation. This is supported by the observation of the conversion of the delithiated h'-Li_xMoO_2 into the monoclinic form at 900°C. Also, the complete oxidization of h'-Li_xMoO_2 over a period of 8 weeks attests to the metastability of the slightly delithiated phase.

Although the crystal structure of the potassium compound "$K_{2+x}Mo_{12}O_{19}$" was not solved, it certainly represents a different structure type than that of the layered Na and Li-Mo-oxides. Comparison with the In and Nd compounds with respect to valence electron count and

O/Mo ratio may provide insight to other compounds which could possess discrete oligomeric clusters of fused Mo_6O_{12} units.

REFERENCES

1. Torardi, C. C.; McCarley, R. E. J. Am. Chem. Soc. 1979, 101, 3963.

2. McCarley, R. E. ACS Symp. Ser. 1983, 211, 273; Philos. Trans. R. Soc. London Ser. A 1982, 308, 141.

3. Carlson, C. D.; Edwards, P. A.; McCarley, R. E., unpublished results, Department of Chemistry, Iowa State University, Ames, Iowa, 1982.

4. McCarley, R. E.; Lii, K. -H.; Edwards, P. A.; Brough, L. F. J. Solid State Chem. 1985, 57, 17.

5. Lii, K. -H.; McCarley, R. E.; Sangsoo, K.; Jacobson, R. A. J. Solid State Chem. 1986, 64, 347.

6. Torardi, C. C.; McCarley, R. E. J. Solid State Chem. 1981, 37, 393.

7. Lii, K. -H., Ph.D. Dissertation, Iowa State University, Ames, Iowa, 1985.

8. Torardi, C. C.; Calabrese, J. C. Inorg. Chem. 1984, 23, 3281.

9. Mattausch, Hj.; Simon, A.; Peters, E. -M. Inorg. Chem. 1986, 25, 3438.

10. Gougeon, P.; McCarley, R. E., unpublished results, Ames Laboratory, Iowa State University, Ames, Iowa, 1985.

11. Hubert, P. H. C. R. Acad. Sc. Paris 1966, 262, 1189.

12. Guillevic, J.; Le Marouille, J. -Y.; Grandjean, D. Acta Crystallogr. 1974, B30, 111.

13. Burdett, J. K.; Hughbanks, T. Inorg. Chem. 1985, 24, 1741.

14. Aleandri, L. E., Ph.D. Dissertation, Iowa State University, Ames, Iowa, 1987, Section 1, Page 20.

15. Delmas, C.; Braconnier, J. J.; Fouassier, C.; Hagenmuller, P. Solid State Ionics 1981, 3/4, 165.

16. Delmas, C.; Fouassier, C.; Hagenmuller, P. Physica 1980, 99B, 81.

17. Fouassier, C.; Delmas, C.; Hagenmuller, P. Mat. Res. Bull. 1975, 10, 443.

18. Fouassier, C.; Matejka, G.; Reau, J. M.; Hagenmuller, P. J. Solid State Chem. 1973, 6, 532.

19. Delmas, C.; Maazarz, A.; Fouassier, C.; Reau, J. M.; Hagenmuller, P. Mat. Res. Bull. 1979, 14, 329.

ACKNOWLEDGEMENTS

First and foremost, I would like to thank Dr. McCarley for his direction, support, and encouragement during the course of this work.

I would also like to thank my fellow group members for their companionship and interesting, but sometimes bizarre, discussions.

I would especially like to extend my appreciation to Kwang-Hwa Lii whose guidance and special friendship have helped me grow as a chemist and a person.

Certainly, I must thank Clark Carlson whose enduring friendship and love have helped me through some very difficult times.

I am also grateful to the scientific community here at Iowa State for their aid throughout my research, especially the members of Dr. Jacobson's group for their assistance in single crystal data collection and structure solutions.

My deepest appreciation goes to Hans Hachgenei for his insight and thoughtful criticism with respect to my dissertation but more importantly for his patience, support, and love.

Finally, I would like to dedicate this thesis to my parents who have provided an infinite source of encouragement.

"Success in the end eclipses
the mistakes along the way."
- Chinese Proverb